

การสังเคราะห์ซีไอโพลด์บีตาขนาดนาโนสำหรับการเปลี่ยนพลาสติกเป็นแก๊สลิ้น




นางสาวธิดารัตน์ กุณะวงษ์

ศูนย์วิทยทรัพยากร
วิทยานิพนธ์นี้เป็นส่วนหนึ่งของการศึกษาตามหลักสูตรปริญญาวิทยาศาสตรมหาบัณฑิต
จุฬาลงกรณ์มหาวิทยาลัย
สาขาวิชาเคมี ภาควิชาเคมี
คณะวิทยาศาสตร์ จุฬาลงกรณ์มหาวิทยาลัย
ปีการศึกษา 2550
ลิขสิทธิ์ของจุฬาลงกรณ์มหาวิทยาลัย



SYNTHESIS OF NANOSIZED ZEOLITE BETA FOR
PLASTIC CONVERSION TO GASOLINE



Miss Thidarat Kunawong

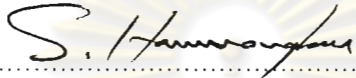
ศูนย์วิทยทรัพยากร
จุฬาลงกรณ์มหาวิทยาลัย

A Thesis Submitted in Partial Fulfillment of the Requirements
for the Degree of Master of Science Program in Chemistry
Department of Chemistry
Faculty of Science
Chulalongkorn University
Academic Year 2007
Copyright of Chulalongkorn University


502095


Thesis Title SYNTHESIS OF NANOSIZED ZEOLITE BETA FOR PLASTIC
 CONVERSION TO GASOLINE
By Miss Thidarat Kunawong
Field of Study Chemistry
Thesis Advisor Aticha Chaisuwan, Ph.D.

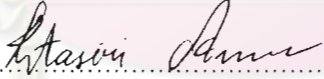
Accepted by the Faculty of Science, Chulalongkorn University in Partial
Fulfillment of the Requirements for the Master's Degree


.....Dean of the Faculty of Science
(Professor Supot Hannongbua, Ph.D.)

THESIS COMMITTEE


.....Chairman
(Professor Sophon Roengsumran, Ph.D.)


.....Thesis Advisor
(Aticha Chaisuwan, Ph.D.)


.....Member
(Amarawan Intasiri, Ph.D.)


.....Member
(Assistant Professor Soamwadee Chaiansutcharit, Ph.D.)


.....Member
(Assistant Professor Kulaya Otaka, Ph.D.)

ธิดารัตน์ ภูณะวงษ์ : การสังเคราะห์ซีโอไลต์บีตาขนาดนาโนสำหรับการเปลี่ยนพลาสติกเป็นแก๊สลิ้น. (SYNTHESIS OF NANOSIZED ZEOLITE BETA FOR PLASTIC CONVERSION TO GASOLINE)

อ.ที่ปรึกษา: คร. อธิชา ฉายสุวรรณ, 150 หน้า.

ได้สังเคราะห์ซีโอไลต์บีตาจากเซโรเจลซิติกาที่เตรียมขึ้นใหม่ซึ่งผสมกับอะลูมิเนียมไอโซโพรพอกไซด์และสารละลายเทระเอทิลแอมโมเนียมไฮดรอกไซด์ตามด้วยการตกผลึกแบบไฮโดรเทอร์มัลที่ 135 องศาเซลเซียส เป็นเวลาต่างๆ กัน ได้สำรวจอิทธิพลของการฉายรังสีอัลตราไวโอเล็ตระหว่างการเกิดเจลต่อสมบัติเชิงเคมี-กายภาพและเชิงเร่งปฏิกิริยา ได้ศึกษาเปรียบเทียบผลของตัวแปรต่างๆ ได้แก่ เวลาในการฉายรังสีอัลตราไวโอเล็ต เวลาในการตกผลึก และอัตราส่วนของซิติกาต่ออะลูมิเนียมในเจลกับซีโอไลต์บีตาที่เตรียมโดยไม่มีการฉายรังสีอัลตราไวโอเล็ต ได้ตรวจสอบลักษณะเฉพาะของซีโอไลต์บีตาด้วยเทคนิคการหักเหรังสีเอกซ์ กล้องจุลทรรศน์แบบส่องกราด อินดักทีฟทีลด์บีเปิดพลาสติกอะตอมมิกอิมิตชันสเปกโทรสโคปิก อะลูมิเนียมแมจิกแองเกิลสปีนนิวเคลียร์แมกเนติกเรโซแนนซ์ การดูดซับไนโตรเจน และการคายแอมโมเนียด้วยการเพิ่มอุณหภูมิแบบตั้งโปรแกรม สามารถสังเคราะห์ซีโอไลต์บีตาที่บริสุทธิ์ด้วยวิธีการฉายรังสีอัลตราไวโอเล็ตหลังการตกผลึกเพียง 16 ชั่วโมง การใช้รังสีอัลตราไวโอเล็ตไม่มีผลต่อโครงสร้างแต่มีผลต่อขนาดอนุภาคของซีโอไลต์บีตาอย่างมีนัยสำคัญ การฉายรังสีอัลตราไวโอเล็ตไม่เพียงทำให้ได้ปริมาณซีโอไลต์บีตาเพิ่มขึ้นแต่ยังทำให้อะลูมิเนียมเข้าไปในตำแหน่งโครงสร้างที่เป็นเทอะซีดรัลได้มากขึ้นเป็นผลให้มีความเป็นกรดเพิ่มขึ้น ได้สำรวจสมบัติเชิงเร่งปฏิกิริยาของซีโอไลต์บีตาที่สังเคราะห์ได้ในการแตกตัวของพอลิโพรพิลีน และพอลิเอทิลีนที่มีความหนาแน่นสูงภายใต้ภาวะต่างๆ การแตกตัวของพอลิเอทิลีนที่มีความหนาแน่นสูงเกิดได้ยากกว่าการแตกตัวของพอลิโพรพิลีน เมื่อใช้ซีโอไลต์บีตาเป็นตัวเร่งปฏิกิริยาการเปลี่ยนของพลาสติกทั้งสองชนิดเพิ่มขึ้นอย่างมากเมื่อเทียบกับไม่ใช้ตัวเร่งปฏิกิริยา ค่าการเปลี่ยนพลาสติกและปริมาณของผลิตภัณฑ์ส่วนที่เป็นของเหลวขึ้นกับอุณหภูมิที่ใช้ในการแตกตัวและอัตราส่วนของพลาสติกต่อตัวเร่งปฏิกิริยา อย่างไรก็ตามอัตราส่วนของซิติกาต่ออะลูมิเนียมในช่วง 40 ถึง 80 ไม่มีผลต่อค่าการเปลี่ยนของพลาสติกและปริมาณผลิตภัณฑ์ การใช้รังสีอัลตราไวโอเล็ตกับตัวอย่างที่มีค่าอัตราส่วนของซิติกาต่ออะลูมิเนียมต่ำคือ 20 ทำให้ได้ค่าการเปลี่ยนและปริมาณผลิตภัณฑ์ที่เป็นของเหลวสูงสุดเนื่องจากค่าความเป็นกรดสูงสุดของตัวเร่งปฏิกิริยานี้ ความเลือกจำเพาะต่อผลิตภัณฑ์ได้รับผลเล็กน้อย ผลิตภัณฑ์ที่เป็นแก๊สที่ได้จากการแตกตัวของพอลิโพรพิลีน และพอลิเอทิลีนที่มีความหนาแน่นสูงส่วนใหญ่เป็นโพรพิน ไอโซบิวทีน และไอสารที่มีจุดหลอมเหลวสูงกว่านอัมลเพนแทน ผลิตภัณฑ์ที่เป็นของเหลวที่ได้จากการแตกตัวของพลาสติกทั้งสองชนิดส่วนใหญ่มีจุดเดือดอยู่ในช่วงของเฮกเซนถึงโนเนน สามารถปรับสภาพตัวเร่งปฏิกิริยาที่ใช้แล้วให้นำกลับมาใช้ใหม่ได้ง่ายด้วยการเผาและความว่องไวยังคงไม่เปลี่ยนแปลงมากนัก

ภาควิชา เคมี ลายมือชื่อนิสิต **ธิดารัตน์ ภูณะวงษ์**
 สาขาวิชา เคมี ลายมือชื่ออาจารย์ที่ปรึกษา **อธิชา ฉายสุวรรณ**
 ปีการศึกษา 2550

4872315423: MAJOR CHEMISTRY

KEY WORD: ZEOLITE BETA / BEA / CATALYTIC CRACKING / HDPE / PP

THIDARAT KUNAWONG: SYNTHESIS OF NANOSIZED ZEOLITE BETA FOR PLASTIC CONVERSION TO GASOLINE.

THESIS ADVISOR: ATICHA CHAISUWAN, Ph.D., 150 pp.

Nanosized zeolite beta was synthesized from a freshly prepared silica xerogel mixed with aluminium isopropoxide and a solution of tetraethylammonium hydroxide, followed by hydrothermal crystallization at 135°C for various periods. The influence of ultrasound irradiation during the gel formation step on physico-chemical and catalytic properties of zeolite beta were investigated. The effects of different parameters: ultrasound irradiation periods, crystallization time and the Si/Al ratios in gel were also studied in comparison with zeolite beta prepared without ultrasound irradiation. The zeolite beta samples were characterized by X-ray diffraction, scanning electron microscopy, ICP-AES, ^{27}Al -MAS-NMR, nitrogen adsorption and ammonia temperature programmed desorption techniques. Pure zeolite beta can be synthesized with employing ultrasound radiation after crystallization for only 16 h. Application of ultrasound radiation did not affect the structures but had significant effect on particle size of zeolite beta. Ultrasound irradiation caused not only yield of zeolite beta increased but also more aluminum incorporated into the tetrahedral framework position resulting in higher acidity. The catalytic property of synthesized zeolite beta was investigated in polypropylene and high density polyethylene catalytic cracking under different conditions. The cracking of high density polyethylene is more difficult than that of polypropylene. When zeolite beta was used as catalyst, the conversions of both plastics are greatly more than that in the absence of catalyst. The plastic conversions and yields of liquid products depend on the cracking temperature and the plastic to catalyst ratio. Nevertheless, the Si/Al ratios in catalyst in the range from 40 to 80 do not affect plastic conversions and product yields. Application of ultrasound radiation to the sample with the low Si/Al ratio of 20 provides the highest conversion as well as liquid product yield due to the highest acidity of the catalyst. The product selectivity is affected slightly. The gas products obtained by polypropylene and high density polyethylene cracking are mainly propene, i-butene and C_5^+ . The liquid products obtained by cracking of both types of plastic are mainly in the boiling point range from C_6 to C_9 . The used catalyst can be regenerated easily by simple calcinations and its activity still does not change significantly.

Department:..... Chemistry..... Student's Signature: *Thidarat Kunawang*
 Field of Study:..... Chemistry..... Advisor's Signature: *A. Chaisuan*
 Academic year:..... 2007.....

ACKNOWLEDGEMENTS

The accomplishment of this thesis can be attributed to the extensive support and assistance from Dr. Aticha Chaisuwan, my thesis advisor. I would like to sincere gratitude to her for valuable advice and guidance in this research as well as extraordinary experiences throughout the work.

I would like to deeply thank Professor Dr. Sophon Roengsumran, Dr. Amarawan Intasiri, Assistant Processor Dr. Soamwadee Chaiansutcharit and Assistant Processor Dr. Kulaya Otaka, from department of chemistry, faculty of science, Ramkhamhaeng University as the chairman and member of this thesis committee, respectively, for all of their kindness and useful advice in the research.

I would like to appreciatively thank PTT Chemical Public Company Limited for supporting the standard mixtures for GC analysis. Moreover, I would like to thank Department of Chemistry, Faculty of Science, Chulalongkorn University for supporting a teacher assistant fund and the valuable knowledge and experience. Furthermore, I would like to thank the Graduate School Chulalongkorn University for a “90th Anniversary Chulalongkorn University” grant for financial support. In addition, Thailand Japan Technology Transfer Project a loan supported by Japan Banks for International Cooperation (TJTTP-JBIC) for instrument support. I also would like to convey the special acknowledgement to the Development and Promotion of Science and Technology Talent Project (DPST) for supporting the scholarship and valuable extraordinary experiences.

Many thanks go in particular to the members of Materials Chemistry and Catalysis Research Unit for their help and encouragement throughout the course of my research and study. Finally, I greatly thank to my family and all of my friends for their help and encouragement during my graduate study.

CONTENTS

	Page
ABSTRACT (THAI)	iv
ABSTRACT (ENGLISH)	v
ACKNOWLEDGEMENTS	vi
CONTENTS	vii
LIST OF TABLES	x
LIST OF FIGURES	xii
LIST OF SCHEMES	xix
LIST OF ABBREVIATIONS	xx
CHAPTER I INTRODUCTION	1
CHAPTER II THEORY	11
2.1 Zeolites	11
2.1.1 Zeolites Structures	12
2.1.2 Acid Sites of Zeolites	15
2.1.3 Shape Selectivity	16
2.2 Zeolite Beta	17
2.2.1 Structure of Zeolite Beta	17
2.2.2 Characterization of Zeolite Beta	18
2.2.2.1 Power X-ray Diffraction (XRD)	19
2.2.2.2 Scanning Electron Microscopy (SEM)	20
2.2.2.3 Nitrogen Adsorption-Desorption Isotherm	21
2.2.2.4 Temperature-Programmed Desorption (TPD)	
of Ammonia	23
2.2.2.5 ²⁷ Al-MAS-NMR	25
2.3 Effect of Parameters on the Zeolite Beta Synthesis	25
2.3.1 Effect of Si/Al ratios	25
2.3.2 Effect of Template	26
2.3.3 Effect of Ultrasound Irradiation	26
2.3.4 Effect of Calcination	28
2.4 The Refining Process	29

	Page
2.5 Catalytic Cracking Mechanisms	31
2.5.1 General Cracking Mechanisms	31
2.5.2 Reactions of Olefins	32
2.5.3 Proposed Cracking Mechanisms of Polymer	34
2.5.4 Reactions of Paraffins	36
CHAPTER III EXPERIMENTS	38
3.1 Instruments and Apparatus	38
3.2 Chemicals and Gases	40
3.3 Preparation Methods of Zeolite Beta	41
3.4 Preparation of Zeolite Beta with Ultrasound Irradiation	43
3.5 Preparation of Zeolite Beta with Various Crystallization Time	43
3.6 Preparation of Zeolite Beta with Various Si/Al Ratios	43
3.7 Removal of Organic Template from the Zeolite Beta Catalysts	44
3.8 Elemental Analysis	45
3.9 Activity of Various Zeolite Beta Catalysts in PP Cracking	45
3.9.1 Effect of Crystallization Time	45
3.9.2 Effect of Si/Al Ratios in Catalyst	46
3.9.3 Effect of Temperature	47
3.9.4 Effect of Polypropylene to Catalyst Ratio	47
3.10 Activity of Various Zeolite Beta Catalysts in HDPE Cracking	47
3.10.1 Effect of Si/Al Ratios in Catalyst	47
3.10.2 Effect of Temperature	47
3.10.3 Effect of HDPE to Catalyst Ratio	47
3.11 Catalyst Regeneration	50
CHAPTER IV RESULTS AND DISCUSSIONS	51
4.1 Effect of Ultrasound Irradiation Period on Formation of Zeolite Beta	51
4.1.1 XRD Results	51
4.1.2 SEM Images	54
4.1.3 Nitrogen Adsorption-Desorption	56
4.2 Effect of Crystallization Time on Formation of Zeolite Beta	58
4.2.1 XRD Results	58
4.2.2 SEM Images	64
4.2.3 Nitrogen Adsorption-Desorption	67

LIST OF TABLES

Table	Page
1.1 Two Basic Types of Plastics.....	2
1.2 Commodity Plastics and Their Uses.....	3
2.1 Features of adsorption isotherms.....	22
2.2 IUPAC classification of pores.....	23
3.1 Required amounts of aluminum isopropoxide in the preparation of zeolite beta samples with various Si/Al ratios in gel of 10, 20, 40, 60 and 80.....	44
4.1 Textural properties of calcined zeolite beta samples.....	57
4.2 Textural properties of calcined zeolite beta samples synthesized without ultrasound irradiation.....	70
4.3 Textural properties of calcined zeolite beta samples synthesized with ultrasound irradiation.....	70
4.4 Comparison of calcined zeolite beta samples with different Si/Al ratios.....	73
4.5 Comparison of O_h/T_d ratios in the calcined zeolite beta samples with different Si/Al ratios.....	79
4.6 Textural properties of calcined zeolite beta with various Si/Al ratios.....	84
4.7 Acidity of calcined zeolite beta catalysts prepared without ultrasound irradiation and the samples prepared by the ultrasound irradiation method with various Si/Al ratios.....	87
4.8 Values of %conversion and %yield obtained by thermal cracking and catalytic cracking of PP over Beta60 and Beta60-US30 samples crystallized for various periods at 380°C.....	88
4.9 Values of %conversion and %yield obtained by catalytic cracking of PP over normal zeolite beta catalysts with various Si/Al ratios.....	93
4.10 Values of %conversion and %yield obtained by catalytic cracking of PP over Beta-US30-24h catalysts with various Si/Al ratios.....	93
4.11 Values of %conversion and %yield obtained by thermal cracking and catalytic cracking of PP over Beta20-US30-24h catalysts at different temperature.....	98

Table	Page
4.12 Conversion and product yield obtained by catalytic cracking of PP over Beta20-US30-24h catalysts with different catalyst amounts at 380°C.....	102
4.13 Values of %conversion and %yield obtained by catalytic cracking of PP using the fresh and the regenerated catalyst.....	107
4.14 Values of %conversion and %yield obtained by thermal cracking and catalytic cracking of HDPE over normal zeolite beta catalysts with various Si/Al ratios.....	111
4.15 Values of %conversion and %yield obtained by thermal cracking and catalytic cracking of HDPE over zeolite beta prepared by ultrasound irradiation method and with various Si/Al ratios.....	112
4.16 Values of %conversion and %yield obtained by thermal cracking and catalytic cracking of HDPE over Beta20-US30-24h at 380°C and 400°C.....	117
4.17 Conversion and product yield obtained by catalytic cracking of HDPE over Beta20-US30-24h catalysts with different catalyst amounts at 400°C	121
4.18 Values of %conversion and yield obtained by catalytic cracking of HDPE using the fresh and the regenerated catalyst	126
4.19 Textural properties of calcined zeolite beta, ZSM-5 and Fe-MFI catalysts.....	130
4.20 Values of %conversion and yield obtained by catalytic cracking of HDPE over zeolite beta, ZSM-5 and Fe-MFI catalysts	131

LIST OF FIGURES

Figure	Page
1.1 World major Thermoplastics 2005 demand	4
2.1 The structure of zeolites.....	11
2.2 A primary building unit of zeolites.....	12
2.3 Secondary building units (SBU) in zeolites structures.....	13
2.4 The structure of sodalite, zeolite A and faujasite-type zeolites.....	14
2.5 Examples of the three types of pore openings in the zeolite molecular sieves.....	14
2.6 The generation of Brønsted and Lewis acid sites in zeolite.....	15
2.7 Three types of selectivity in zeolites: reactant, product and transition-state shape selectivity	16
2.8 Zeolite beta polymorphs.....	18
2.9 Diffraction of X-ray by regular planes of atoms.....	19
2.10 Simulated powder patterns of materials with stacking disorder in the zeolite beta family.....	20
2.11 Scanning electron micrograph of a zeolite beta sample	21
2.12 The IUPAC classification of adsorption isotherm.....	22
2.13 SEM images of the zeolite A samples obtained at 50°C (A) after 13 h of synthesis in the absence of ultrasound, and (B) after 10 h of synthesis in the presence of ultrasound.....	27
2.14 Diagram of a typical sonochemical apparatus.....	28
2.15 Distilling crude and product disposition.....	29
2.16 Cracking mechanisms illustrated by the reaction of n-heptene.....	32
2.17 Monomolecular cracking mechanisms.....	34
2.18 Bimolecular cracking mechanism.....	35
3.1 Apparatus for catalytic cracking.....	48
3.2 Apparatus for vacuum distillation.....	49
4.1 XRD patterns of the as-synthesized zeolite beta samples, (A) prepared without ultrasound irradiation; (B), (C), (D), and (E) synthesized with ultrasound irradiation for 30, 60, 90, and 120 min, respectively.....	52

Figure	Page
4.2 XRD patterns of the calcined zeolite beta samples, (A) prepared without ultrasound irradiation; (B), (C), (D), and (E) synthesized with ultrasound irradiation for 30, 60, 90, and 120 min, respectively	53
4.3 SEM images of calcined zeolite beta synthesized without and with ultrasound irradiation for various periods: (A) Beta60, (B) Beta60 with magnification of x 50,000 (C) Beta60-US30 (D) Beta60-US60 (E) Beta60-US90 and (F) Beta60-US120	55
4.4 N ₂ adsorption-desorption isotherms of zeolite beta samples prepared without and with the application of ultrasound irradiation in the gel formation step for various periods	57
4.5 MP plots for pore-size distribution of zeolite beta samples	58
4.6 XRD patterns of the as-synthesized zeolite beta samples prepared with ultrasound irradiation and crystallized for various periods: (A) 8 h; (B) 12 h; (C) 16 h; (D) 20 h; (E) 24 h; (F) 48 h; (G) 72 h; and (H) 96 h.	59
4.7 XRD patterns of the as-synthesized zeolite beta samples prepared without ultrasound irradiation and crystallized for various periods: (A) 8 h; (B) 12 h; (C) 16 h; (D) 20 h; (E) 24 h; (F) 48 h; (G) 72 h; and (H) 96 h.	60
4.8 XRD patterns of the calcined zeolite beta samples synthesized with ultrasound irradiation and crystallized for various periods: (A) 8 h; (B) 12 h; (C) 16 h; (D) 20 h; (E) 24 h; (F) 48 h; (G) 72 h; and (H) 96 h.	62
4.9 XRD patterns of the calcined zeolite beta samples synthesized without ultrasound irradiation and crystallized for various periods: (A) 8 h; (B) 12 h; (C) 16 h; (D) 20 h; (E) 24 h; (F) 48 h; (G) 72 h; and (H) 96 h.	63
4.10 SEM images of (A) xerogel and (B-H) Beta60 samples crystallized at 135°C for various periods: (B) 12 h; (C) 16 h; (D) 20 h; (E) 24 h; (F) 48 h; (G) 72 h and (H) 96 h	65
4.11 SEM images of (A) xerogel and (B-H) Beta60-US30 samples crystallized at 135°C for various periods: (B) 12 h; (C) 16 h; (D) 20 h; (E) 24 h; (F) 48 h; (G) 72 h and (H) 96 h	66
4.12 N ₂ adsorption-desorption isotherms of calcined zeolite beta prepared without ultrasound irradiation: (A) silica xerogel and samples crystallized for 16 and 20 h, (B) samples crystallized for 24 - 96 h	68

Figure	Page
4.13 N ₂ adsorption-desorption isotherms of calcined zeolite beta prepared with the application of ultrasound irradiation and with various periods of crystallization: (A) silica xerogel and samples crystallized for 16 and 24 h, (B) samples crystallized for 48 - 96 h.....	69
4.14 BJH pore-size distributions of silica xerogel.....	71
4.15 MP pore-size distributions of zeolite beta samples synthesized without ultrasound irradiation and with various periods of crystallization.....	72
4.16 MP pore-size distributions of zeolite beta samples synthesized with ultrasound irradiation and with various periods of crystallization.....	72
4.17 XRD patterns of calcined zeolite beta catalysts prepared without ultrasound irradiation and with different Si/Al ratios in gel: (A) 10; (B) 20; (C) 40; (D) 60; and (E) 80.....	75
4.18 XRD patterns of calcined samples synthesized by ultrasound irradiation method with different Si/Al ratios in gel: (A) 10; (B) 20; (C) 40; (D) 60; and (E) 80.....	76
4.19 ²⁷ Al-MAS-NMR spectra of calcined zeolite beta catalysts prepared without ultrasound irradiation and with different Si/Al ratios in catalyst (A) 15.0; (B) 23.6; (C) 27.7 and (D) 27.6.....	78
4.20 ²⁷ Al-MAS-NMR spectra of zeolite beta samples synthesized by ultrasound irradiation method and with different Si/Al ratios in catalyst (A) 11.6; (B) 22.9; (C) 28.2 and (D) 26.9.....	79
4.21 SEM images of calcined zeolite beta samples prepared with and without application of ultrasound radiation and with different Si/Al ratios.....	81
4.22 N ₂ adsorption-desorption isotherms of zeolite beta catalysts prepared without ultrasound irradiation and with various Si/Al ratios in catalyst.....	82
4.23 N ₂ adsorption-desorption isotherms of zeolite beta samples synthesized by ultrasound irradiation method with different Si/Al ratios in catalyst.....	83
4.24 MP plots for pore size distribution of calcined zeolite beta samples prepared without ultrasound irradiation and with different Si/Al ratios.....	83
4.25 MP plots for pore size distribution of calcined zeolite beta samples synthesized by ultrasound irradiation method and with different Si/Al ratios.....	84

Figure	Page
4.26 NH ₃ -TPD profiles of of zeolite beta catalysts prepared without ultrasound irradiation and with various Si/Al ratios in catalyst of (A) 15.0; (B) 23.6; (C) 27.7 and (D) 27.6.....	86
4.27 NH ₃ -TPD profiles of zeolite beta samples synthesized by ultrasound irradiation method with different Si/Al ratios in catalyst (A) 11.6; (B) 22.9; (C) 28.2 and (D) 26.9.....	86
4.28 Accumulative volume of liquid fractions obtained by catalytic cracking of PP over Beta60 samples crystallized for various time at 380°C.....	89
4.29 Distribution of gas fraction obtained by the thermal cracking and catalytic cracking of PP over Beta60 samples crystallized for various time at 380°C.....	90
4.30 Carbon number distribution of liquid fractions from thermal cracking and catalytic cracking of PP over Beta60 samples crystallized for various time at 380°C.....	91
4.31 Accumulative volume of liquid fractions from catalytic cracking of PP over various zeolite beta catalysts with different Si/Al ratios at 350°C.....	94
4.32 Distribution of gas fraction obtained by catalytic cracking of PP over Beta-24h catalysts with various Si/Al ratios at 350°C.....	95
4.33 Distribution of gas fraction obtained by catalytic cracking of PP over various Beta-US30-24h catalysts with different Si/Al ratios at 350°C.....	95
4.34 Carbon number distribution of distillate oil obtained by catalytic cracking of PP over Beta-US30-24h catalysts with various Si/Al ratios at 350°C.....	96
4.35 Carbon number distribution of distillate oil obtained by catalytic cracking of PP waste over Beta-24h catalysts with various Si/Al ratios at 350°C.....	97
4.36 Carbon number distribution of commercial SUPELCO standard gasoline fraction.....	97
4.37 Accumulative volume of liquid fractions from catalytic cracking of PP over Beta20-US30-24h catalysts at different temperature.....	99
4.38 Distribution of gas fraction obtained by catalytic cracking of PP over Beta20-US30-24h catalysts at different temperature.....	100
4.39 Carbon number distribution of distillate oil obtained by catalytic cracking of PP over Beta20-US30-24h catalysts at different temperature.....	101

Figure	Page
4.40 Accumulative volume of liquid fractions from catalytic cracking of PP over Beta20-US30-24h catalysts with different catalyst amounts at 380°C	103
4.41 Distribution of gas fraction obtained by catalytic cracking of PP over Beta20-US30-24h catalysts with different catalyst amounts at 380°C.....	104
4.42 Carbon number distribution of distillate oil obtained by catalytic cracking of PP over Beta20-US30-24h catalysts with different catalyst amounts at 380°C.....	104
4.43 XRD patterns of (A) the calcined unused (B) the 1 st regenerated Beta20-US30-24h and (C) the 2 nd regenerated Beta20-US30-24h catalysts	105
4.44 SEM images of the 3 rd regenerated Beta20-US30-24h sample with different magnification (A) x20,000 and (B) x50,000 times.....	106
4.45 N ₂ adsorption-desorption isotherms of the fresh and the regenerated Beta20-US30-24h sample.....	106
4.46 Accumulative volume of liquid fraction obtained by catalytic cracking of PP using the fresh and the regenerated Beta20-US30-24h catalysts	108
4.47 Distribution of gas fraction obtained by catalytic cracking of PP using the fresh and the regenerated Beta20-US30-24h catalysts.....	109
4.48 Carbon number distributions of liquid fraction obtained by catalytic cracking of PP using the fresh and the regenerated Beta20-US30-24h catalysts	109
4.49 Accumulative volume of liquid fraction obtained by catalytic cracking of HDPE using zeolite beta with different Si/Al ratio	113
4.50 Accumulative volume of liquid fraction obtained by catalytic cracking of HDPE using zeolite beta prepared by ultrasound method with different Si/Al ratios	113
4.51 Distribution of gas fraction obtained by thermal cracking and catalytic cracking of HDPE using normal zeolite beta with various Si/Al ratios.....	114
4.52 Distribution of gas fraction obtained by thermal cracking and catalytic cracking of HDPE using zeolite beta synthesized by ultrasound method with different Si/Al ratios	114

Figure	Page
4.53 Carbon number distribution of liquid fraction from catalytic cracking of HDPE over normal zeolite beta with various Si/Al ratios	116
4.54 Carbon number distribution of liquid fraction from catalytic cracking of HDPE over zeolite beta synthesized by ultrasound irradiation method with various Si/Al ratios	116
4.55 Accumulative volume of liquid fraction obtained by catalytic cracking of HDPE using Beta20-US30-24h at 380°C and 400°C	118
4.56 Distribution of gas fraction obtained by thermal cracking and catalytic cracking of HDPE using Beta20-US30-24h at 380°C and 400°C	119
4.57 Carbon number distribution of liquid fraction from catalytic cracking of HDPE over Beta20-US30-24h at 380°C and 400°C	120
4.58 Accumulative volume of liquid fractions from catalytic cracking of HDPE over Beta20-US30-24h catalysts with different catalyst amounts at 400°C	122
4.59 Distribution of gas fraction obtained by catalytic cracking of HDPE over Beta20-US30-24h catalyst with different catalyst amounts at 400°C	123
4.60 Carbon number distribution of distillate oil obtained by catalytic cracking of HDPE over Beta20-US30-24h catalysts with different catalyst amounts at 400°C	123
4.61 XRD patterns of (A) the calcined unused (B) the 1 st regenerated Beta20-US30-24h and (C) the 2 nd regenerated Beta20-US30-24h catalysts	124
4.62 SEM images of the 3 rd regenerated Beta20-US30-24h sample with different magnification (A) x20,000 and (B) x50,000 times	125
4.63 N ₂ adsorption-desorption isotherms of the fresh and the regenerated Beta20-US30-24h sample	125
4.64 Accumulative volume of liquid fraction obtained by catalytic cracking of HDPE waste using the fresh and the regenerated Beta20-US30-24h catalyst	127
4.65 Distribution of gas fraction obtained by catalytic cracking of HDPE using the fresh and the regenerated Beta20-US30-24h catalyst	128
4.66 Carbon number distributions of liquid fraction obtained by catalytic cracking of HDPE using the fresh and the regenerated Beta20-US30-24h catalyst	129

Figure	Page
4.67 Distribution of gas fraction obtained by catalytic cracking of HDPE over zeolite beta, ZSM-5 and Fe-MFI catalysts.....	132
4.68 Carbon number distributions of liquid fraction obtained by catalytic cracking of HDPE over zeolite beta, ZSM-5 and Fe-MFI catalysts.....	133
A-1 Gas chromatogram of standard mixture gas.....	145
A-2 Gas chromatogram of gas product obtained from catalytic cracking of PP waste over Beta20-US30-24h at 400°C.....	146
A-3 Gas chromatogram of standard gasoline (SUPELCO).....	147
A-4 Liquid chromatogram of liquid product obtained from catalytic cracking of PP waste over Beta20-US30-24h at 400°C.....	148
A-5 XRD pattern of plastic waste. Insert shows the XRD patterns for HDPE.....	149
A-6 XRD pattern of plastic waste. Insert shows the XRD patterns for PP.....	149

LIST OF SCHEMES

Scheme	Page
3.1 The GC heating program for gas analysis	40
3.2 The GC heating program for liquid analysis	40
3.3 Diagram of the synthesis procedure of zeolite beta	42
3.4 A heating program for removal of organic template from the pores of zeolite beta	44
3.5 Catalytic cracking of HDPE and PP using zeolite beta as catalyst	49



ศูนย์วิทยทรัพยากร
จุฬาลงกรณ์มหาวิทยาลัย

LIST OF ABBREVIATIONS

BET	Brunauer- Emmett-Teller
BJH	Barret, Joyner, and Halenda
°C	degree Celsius
cps	counts per second
g	gram (s)
GC	Gas Chromatography
h	hour (s)
HDPE	High density polyethylene
ICP-AES	Inductively Coupled plasma-Atomic Emission Spectrometer
M	molar
MAS-NMR	Magic-angle-spinning-nuclear magnetic resonance
mg	milligram (s)
min	minute (s)
PP	Polyethylene
ppm	part per million or mg/l
SEM	Scanning Electron Microscopy
TEAOH	Tetraethylammoniumhydroxide
TPD	Temperature-Programmed Desorption
XRD	X-ray Diffraction
%	percent

ศูนย์วิทยทรัพยากร
จุฬาลงกรณ์มหาวิทยาลัย

CHAPTER I

INTRODUCTION

In recent years, Plastics have become the material of choice for wide-ranging applications: household, agriculture, construction, packaging, etc. The world's plastics consumption has increased rapidly from around 5 million tones in the 1950s to nearly 170 million tones today. Packaging is the largest single sector of plastics use in the UK [1]. It is not without reason that plastics have experienced such rapid development. Plastics are materials with extremely wide spectrum of possibilities. Their properties can be summarized briefly as follows [1, 2]:

- Plastics are light. Their density varies between 0.8 and 2.2 g/cm³. They are thus lighter than metal and ceramics, reducing fuel consumption during transportation.
- Plastics have high chemical, water and impact resistance.
- Plastics are often transparent and can be colored as desired.
- Plastics are excellent thermal and electrical insulators.
- Plastics exhibit a wide, variable spectrum of mechanical properties. They can be soft and elastic as well as hard and rigid.
- Plastics are extreme durability.
- Plastics are good safety and hygiene properties for food packaging.
- Plastics are relatively inexpensive to produce
- Plastics can be reused and recycled by means of a number of different methods.

จุฬาลงกรณ์มหาวิทยาลัย

Plastics can be classified as thermoplastic and thermosetting resins (Table 1.1). Thermoplastics make up 80% of the plastics produced today, while thermosets make up the remaining 20% of plastics produced [3].








Table 1.1 Two Basic Types of Plastics [4]

Thermoplastics resins	Thermosetting resins
Softens when exposed to heat & return to the original condition when cooled.	Becomes permanently hard and rigid when heated and cannot be softened by reheating
Can be shaped by extrusion or molding processes	More rigid and can crack/chip on impact
Are recyclable and can be transparent	Not recyclable and transparent
Examples: polyvinylchloride (PVC), polypropylene (PP), polyethylene (PE), polyethylene terephthalate (PET), polystyrene (PS), etc	Examples: polyesters, polyurethane (PU), melamine etc.

Most consumers recognize the types of plastics by the numerical coding system created by the American Society of Plastics Industry in the late 1980s. There are six different types of plastic resins that are commonly used to package household products. The identification codes listed below can be found on the bottom of most plastic packaging [5]. These types and their most common uses are shown in Table 1.2.

ศูนย์วิทยทรัพยากร
จุฬาลงกรณ์มหาวิทยาลัย

Table 1.2 Commodity Plastics and Their Uses [1]

Type	Abbreviation	Major Uses
	PET	Polyethylene terephthalate - Fizzy drink bottles and oven-ready meal trays.
	HDPE	High-density polyethylene - Bottles for milk and washing-up liquids.
	PVC	Polyvinyl chloride - Food trays, cling film, bottles for squash, mineral water and shampoo.
	LDPE	Low density polyethylene - Carrier bags and bin liners.
	PP	Polypropylene - Margarine tubs, microwaveable meal trays.
	PS	Polystyrene - Yoghurt pots, foam meat or fish trays, hamburger boxes and egg cartons, vending cups, plastic cutlery, protective packaging for electronic goods and toys.
	OTHER	Any other plastics that do not fall into any of the above categories. - An example is melamine, which is often used in plastic plates and cups.

Chemical Market Associates, Inc. (CMAI), a Houston-based global chemicals and plastics consulting firm, estimates that in 2005, nearly 165 million metric tons of commodity plastics were consumed worldwide. An average weight composition of the different type of plastics present in Western Europe is shown in Figure 1.1.

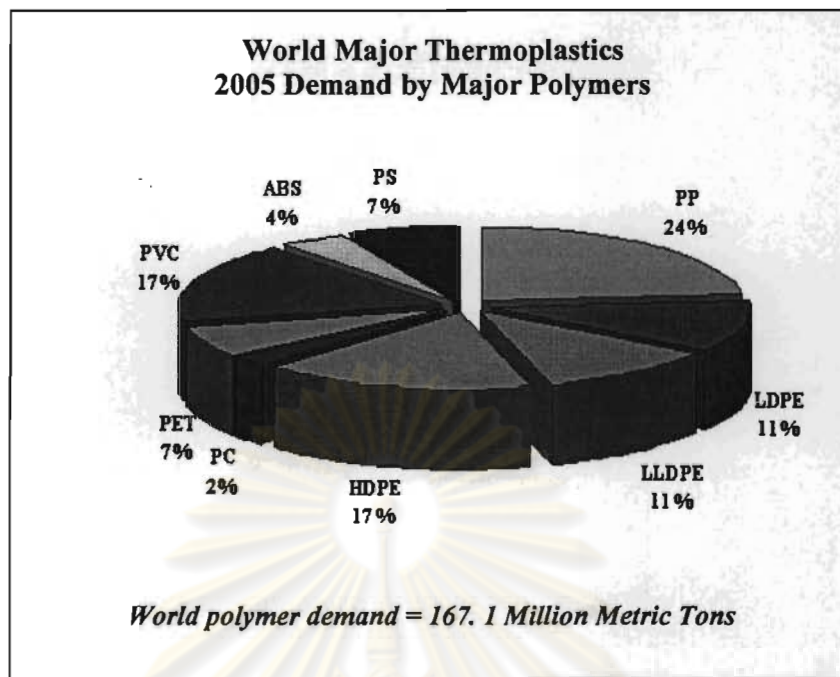


Figure 1.1 World major Thermoplastics 2005 demand (CMAI) [6]

Demand for Global Thermoplastics is dominated by Polyolefins (PP & PE). They represent over 63 % of all the commodity resins consumed on an annual basis. PP represents the single largest category at 24 %. PE is the largest category including LDPE, LLDPE & HDPE. Polyethylene can be found in the market in several grades [7, 8]:

1. Low density polyethylene (LDPE) is an ethylene homopolymer produced in a high pressure uncatalyzed process, which contains long and short branches; these branches in LDPE prevent a good packing of polymer molecules and in consequence the polymer melts at low temperatures.

2. High density polyethylene (HDPE) was firstly obtained in 1958 by the use of Phillips and Ziegler-Natta catalysts. This grade, which consists in unbranched polyethylene molecular chains, has a higher melting temperature, but also a higher fragility.

3. Linear low density polyethylene (LLDPE) was produced in the 1980s by copolymerization of ethylene with other olefins like 1-hexene. Thus, a great quantity of short branches was added to the main polyethylene chain, achieving intermediate properties between HDPE and LDPE.

The disposal of plastics products also contributes significantly to their environmental impact because most plastics are non-degradable. There are many alternatives to manage plastic waste such as landfill, recycling, and incineration; however, each of these methods has disadvantages. Landfill treatment of plastic waste is less desirable due to high cost, poor biodegradability and the possibility of unacceptable emission [9, 10]. Incineration of plastic waste finds strong social rejection because of possible atmospheric contamination. Recycling is a popular recovery path but recycled plastic product often costs more than virgin plastic. In 2006, only about 3.5% of all plastics generated are recycled compared to 34% of paper, 22% of glass and 30% of metals. At this time, plastics recycling only minimally reduce the amount of virgin resources used to make plastics. Recycling papers, glass and metal, materials that are easily recycled more than once, saves far more energy and resources than are saved with plastics recycling [5].

Recycling process is divided into two groups: mechanical recycling and chemical recycling. Mechanical recycling involves the melting and re-moulding of used thermoplastics for the production of low grade products. Chemical recycling embraces a variety of processes designed to convert plastic waste into petrochemical feedstock for use in the production of refined chemicals or fuels [11].

An alternative strategy is chemical recycling, which has attracted much interest recently with the aim of converting waste polymers into basic petrochemicals to be used as feedstock or fuel for a variety of downstream processes. Two main chemical recycling routes are the thermal and catalytic degradation of waste plastic [12].

1. Thermal degradation requires high operating temperature, typically more than 500°C and even up to 900°C, and proceeds with low yields into the corresponding raw monomers [13, 14]. Moreover, thermal conversion of PE and PP leads to a wide product distribution with poor economical value, which should be further upgraded [15].

2. Catalytic degradation of plastic waste is a method to obtain valuable products from polymers [16]. Catalytic cracking have several advantages over a purely thermal process. First, catalysts promote the degradation reaction to occur at lower temperature, with implies lower energy consumptions. Second and most importantly, the shape selectivity exhibited by certain catalysts allows the formation

of a narrower distribution of products, which may be directed towards light and aromatic hydrocarbons with higher market values [11].

Since catalytic technology is the key technology for petroleum refining and petrochemical processing and catalyst is the core of catalytic technology, the development of new catalysts would have a great impact on petroleum refining and petrochemical industry [17]. A number of authors have reported promising results on the cracking of polyolefins over several acid catalysts like zeolites, clay, and mesostructured materials [18-21]. Differences in the catalytic activities of these solids have usually been related to their acid properties, the strength and number of acid sites [11]. Zeolite beta is one of the most attractive zeolite because of the three-dimensional large-pore channel system, large available micropore volume, and the presence of active sites in different concentrations that are useful in a number of acid-catalyzed reactions [22]. Several works have been published using zeolite beta as solid-acid catalysts for catalytic cracking [23-30]. Some of the studies reported in the literature will be reviewed below.

R. Nakao *et al.* [23] studied activity of homemade BEA zeolite prepared by a hydrothermal synthesis method (BEA(HTS)) in catalytic cracking of hydrocarbons compared with commercial BEA zeolites. The results showed that homemade BEA had more Brønsted acid sites than commercial BEA zeolites, and exhibited much higher activity in catalytic cracking of hydrocarbons, especially *n*-heptane. The initial activity of BEA(HTS) was about three times as high as that of HZSM-5. In addition, BEA (HTS) gave high *n*-heptane conversion even after the regeneration treatment.

L. Bonetto *et al.* [24] studied zeolite beta catalysts with different crystal sized in catalytic cracking of gas-oil. The sample with an average crystal size of 0.4 μm showed an optimum compromise between stability, activity and selectivity. This sample, before and after steaming, gave a slightly lower selectivity to gasoline than a high and a low unit cell size USY zeolite, respectively. The optimum zeolite beta produced more liquefied petroleum gas alkenes that were useful for alkylation gasoline production. Zeolite beta with the same Si/Al ratio, but with crystal size in a narrow distribution countered at ca. 0.17, 0.40 and 0.70 μm were used in order to study the stability. The result showed that the stability of zeolite beta slightly increased with increasing crystal size.

G. Manos *et al.* [25] explored the catalytic cracking of HDPE over ultrastable Y, Y, β zeolites, mordenite and ZSM-5 at 360°C. The structure of the zeolite framework has shown a significant influence on the product distribution. Over large-pore USY, Y and β zeolites, alkanes were the main products with less amounts of alkenes and aromatics and only very small amounts of cycloalkanes and cycloalkenes. Medium-pore mordenite and ZSM-5 gave alkenes as major products. The hydrocarbons formed with medium-pore zeolites were lighter than those formed with large-pore zeolites. A similar order was found regarding the bond saturation:

(more alkenes) ZSM-5 < mordenite < β < Y < USY (more alkanes)

D.P. Serrano *et al.* [26] reported the catalytic cracking of polyolefin mixture consisting of 46.5 wt% LDPE, 25 wt% HDPE and 28.5 wt% PP at 400°C over a variety of acid solids as catalysts. The activity order was found as follow:

n-HZSM-5 > H-beta > HMCM-41 >> SiO₂-Al₂O₃ > HZSM-5 > HY > thermal degradation

The activity order found for the different catalysts was related to their respective properties and the nature of the polyolefin mixture. Zeolite beta leads to a high conversion because the presence of a high external surface area enhances its cracking activity. The external acid sites are not sterically hindered for the conversion of the bulky polyolefin molecules. Significant differences are observed in the product distribution: n-HZSM-5 shows the highest selectivity toward C₁₋₄ (50 wt %), H-beta leads mainly to liquid hydrocarbon C₅₋₁₂ (60 wt %), whereas HMCM-41 yields both C₅₋₁₂ (54 wt %) and C₁₃₋₃₀ (32 wt %) fractions. Regarding the selectivity by carbon atom number, in all cases C₄ fraction was the major products, although its value changes widely depending on the catalyst.

A. Marcilla *et al.* [27, 28] studied the effect of the addition of a nanocrystalline H-beta zeolite in the pyrolysis of a commercial LDPE using dynamic conditions in a thermobalance and in a batch reactor. The results have been compared with those obtained using a HZSM-5 zeolite. The results presented the great catalytic effect of H-Beta, with an important influence over the decomposition of the polymer even at very low zeolite concentration. Although this mixture had a saturating effect at a certain concentration of catalyst (around 7%), a remarkable effect in the first steps of LDPE decomposition as increasing the catalyst loading has been observed, which has been attributed to the external acid sites presents in the nanocrystalline zeolite. The HZSM-5 zeolite produced a gas richer in C₃ compounds than H-beta zeolite,

whereas the gas obtained in the catalytic cracking of LDPE with H-beta produced a gas richer in $C_4 + C_5$ than HZSM-5. The H-beta zeolite permits to obtain a gas with an elevated weight fraction of isobutane as compared with the HZSM-5 zeolite. This different behaviour can be explained by the different pore structure: the higher the pore size, the higher the isobutane/*n*-butane ratio.

J. Aguado *et al.* [29] have investigated and compared the behavior of six acid solids of varying acid and textural characteristics for their catalytic activity in the degradation of LDPE, HDPE, and two plastics of recycled polyethylene of urban and agricultural origins using thermogravimetric and differential thermal analysis. The catalysts used in this work were three zeolitic materials (standard ZSM-5, nanocrystalline *n*-ZSM-5 and Beta) and three mesostructured solids (sol-gel Al-MCM-41 (sg), hydrothermal Al-MCM-41 (hy) and Al-SBA-15). The catalytic activity of each acid solid has been related to its capacity to shift the degradation reaction to lower temperatures. Despite showing strong acid properties, standard ZSM-5 zeolite exhibited a very low catalytic activity on most plastics, which was attributed to diffusional impediments that affected the access of the bulky polymer molecules to its internal active sites. These impediments were partly overcome in the case of Beta zeolite and even more markedly with nanocrystalline *n*-ZSM-5, which exhibited the strongest catalytic activity due to a combination of strong acid properties and large external surface area. Owing to their non-crystalline nature, mesostructured solids showed weaker acid properties than their zeolitic counterparts. However, this disadvantage was partly compensated by the presence of larger pores that reduced diffusional hindrances. Thus, Al-MCM-41 (hy) exhibited one of the highest catalytic activities, largely surpassing the performance of crystalline solids with stronger acid properties. The catalytic activity of all the acid solids tested in this work was significantly reduced when they were used on waste plastics. This deactivating effect was more notable in mesostructured solids.

Recently, Y. J. Lee *et al.* [30] reported the influence of nanocrystalline H-Beta zeolite in liquid-phase degradation of high-density polyethylene at 380 °C. Nanocrystalline H-Beta zeolite with a crystallite size of about 10 nm and low Si/Al ratio (10.7) was found to be an efficient catalyst in the liquid-phase degradation of HDPE, producing a large amount of liquid products (80%) with high selectivities for C7 - C12 hydrocarbons that are suitable as fuels. HDPE of 10 g could be completely

converted to lower hydrocarbons even with 0.03 g of the nanocrystalline H-Beta zeolite at 380 °C. Both the crystallite size and acidity of H-Beta zeolites are important factors influencing their catalytic activity and product distribution. The high activity and high liquids yield of nanocrystalline Beta zeolites can be rationalized by considering the rapid cracking of HDPE over the strong acid sites on the external surface and fast mass transfer of cracked fragments in the pores of nanocrystalline H-Beta zeolite. The decreased intracrystalline residence time of cracked fragments leads to less cracking reactions, resulting in high liquid products yield.

As previously reported, zeolite beta has efficiency in the catalytic cracking of polyolefin. The interconnected large pore network, high surface area and strong acidity distribution of this catalyst allow plastic wastes to be degraded with high activity. The obtained products were controlled by pore size, acid strength, and particle size of the catalyst. The role of nanocrystalline catalysts in polyolefin cracking are very important because the increase of external surface area leads to the rapid primary cracking of HDPE over the strong acid sites on the external surface and fast mass transfer of cracked fragments in the pores of nanocrystalline zeolite, resulting in high liquid products yield. This work intends to synthesize nanosized zeolite beta catalyst and study the influence of ultrasound irradiation during the gel formation step on physico-chemical properties and use in catalytic cracking of high density polyethylene and polypropylene wastes. Moreover, different parameters: ultrasound irradiation periods, crystallization time and the Si/Al ratios in gel were also studied in comparison with zeolite beta prepared without ultrasound irradiation.

Objective

To study the influence of ultrasound irradiation during the gel formation step on physico-chemical and catalytic properties of zeolite beta.

Scopes of This Work

1. To synthesize zeolite beta catalyst and study the effect of ultrasound irradiation periods during gel formation step, crystallization time, and Si/Al ratios.
2. To investigate the efficiency and stability of zeolite beta for cracking of polypropylene and high density polyethylene wastes.
3. To study activity of regenerated zeolite beta catalyst.



ศูนย์วิทยทรัพยากร
จุฬาลงกรณ์มหาวิทยาลัย

CHAPTER II

THEORY

2.1 Zeolites

Zeolites are crystalline aluminosilicates that contain uniform pores and cavities with molecular dimensions. The structures of zeolites consist of an extensive three-dimensional network of SiO_4 and AlO_4 tetrahedral. The tetrahedral are cross-linked by the sharing of oxygen atoms as shown in Figure 2.1

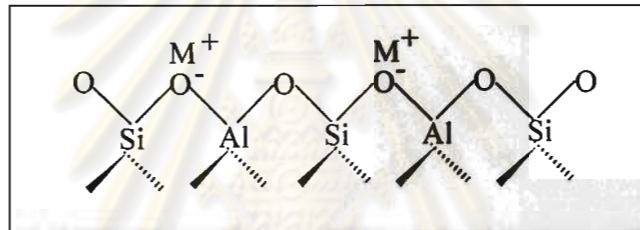
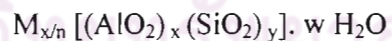


Figure 2.1 The structure of zeolites. [31]

The AlO_2^- tetrahedral in the structure determines the framework charge. This is balanced by cations that occupy nonframework positions. The structure formula of a zeolite is best expressed for the crystallographic unit cell as:



Where M is the cation of valence n, generally from the group I or II ions, although other metals, nonmetals, and organic cations are also possible, w is the number of water molecules. Water molecules presented are located in the channels and cavities, as the cations that neutralize the negative charge created by the presence of the AlO_2^- tetrahedral unit in the structure. The y/x usually has values of 1-5 depending upon the structure. The sum (x+y) is the total number of tetrahedral in the unit cell. The portion [] represents the framework composition.

The marvelous importance of zeolites and related materials in a variety of catalytic processes can be attributed to their superior properties in comparison with other types of materials. Some of their advantages are listed below:

1. Large surface area and adsorption capacity
2. The possibility of controlling the adsorption properties by tuning the hydrophobicity or hydrophilicity of the materials
3. The pore openings and cavities in the range of 5-12 Å
4. Insoluble materials and well defined pore structures
5. Different types, different properties
6. The presence of shape and size selectivities

2.1.1 Zeolite Structures [31]

The structure of zeolite consisted of a three-dimension framework of the tetrahedral primary building units when tetrahedral atoms are silicon or aluminum as shown in Figure 2.2

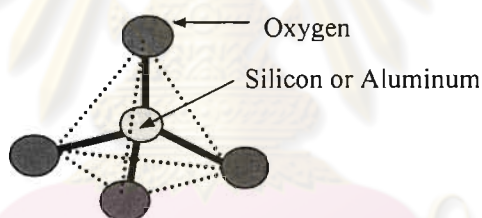


Figure 2.2 A primary building unit of zeolites.

Zeolites have a common subunit of structure so called primary building units of $(\text{Al,Si})\text{O}_4$ tetrahedral, therein the Si or Al distribution is neglected. A secondary building unit (SBU) consists of selected geometric groupings of those tetrahedral. There are sixteen such building units, which can be used to describe all of the known zeolite structures; for example, 4, 5, 6 and 8-member single rings, 4-4, 6-6, and 8-8-member double rings, and 4-1,5-1 and 4-4-1 branched rings. The secondary building units (SBU) are shown in Figure 2.3. Most zeolite framework can be generated from different SBU.

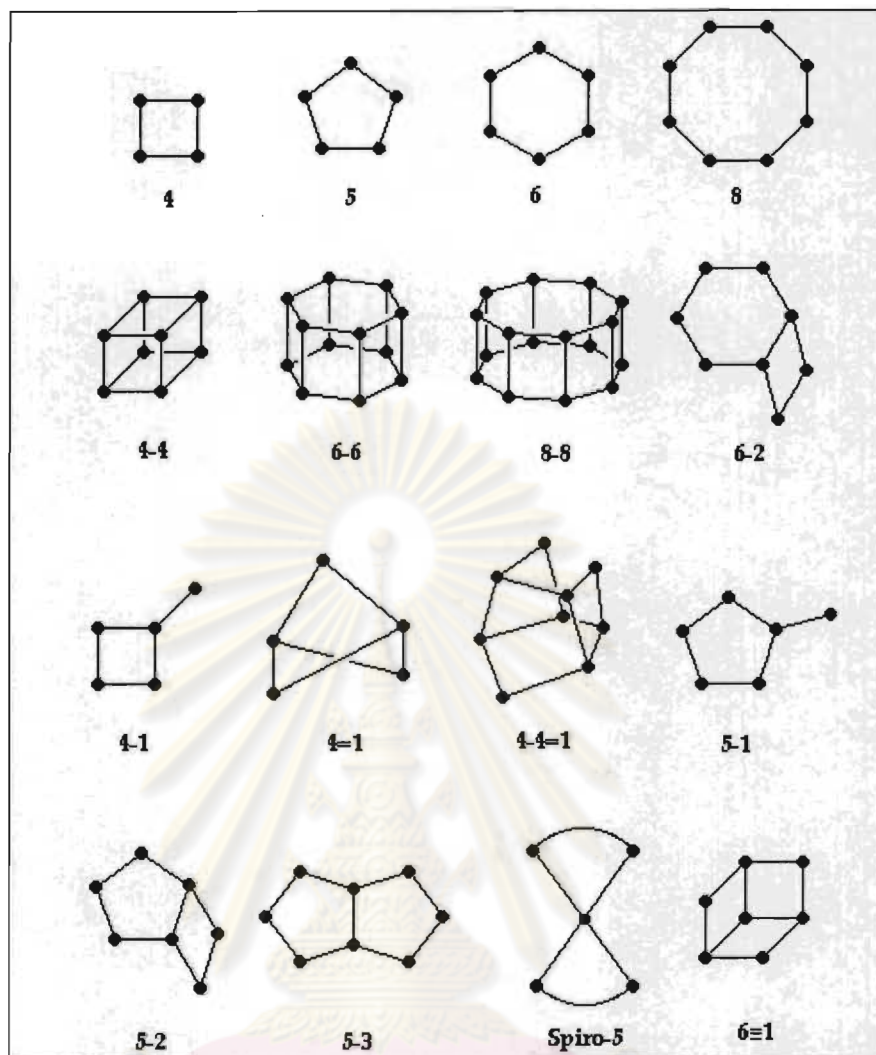


Figure 2.3 Secondary building units (SBU) in zeolites structures. [32]

Most zeolite frameworks can be generated from several different SBUs. For example, the sodalite framework can be built from either the single 6-member ring or the single 4-member ring. Some of them are shown in Figure 2.4

จุฬาลงกรณ์มหาวิทยาลัย

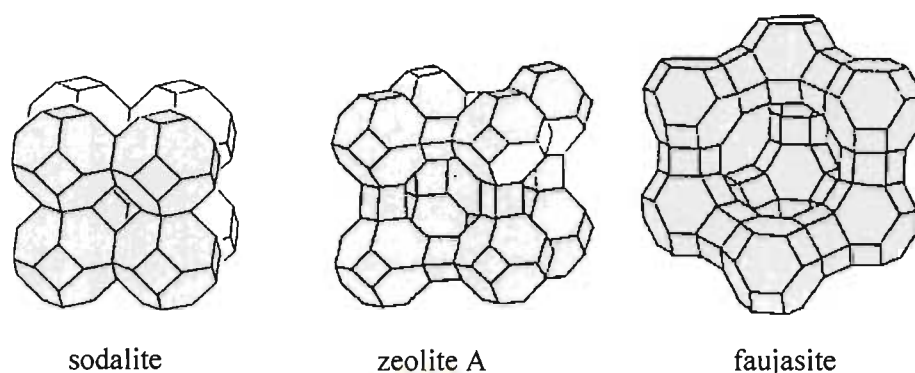


Figure 2.4 The structure of sodalite, zeolite A and faujasite-type zeolites [33]

The different ring sizes found in zeolites, based on the different number of tetrahedral atoms defining the opening, are shown in Figure 2.5. The ring sizes are often mentioned as the number of oxygen atoms which are equal to the number of tetrahedral atoms.

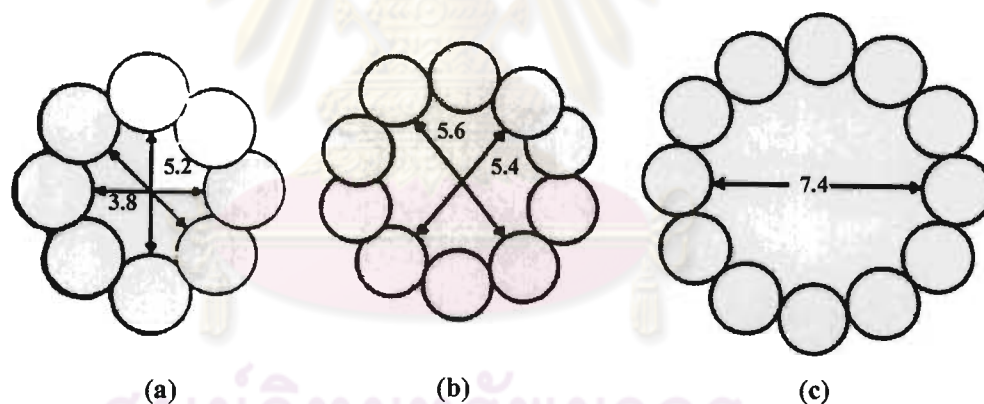


Figure 2.5 Examples of the three types of pore openings in the zeolite molecular sieves

- (a) an 8 ring pore opening (small pore)
- (b) a 10 ring pore opening (medium pore)
- (c) a 12 ring pore opening (large pore)

2.1.2 Acid Sites of Zeolites

Most industrial application of zeolites are based upon technology adapted from the acid silica/alumina catalysts originally developed for the cracking reaction [34-36]. This means that the activity required is based upon the production of Brønsted acid sites arising from the creating 'hydroxyls' within the zeolites pore structure. These hydroxyls are formed by ammonium exchange followed by a calcination step. Zeolites as normally synthesized usually have Na^+ balancing the framework charges, but these can be readily exchanged for protons by direct reaction with an acid, giving hydroxyl groups, the Brønsted acid sites. Alternatively, if the zeolite is not stable in acid solution, it is common to use the ammonium, NH_4^+ , salt, and then heat it so that ammonia is driven off, leaving a proton. Further heating removes water from Brønsted site, exposing a tricoordinated Al ion, which has electron-pair acceptor properties; this is identified as a Lewis acid site. A scheme for the formation of these sites is shown in Figure 2.6. The surfaces of zeolites can thus display either Brønsted or Lewis acid sites, or both, depending on how the zeolite is prepared. Brønsted sites are converted into Lewis sites as the temperature is increased above 500°C , and water is driven off.

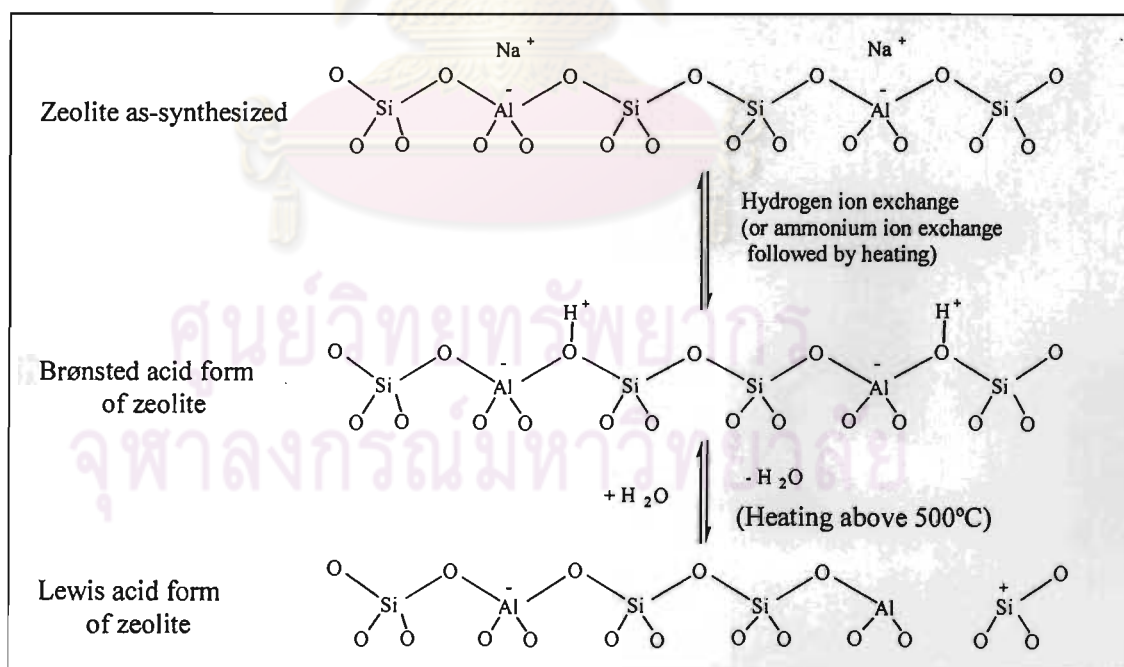


Figure 2.6 The generation of Brønsted and Lewis acid sites in zeolite [37].

2.1.3 Shape Selectivity

Shape selectivity plays a very important role in catalysis. Highly crystalline and regular channel structures are among the principal features that zeolite used as catalysts offer over other materials. Shape selectivity is divided into 3 types: reactant shape selectivity, product shape selectivity and transition-state shape selectivity. These types of selectivities are shown in Figure 2.7. Reactant shape selectivity results from the limited diffusivity of some reactants, which cannot effectively enter and diffuse inside the zeolites. Product shape selectivity occurs when diffusing product molecules cannot rapidly escape from the crystal, and undergo secondary reactions. Restricted transition-state shape selectivity is a kinetic effect arising from the local environment around the active site: the rate constant for a certain reaction mechanism is reduced if the necessary transition state is too bulky to form readily.

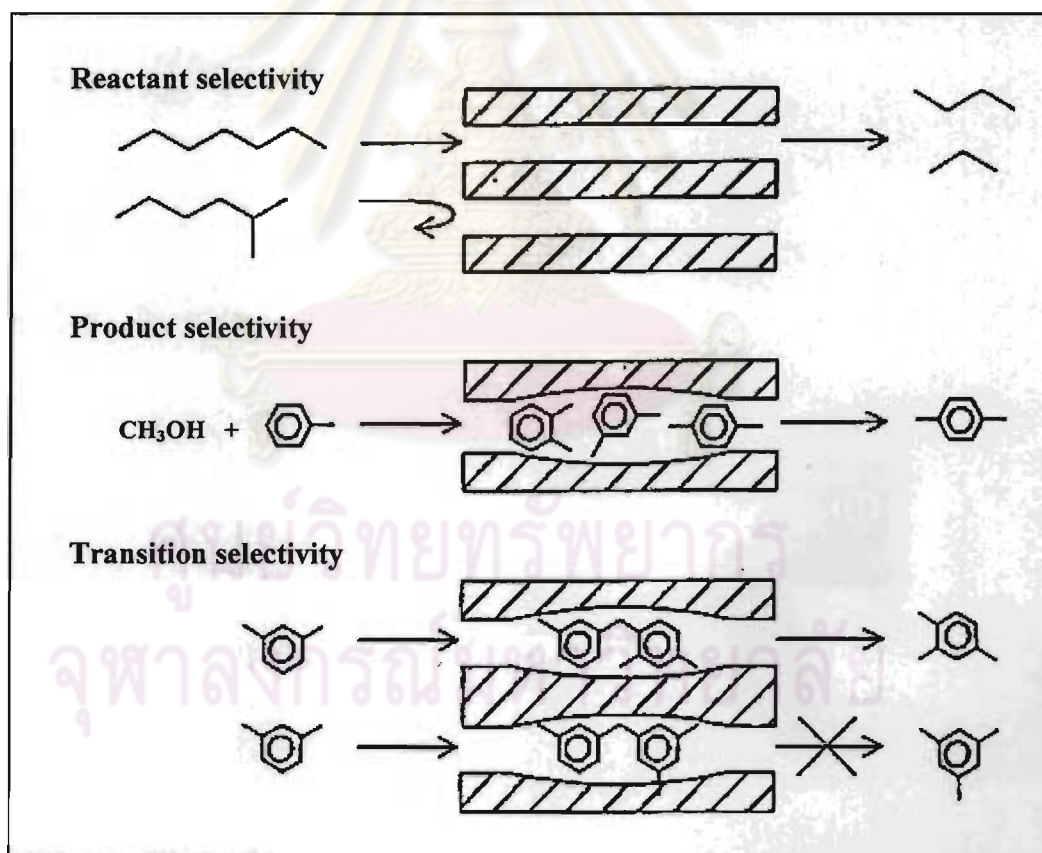
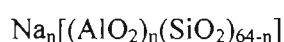


Figure 2.7 Three types of selectivity in zeolites: reactant, product and transition-state shape selectivity [33].

2.2 Zeolite Beta

Zeolite beta is an old zeolite discovered before Mobil began the “ZSM” naming sequence. A zeolite beta which is high silica zeolite was initially synthesized by Wadlinger *et al.* [38] using tetraethylammonium hydroxide as the organic template. The unit cell composition of zeolite beta is:



The structure of zeolite beta was recently determined because the structure is very complex and interest was not high until it becomes important for some dewaxing process.

Zeolite beta is generally formed as a very small catalyst, less than 1 μm which diminish its stability. On the other hand, it is known that the crystal size of a zeolite catalyst can influence the reaction activity and selectivity [39]. Zeolite beta have been used as a cracking catalyst for higher production of olefins, and an increase in the formation of these products was observed, as well as in the catalyst stability by increasing the crystallite size.

2.2.1 Structure of Zeolite Beta

The tetrahedral framework of zeolite beta is disordered along the [001]. The disordered structure and the three simple ordered polymorphs and related though layer displacements on 001 planes. Zeolite beta exhibits characteristic properties of the presence of 12-member-ring connected together in three dimensions cause two different type channels: straight channel (100) and sinusoidal channel (001) [40, 41]. The smaller building units are double six-ring units connected by two four-rings and four five-rings unit. These are connected to form chains along the [001] direction [42]. The three polymorphs of zeolite beta show in Figure 2.8.

1. Polymorph A: tetragonal crystal system, two different pore opening dimensions: 0.60 x 0.56 nm and 0.60 x 0.73 nm
2. Polymorph B: monoclinic crystal system, two different pore opening dimensions: 0.68 x 0.55 nm and 0.68 x 0.73 nm
3. Polymorph C

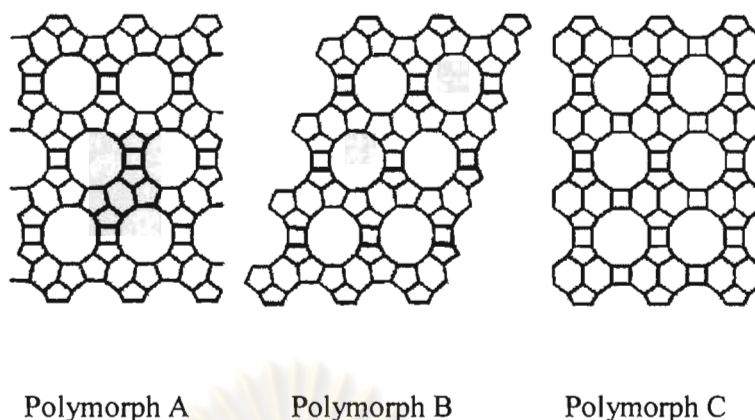


Figure 2.8 Zeolite beta polymorphs [43]

Ordinarily, zeolite beta consists of an intergrowth hybrid of two distinct structures termed polymorphs A and B and the polymorphs grow as two-dimensional sheets and the sheets randomly alternate between the two. A hypothetical polymorph C, closely related to A and B, was first described by Newsam *et al.* in 1988 [44, 45]. Recently, Corma *et al.* synthesized the pure polymorph C structure either in the presence of fluoride anions [46] or in a fluoride-free system under alkaline conditions [47]. Synthesis of zeolite beta was carried out in wide range of Si/Al molar ratios (from 0 to infinity).

2.2.2 Characterization of Zeolite Beta

Zeolite beta has a strong acidity and large specific surface area. Reliable characterization of the zeolite structure requires the use of five independent techniques:

- (a) X-ray powder diffraction (XRD)
- (b) Scanning electron microscopy (SEM)
- (c) Nitrogen adsorption-desorption isotherm
- (d) Temperature-programmed desorption (TPD) of ammonia
- (e) Solid state ^{27}Al -MAS-NMR

2.2.2.1 Powder X-ray Diffraction (XRD) [48]

X-ray powder diffraction (XRD) is an instrumental technique used to identify minerals, as well as other crystalline materials. XRD is a technique in which a collimated beams of nearly monochromatic. X-rays is directed onto the flat surface of a relatively thin layer of finely ground material. XRD can provide additional information beyond basic identification. If the sample is a mixture, XRD data can be analyzed to determine the proportion of the different minerals present. Other information obtained can include the degree of crystallinity of the minerals present, possible deviations of the minerals from their ideal compositions, the structural state of the minerals and the degree of hydration for minerals that contain water in their structure. Figure 2.9 shows a monochromatic beam of X-ray incident on the surface of crystal at an angle θ . The scattered intensity can be measured as a function of scattering angle 2θ . The resulting XRD pattern efficiently determines the different phases present in the sample.

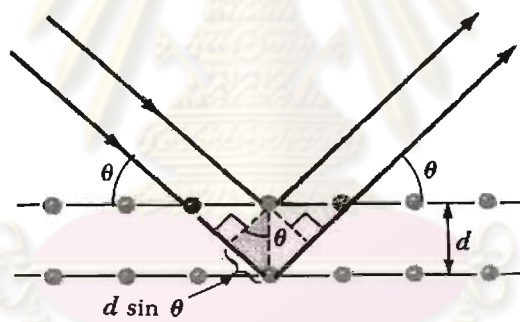


Figure 2.9 Diffraction of X-ray by regular planes of atoms [49]

Using this method, Braggs' law is able to determine the interplanar spacing of the samples, from diffraction peak according to Bragg angle.

$$n\lambda = 2 d \sin\theta$$

Where the integer n is the order of the diffracted beam, λ is the wavelength; d is the distance between adjacent planes of atoms (the d -spacings) and θ is the angle of between the incident beam and these planes.

In the simulated powder pattern of zeolite beta, shown in Figure 2.10, the intensity is plotted against the diffraction angle 2θ . Diffraction patterns are simulated for materials in the disordered series indicated in steps of 10% intergrowth.

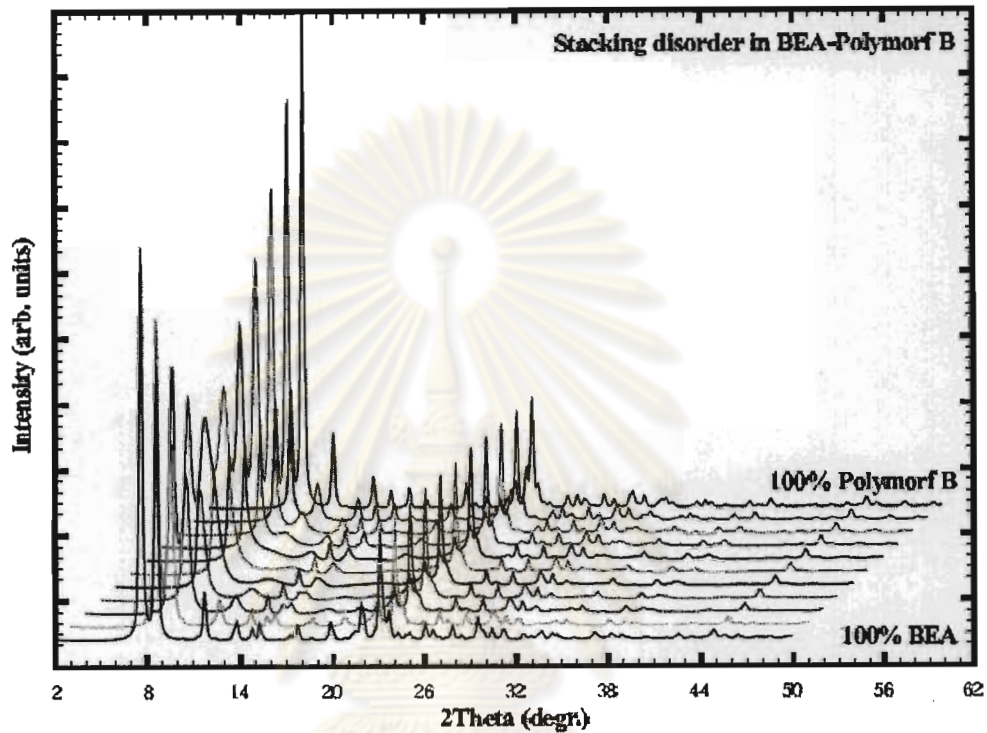


Figure 2.10 Simulated powder patterns of materials with stacking disorder in the zeolite beta family

2.2.2.2 Scanning Electron Microscopy (SEM) [50, 51]

Scanning electron microscope (SEM) uses a focused beam of high-energy electrons to generate a variety of signals at the surface of solid specimens. The signals that derive from electron-sample interactions reveal information about the sample including external morphology (texture), chemical composition, and crystalline structure and orientation of materials making up the sample. In most applications, data are collected over a selected area of the surface of the sample, and a 3-dimensional image is generated that displays spatial variations in these properties.

Areas ranging from approximately 1 cm to 5 microns in width can be imaged in a scanning mode using conventional SEM techniques (magnification ranging from 20X to approximately 30,000X, spatial resolution of 50 to 100 nm). The SEM is also capable of performing analyses of selected point locations on the sample; this approach is especially useful in qualitatively or semi-quantitatively determining chemical compositions (using EDS), crystalline structure, and crystal orientations (using EBSD). The morphology of the uniform zeolite beta can be easily observed in SEM as Figure 2.11 if the sample is conventionally prepared.

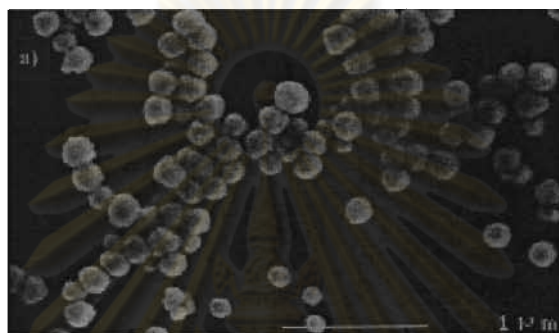


Figure 2.11 Scanning electron micrograph of a zeolite beta sample [30]

2.2.2.3 Nitrogen Adsorption-Desorption Isotherm

The N_2 adsorption technique is used to determine the physical properties of microporous molecular sieves, such as the surface area, pore volume, pore diameter and pore-size distribution of solid catalysts.

Adsorption of gas by a porous material is described by an adsorption isotherm, the amount of adsorbed gas by the material at a fixed temperature as a function of pressure. Porous materials are frequently characterized in terms of pore sizes derived from gas sorption data. IUPAC conventions have been proposed for classifying pore sizes and gas sorption isotherms that reflect the relationship between porosity and sorption. The IUPAC classification of adsorption isotherms is illustrated in Figure 2.12. Six types of isotherms are characteristic of adsorbents that are microporous (type I), nonporous or macroporous (types II, III, and VI) or mesoporous (types IV and V).

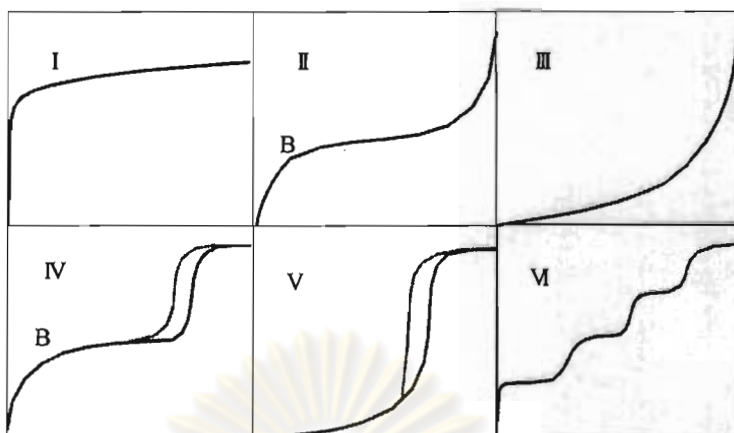


Figure 2.12 The IUPAC classification of adsorption isotherm. [52]

Adsorption isotherms are described as shown in Table 2.1 based on the strength of the interaction between the sample surface and gas adsorbate, and the existence or absence of pores. Pore types are classified as shown in Table 2.2.

Table 2.1 Features of adsorption isotherms [53]

Type	Features	
	Interaction between sample surface and gas adsorbate	Porosity
I	Relatively strong	Micropores
II	Relatively strong	Nonporous
III	Weak	Nonporous
IV	Relatively strong	Mesopore
V	Weak	Micropores or Mesopore
VI	Relatively strong Sample surface has an even distribution of energy	Nonporous

Table 2.2 IUPAC classification of pores [54]

Pore Type	Pore diameter / nm
Micropore	Up to 2
Mesopore	2 to 50
Macropore	50 to up

Pore size distribution is measured by the use of nitrogen adsorption/desorption isotherm at liquid nitrogen temperature and relative pressures (P/P_0) ranging from 0.05-0.1. The large uptake of nitrogen at low P/P_0 indicates filling of the micropores ($<20 \text{ \AA}$) in the adsorbent. The linear portion of the curve represents multilayer adsorption of nitrogen on the surface of the sample, and the concave upward portion of the curve represents filling of mesopores and macropores.

The multipoint Brunauer, Emmett and Teller (BET) [55] method is commonly used to measure total surface area.

$$\frac{1}{W[(P_0/P)-1]} = \frac{1}{W_m C} + \frac{C-1}{W_m C} (P/P_0)$$

Where W is the weight of nitrogen adsorbed at a given P/P_0 , and W_m is the weight of gas to give monolayer coverage, and C is a constant that is related to the heat of adsorption. A linear relationship between $1/W [(P_0/P)-1]$ and P/P_0 is required to obtain the quantity of nitrogen adsorbed. This linear portion of the curve is restricted to a limited portion of the isotherm, generally between 0.05-0.30. The slope and intercept are used to determine the quantity of nitrogen adsorbed in the monolayer and calculate the surface area. For a single point method, the intercept is taken as zero or a small positive value, and the slope from the BET plot is used to calculate the surface area. The surface area reported depends upon the method used, as well as the partial pressures at which the data are collected.

2.2.2.4 Temperature-Programmed Desorption (TPD) of Ammonia [56]

Temperature-Programmed Desorption (TPD) is one of the most widely used and flexible techniques for characterizing the acid sites on oxide surfaces.

Determining the quantity and strength of the acid sites on alumina, amorphous silica-alumina, and zeolites is crucial to understanding and predicting the performance of a catalyst. For several significant commercial reactions (such as n-hexane cracking, xylene isomerization, propylene polymerization, methanol-to-olefins reaction, toluene disproportionation, and cumene cracking), all reaction rates increase linearly with Al content (acid sites) in H-ZSM-5. The activity depends on many factors, but the Brønsted-acid site density is usually one of the most crucial parameters.

Preparation

Samples are degassed at 100°C for one hour in flowing helium to remove water vapour and to avoid pore damage from steaming which may alter the structure of zeolites. The samples are then temperature programmed to 500°C at a ramp rate of 10°C/minute and held at that temperature for two hours to remove strongly bound species and activate the sample. Finally the sample is cooled to 120°C in a stream of flowing helium.

Adsorption

Next the sample is saturated with the basic probe at 120°C; this temperature is used to minimize physisorption of the ammonia or organic amines. For ammonia, two techniques are available to saturate the sample: pulsing the ammonia using the loop or continuously flowing ammonia. Pulsing the ammonia allows the user to compare the quantity of ammonia adsorbed (via pulse adsorption) to the quantity desorbed for the subsequent TPD. After saturation with ammonia, pyridine, or propyl amine, the sample is purged for a minimum of one hour under a flow of helium to remove any of the physisorbed probes.

Desorption

The temperature-programmed desorption is easily performed by ramping the sample temperature at 10°C/minute to 500°C. It is a good rule of thumb that the end temperature during the TPD not exceed the maximum temperature used in the preparation of the sample.

Exceeding the maximum preparation temperature may liberate additional species from the solid unrelated to the probe molecule and cause spurious results.

During the TPD of ammonia or the non-reactive probes (pyridine or *t*-butyl amine), the built-in thermal conductivity detector (TCD) will monitor the concentration of the desorbed species. For the reactive probes (propyl amines), a mass spectrometer is required to quantify the density of acid sites. For these probes, several species may be desorbing simultaneously: amine, propylene, and ammonia.

2.2.2.5 ^{27}Al -MAS-NMR [57]

Another important characterization technique for microporous materials is solid state NMR. ^{27}Al -MAS-NMR spectroscopy has been employed to distinguish between tetrahedrally and octahedrally coordinated aluminum in the framework at approximately 50 and 0 ppm, respectively. Therefore, the amount of framework aluminum can be determined.

2.3 Effect of Parameters on Zeolite Beta Synthesis

2.3.1 Effect of Si/Al ratios

A. Simon-Masseron *et al.* [58] investigated influence of the Si/Al ratio and crystal size on the acidity and activity of HBEA zeolites. Three HBEA samples were prepared through ion exchange followed by calcination under dry air flow at 550°C from parent samples synthesized with different total Si/Al ratios or crystal sizes and characterized by various techniques. Remarkable differences were found between the concentration (and concentration ratio) of Lewis and Brønsted acidic sites of HBEA zeolite resulting from the transformation of samples synthesized with different total Si/Al ratio or crystal sizes. As could be expected, the greater the Si/Al ratio and the larger the crystal size, the more stable the synthesized sample, hence the lower the degradations undergone by the zeolite framework during the exchange and calcination steps necessary to prepare the acidic form of the zeolite. Therefore, HBEA samples with a large concentration of protonic sites and practically no Lewis acid sites can be obtained from samples synthesized with a relatively high Si/Al ratio (above 15) and

large crystals; on the opposite, HBEA zeolites with predominantly Lewis acid sites will be prepared from samples synthesized with a low Si/Al ratio and small crystals.

2.3.2 Effect of Template

Y. Zheng *et al.* [59] reported the amount of template agent plays an important role in the determination of the crystal sizes of zeolite beta. More template agent leads to more silica species dissolved to the liquid phase so that more and smaller inorganic–organic compositions can be formed. Thus, the crystal size of synthesized zeolite reduces. The morphology of crystalline zeolite was changed from square to spherical shape. With the size reducing from micro-size to nano-size, the pore volume greatly increased and micropore volume decrease due to the formation of mesopores. The water content in the initial gel did not significantly influence the crystalline size and framework Si/Al ratio of zeolite beta.

2.3.3 Effect of Ultrasound Irradiation

Ö. Andaç *et al.* [60] reported that highly crystalline zeolite A could be synthesized from a clear-to-the-eye aluminosilicate solution in the presence of ultrasound. Sonocrystallization has been demonstrated to offer the possibilities of increasing the nucleation and crystallization rates of zeolites, improving the yield and particle size distribution of the product crystals, and directing the synthesis towards different crystal phases. The effects of varying the frequency and power of ultrasound and applying sonocrystallization to different zeolite synthesis systems were also investigated in this work in order to develop a better understanding of the range of possibilities offered by the technique. Figure 2.13(A) shows SEM images of the zeolite A samples obtained at 50°C after 13 h of synthesis in the absence of ultrasound, and Figure 2.13B shows that prepared after 10 h of synthesis in the presence of ultrasound. It can be easily inferred from the figure that the particles in the sample prepared in the presence of ultrasound were larger than that prepared in the absence of ultrasound.

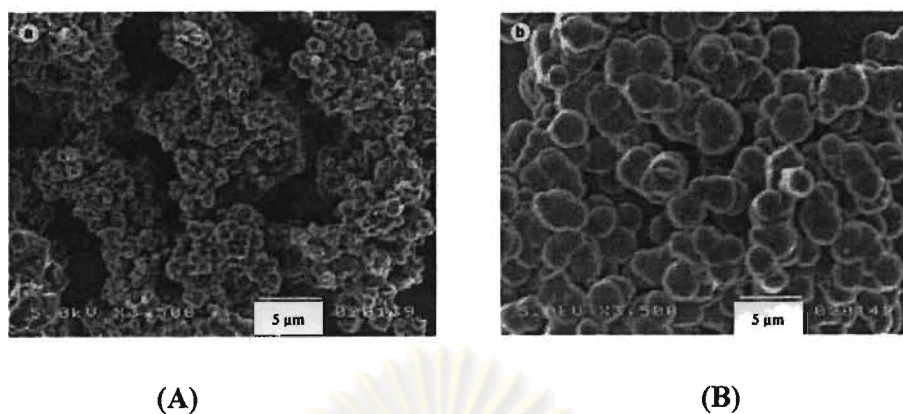


Figure 2.13 SEM images of the zeolite A samples obtained at 50°C (A) after 13 h of synthesis in the absence of ultrasound, and (B) after 10 h of synthesis in the presence of ultrasound.

The chemical applications of ultrasound, "sonochemistry", have become an exciting new field of research during the past decade. Scientists know that the chemical effects of ultrasound are diverse and include substantial improvements in both stoichiometric and catalytic chemical reactions. In some cases, ultrasonic irradiation can increase reactivities by nearly a millionfold. The chemical effects of ultrasound fall into three areas: homogeneous sonochemistry of liquids, heterogeneous sonochemistry of liquid-liquid or liquid-solid systems, and sonocatalysis (which overlaps the first two). Because cavitation can take place only in liquids, chemical reactions do not generally occur during the ultrasonic irradiation of solids or solid-gas systems. Ultrasound has proved extremely useful in the synthesis of a wide range of nanostructured materials, including high surface area transition metals, alloys, carbides, oxides and colloids. Sonochemical decomposition of volatile organometallic precursors in high boiling solvents produces nanostructured materials in various forms with high catalytic activities. Nanometer colloids, nanoporous high surface area aggregates, and nanostructured oxide supported catalysts can all be prepared by this general route [61].

Power ultrasound produces its chemical effects through the phenomenon of cavitation. Cavitation is the production of microbubbles in a liquid when a large negative pressure is applied to it [62]. Ultrasonic irradiation differs from traditional

energy sources (such as heat, light, or ionizing radiation) in duration, pressure, and energy per molecule. Because of the immense temperatures and pressures and the extraordinary heating and cooling rates generated by cavitation bubble collapse, ultrasound provides an unusual mechanism for generating high-energy chemistry. Figure 2.14 shows a typical sonochemical apparatus. Ultrasound can easily be introduced into a chemical reaction in which there is good control of temperature and ambient atmosphere. The titanium rod shown immersed in the reaction liquid is driven into vibration by a piezoelectric, which vibrates when subjected to an alternating current electric field. The usual piezoelectric ceramic is PZT, a lead zirconate titanate material.

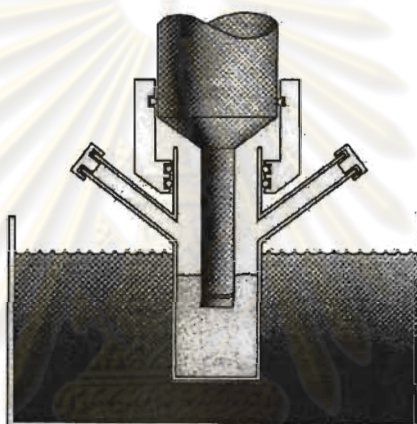


Figure 2.14 Diagram of a typical sonochemical apparatus [63].

2.3.4 Effect of Calcination

J. He *et al.* [64] studied new methods to remove the templates from porous materials with high porosity and poor structural stability have been proposed in the light of analysis of the decomposition process of the organic templates. Microwave irradiation and two-step calcination are shown to be more favorable than conventional calcination in that the new methods have beneficial effects on both the structural order and surface acidity. Two-step calcination is particularly effective because it is more convenient and reproducible than microwave irradiation. The results show that microwave irradiation and two-step calcination are more effective than conventional calcination in that the new methods of template removal are beneficial not only to the

crystal structure of zeolite β and MCM-41, but also to the surface acidity in the case of zeolite β . Two-step calcination is particularly preferable since it is more convenient and reproducible.

2.4 The Refining Process [65, 66]

Every refinery begins with the separation of crude oil into different fractions by distillation (Figure 2.15). The fractions are further treated to convert them into mixtures of more useful saleable products by various methods such as cracking, reforming, alkylation, polymerization and isomerisation. These mixtures of new compounds are then separated using methods such as fractionation and solvent extraction. Impurities are removed by various methods, e.g. dehydration, desalting, sulphur removal and hydrotreating.

Refinery processes have developed in response to change market demands for certain products. With the advent of the internal combustion engine the main task of refineries became the production of petrol. The quantity of petrol available from distillation alone was insufficient to satisfy consumer demand. Refineries began to look for ways to produce more and better quality petrol. Two types of processes have been developed:

- Breaking down large, heavy hydrocarbon molecules
- Reshaping or rebuilding hydrocarbon molecules.

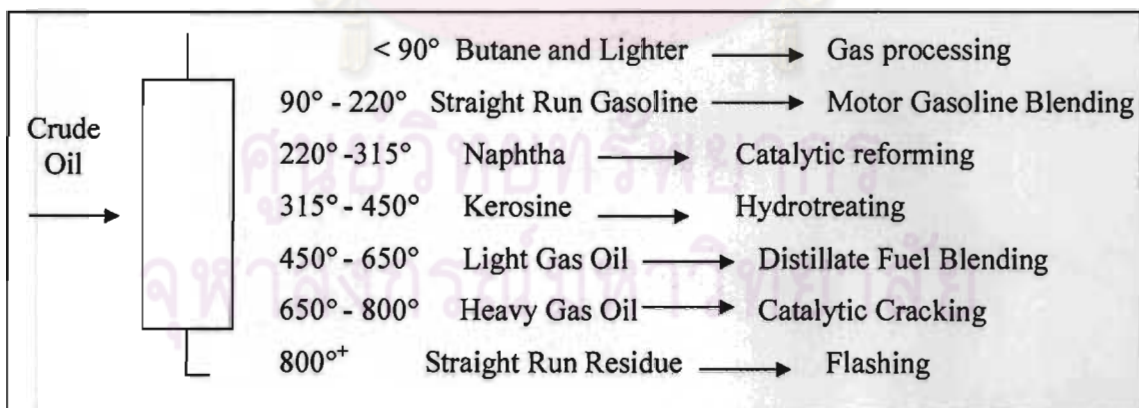


Figure 2.15 Distilling crude and product disposition

Cracking processes break down heavier hydrocarbon molecules (high boiling point oils) into lighter products such as petrol and diesel. These processes include catalytic cracking, thermal cracking and hydrocracking.

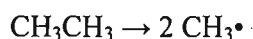
- **Catalytic cracking** [67] is used to convert heavy hydrocarbon fractions obtained by vacuum distillation into a mixture of more useful products such as petrol and light fuel oil. In this process, the feedstock undergoes a chemical breakdown, under controlled heat (450°C-500°C) and pressure. Small pellets of silica-alumina have proved to be the most effective catalysts. The cracking reaction yield petrol, LPG, unsaturated olefin compounds, cracked gas oils, a liquid residue called cycle oil, light gasses and a solid coke residue. Cycle oil is recycled to cause further breakdown and the coke, which forms a layer on the catalyst, is removed by burning. The other products are passed through fractionators to be separated and separately processed.

- **Thermal cracking** [68]

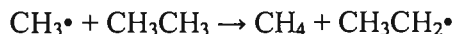
In thermal cracking elevated temperatures (~800°C) and pressures (~700kPa) are used. An overall process of disproportionation can be observed, where "light", hydrogen-rich products are formed at the expense of heavier molecules which condense and are depleted of hydrogen. The actual reaction is known as homolytic fission and produces alkenes, which are the basis for the economically important production of polymers.

A large number of chemical reactions take place during steam cracking, most of them based on free radicals. Computer simulations aimed at modeling what takes place during steam cracking have included hundreds or even thousands of reactions in their models. The main reactions that take place include:

1. Initiation reactions, where a single molecule breaks apart into two free radicals. Only a small fraction of the feed molecules actually undergo initiation, but these reactions are necessary to produce the free radicals that drive the rest of the reactions. In steam cracking, initiation usually involves breaking a chemical bond between two carbon atoms, rather than the bond between a carbon and a hydrogen atom.



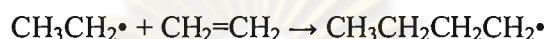
2. Hydrogen abstraction, where a free radical removes a hydrogen atom from another molecule, turning the second molecule into a free radical.



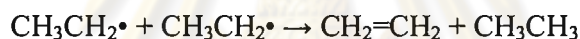
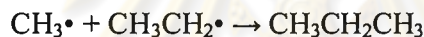
3. Radical decomposition, where a free radical breaks apart into two molecules, one an alkene, the other a free radical. This is the process that results in the alkene products of steam cracking.



4. Radical addition, the reverse of radical decomposition, in which a radical reacts with an alkene to form a single, larger free radical. These processes are involved in forming the aromatic products that result when heavier feedstocks are used.



5. Termination reactions, which happen when two free radicals react with each other to produce products that are not free radicals. Two common forms of termination are *recombination*, where the two radicals combine to form one larger molecule, and *disproportionation*, where one radical transfers a hydrogen atom to the other, giving an alkene and an alkane.



- **Hydrocracking** can increase the yield of petrol components, as well as being used to produce light distillates. It produces no residues, only light oils. Hydrocracking is catalytic cracking in the presence of hydrogen. The extra hydrogen saturates, or hydrogenates the chemical bonds of the cracked hydrocarbons and creates isomers with the desired characteristics. Hydrocracking is also a treating process, because the hydrogen combines with contaminants such as sulphur and nitrogen, allowing them to be removed.

2.5 Catalytic Cracking Mechanisms

2.5.1. General Cracking Mechanisms [69]

In general, for components with equal carbon numbers, the rate of cracking decreases in the order: i-olefins > n-olefins > i-paraffins ≈ naphthenes > n-paraffins > aromatics. The cracking mechanism can be seen as a chain mechanism that involves the intermediate formation of carbocations, positively charged hydrocarbon species.

Carbocations include both carbenium ions (e.g. $R_1-CH_2-C^+H-R_2$, $R_1-CH=C^+-R_2$) and carbonium ions (e.g. $R_1-CH_2-C^+H_3-R_2$, $R_1-CH=C^+H_2-R_2$). In carbenium ions, the charge carrying carbon atom can be di- or tri-coordinated, while in carbonium ions, the charge carrying carbon atom is tetra- or pentacoordinated. The stability of the carbocations decreases in the order tertiary > secondary > primary [70]. Cracking of hydrocarbons is primarily a reaction that proceeds through adsorbed carbenium ion intermediates.

2.5.2. Reactions of Olefins

The formation of carbenium ions from olefins can easily proceed by addition of the proton from a Brønsted acid site of the catalyst to the carbon-carbon double bond. Cracking of the adsorbed carbenium ion proceeds through the β -scission mechanism [71,72] or through the protonated cyclopropane mechanism [73]. An illustration is given in Fig. 2.16.

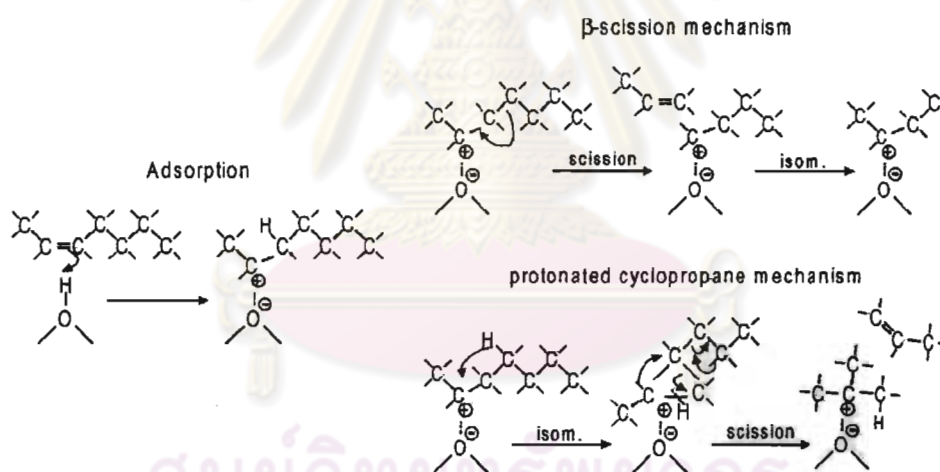
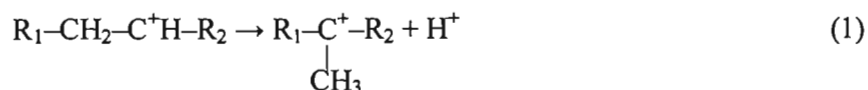


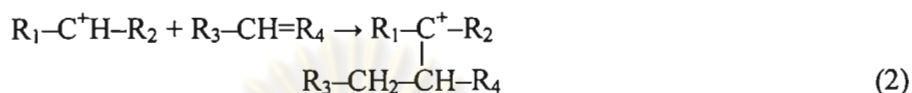
Figure 2.16 Cracking mechanisms illustrated by the reaction of n-heptene; adsorption at a Brønsted acid site leads to formation of an adsorbed carbenium ion that can be cracked. Both the β -scission mechanism [69, 70] and the protonated cyclopropane mechanism [66] are shown.

Other reactions of the adsorbed carbenium ion are [74, 75]:

1. Isomerization to a more stable carbenium ion, for example, through a methyl shift:



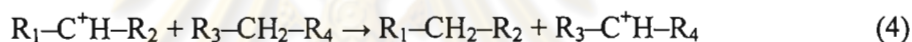
2. Oligomerization with olefin in a bimolecular reaction to form a larger adsorbed carbenium ion:



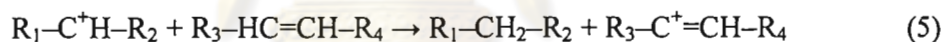
3. Desorption with deprotonation to form an olefin (the opposite of adsorption):



4. Desorption with hydride abstraction from a paraffin to form new paraffin from the carbenium ion and new carbenium ion from the paraffin (H-transfer reaction):



5. Desorption with hydride abstraction from (cyclic) olefins or coke (precursors) to form paraffin and a more aromatic compound (H-transfer reaction):



The bimolecular reactions (2), (4) and (5) can occur if the pore size of the catalyst is large enough to accommodate the reactive intermediates, or they should occur on the outer surface of the zeolite particles. If the pores are too small, as in the case of ZSM-5 (0.53 nm × 0.56 nm), these reactions cannot take place with the larger (gasoline) components, although oligomerization or dimerization of small (C₂-C₄) olefins could be possible. For example, in the Mobil olefins to gasoline and distillates process (MOGD) coupling of light hydrocarbons is catalyzed by ZSM-5.

With ZSM-5, cracking through dimeric intermediates has only been reported in the reactions of relatively small *n*-olefins (C₄-C₆). Abbot and Wojciechowski [76] have studied cracking of *n*-olefins from C₅ to C₉ at 678K with ZSM-5 and found that cracking of pentene solely took place through a dimeric/disproportionation mechanism. Cracking of heptene and larger molecules proceeded mainly through monomolecular cracking and at 678 K; hexene represented the transition case of the

two mechanisms and was cracked by both monomolecular cracking and through dimeric intermediates.

With Y-type zeolites, the dimeric mechanism is a more important reaction route; for example, it has been found that cracking of C_7 took place for 25% via a dimeric disproportionation reaction at 746K and for 32% at 673K.

2.5.3. Proposed Cracking Mechanisms of Polymer [77]

For ZSM-5 the cracking reactions of larger C_7^+ olefins are restricted to simple β -scission reactions. The relatively straight chains (or parts of it) can enter the pores of ZSM-5, are adsorbed, split-off small olefins, and desorb. For example, the reaction of n-heptene over ZSM-5 (for simplicity only the β -scission mechanism) is shown in Fig.2.17. The adsorbed C_7 -carbenium ion is cracked to propene and C_4 -carbenium ion. Then C_4 -carbenium isomerizes to butene or is cracked to two ethene molecules.

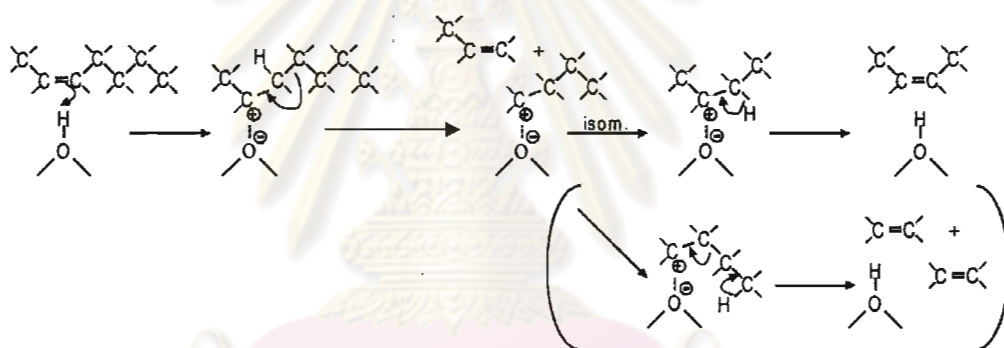


Figure 2.17 Monomolecular cracking mechanisms (only mechanism possible with ZSM-5).

Generally, the second reaction, formation of ethene, is energetically less favorable because it involves the formation of two primary carbenium ions. However, due to the small pores of ZSM-5, the electrical field in the pores is larger and a relatively large interaction between the catalyst and the adsorbed carbenium ions shall exist. It is believed that the oxygen atoms of a zeolite structure play a role in solvating carbocations, delocalizing the positive charge into the framework. The smaller the size of the pores of the zeolite, the closer the different oxygen atoms are to the adsorbed reaction intermediates and the higher the possible interaction. So possibly,

as a result of increased stabilization of the intermediates, the formation of ethene is enhanced when small pore-zeolites such as ZSM-5 are involved.

On the base catalyst, with zeolite Y as active species (pore size 0.74 nm) adsorbed C_4 -carbenium species and new heptene molecule to form an adsorbed C_{11} -carbenium ion. The C_{11} carbenium ion is cracked to hexane and C_5 -carbenium ion. This bimolecular cracking mechanism proposed by Williams *et al.* [74] is illustrated in Fig. 2.18. Also, the adsorbed heptene carbenium ion could oligomerize before cracking.

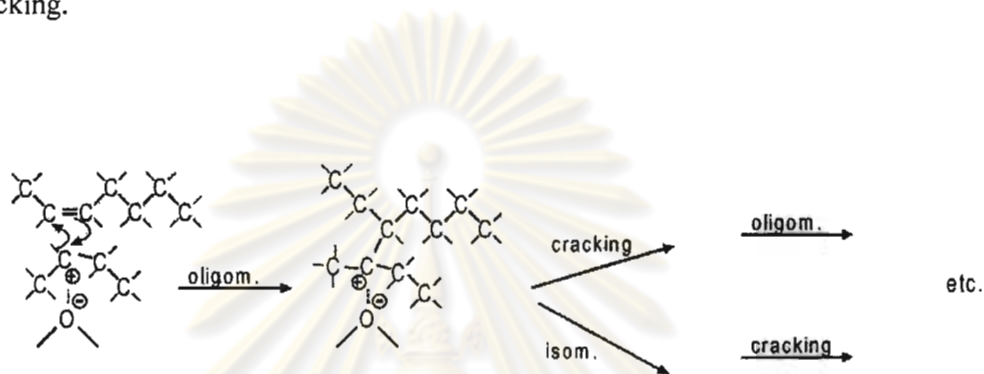


Figure 2.18 Bimolecular cracking mechanism that can occur on zeolite Y in addition to the monomolecular mechanism.

Because of the larger adsorption strength of larger hydrocarbons, the bimolecular mechanism have an important contribution in the cracking mechanism of the heavier gasoline-range olefins, provided that the catalyst pore size is large enough to accommodate the reaction intermediates. Aromatics and highly branched components, therefore, are too large to react through bimolecular mechanisms. Linear components are the most likely ones to react through this mechanism.

According to this proposed mechanism, the active site of ZSM-5 is the acid site itself, while the active site in zeolite Y can be represented by the adsorbed carbenium ion. The reaction intermediates with ZSM-5 contain the number of carbon atoms (C_5 – C_{11}), while the (surface) intermediates with the base catalyst can be much larger. As a result, the cracking products from ZSM-5 will be mainly C_3 , C_4 , and to some extent also C_2 olefins, while with the zeolite Y base catalyst larger fragments can be formed.

This agrees with the results that can be found in literature; the main products from *n*-olefins and *i*-olefins cracking on ZSM-5 are light olefins with a high selectivity for propene, *i*-butene, and in some cases the increased yields of ethene are reported.

There are no major reports that explicate a mechanism for the catalytic cracking of PE and PP using zeolite beta as catalyst. The catalytic mechanism that can occur on ZSM-5 and zeolite Y should be used for elucidate the mechanism of zeolite beta. The catalytic cracking of PP and PE is initiated by attack of low molecular weight carbonium ion (R^+) on a very small number of on-chain hydrogen atoms attached to tertiary carbon atoms in polymer chains. The direction of this reaction mostly obeys the stability rule of carbonium ions: primary \ll secondary \ll tertiary. The mechanism begins with the rapid cracking of polymer over the acid sites on external surface and then fast mass transfer of cracked fragments in the pore of zeolite beta. The selectivity to products depend on shape and size selectivity that control by pore size and pore structure of zeolite beta.

2.5.4. Reactions of Paraffins

Compared to olefins, paraffins have a lower reactivity towards cracking due to a more difficult formation of carbenium ions. Direct formation of a carbenium ion requires the abstraction of a hydride ion. This may proceed at Lewis acid sites or adsorbed carbenium ions can react with paraffins in a bimolecular-type of mechanism. The latter mechanism requires the presence of the adsorbed carbenium ions and can take place if the pore size of the catalyst is large enough to accommodate the necessary transition state (as is the case in zeolite Y and not in ZSM-5).

Indirect formation of carbenium ions is proposed to proceed through the formation of carbonium ions; paraffin reacts with a proton from a Brønsted acid site and the resulting adsorbed carbonium ion is cracked to an adsorbed carbenium ion and hydrogen or a small olefin. The formation of a carbonium ion requires an energetically unfavorable transition state and has high activation energy. This mechanism for activation of paraffins will only be significant in the absence of olefins and is favored by high temperatures, low hydrocarbon partial pressures and low conversions of the paraffins. The occurrence is not expected to be significant when cracking a gasoline mixture that contains olefins. The olefin can easily form

carbenium ions and cause cracking of paraffins through the bimolecular cracking mechanisms as discussed above.



ศูนย์วิทยทรัพยากร
จุฬาลงกรณ์มหาวิทยาลัย

CHAPTER III

EXPERIMENTS

3.1 Instruments and Apparatus

Ultrasonic Probe

During the synthesis procedure, the gel mixture was introduced in a 300-ml autoclave into which a ultrasonic probe was inserted through the bottom of the autoclave. The ultrasonicator (SONICS, VC 505) consisted of a power supply (net power output: 500 Watts, frequency: 20 kHz), sealed converter (piezoelectric lead zirconate titanate crystals) and a titanium alloy probe (13-mm-diameter tip). The mixture was subjected to ultrasound irradiation with an amplitude of 40% for various periods.

Ovens and Furnaces

The gel mixture was crystallized at 135°C in a Memmert UM-500 oven. Heating of any solid sample at 110°C was carried out using the same oven. Calcination of the solid catalysts at 550°C was achieved in a Carbolite RHF 1600 muffle furnace with programmable heating rate of 1°C/min.

X-ray Powder Diffractometer (XRD)

The X-ray powder diffractometer was used for investigation of the phase purity and structure of zeolite beta catalysts. The XRD patterns were collected on a Rigaku, Dmax 2200/ultima plus X-ray powder diffractometer with a monochromator and Cu K_α radiation (40 kv. 30 mA). The 2-theta angle was ranged from 5 to 40 degree with scan speed of 5 degree/min and sampling width of 0.02 degree. The scattering slit, divergent slit and receiving slit were fixed at 0.5 degree, 0.5 degree, and 0.3 mm, respectively. The measured diffractograms were analyzed using MDI software (Jade6.5).

Scanning Electron Microscope (SEM)

JEOL JSM-6480LV scanning electron microscope was used for the identification of the morphology and particle size of zeolite beta catalysts. In order to avoid charging of samples and obtain good quality of micrographs, the catalysts were dispersed in absolute ethanol in ultrasonic water bath before gradually evaporated on glass slide and coated with sputtering gold under vacuum prior to the SEM measurements.

NMR Spectrometer

Solid state ^{27}Al -MAS-NMR spectra were performed using the Bruker Advance DPX 300 MHz NMR spectrometer.

ICP-AES Spectrometer

Aluminum content in the catalysts was analyzed by using the Perkin Elmer Plasma-1000 inductively coupled plasma-atomic emission spectrometer (ICP-AES).

Nitrogen Adsorptometer

The catalyst porosity in terms of nitrogen adsorption-desorption isotherms of zeolite beta catalysts were performed in a BELSORP-II instrument. The catalysts were outgassed at 400°C at 3 h before the surface area measurements. Surface areas and micropore volume of the catalysts were calculated by using the BET equation. The external surface areas were obtained from the analysis of adsorption branch of the isotherm by the t-plot method.

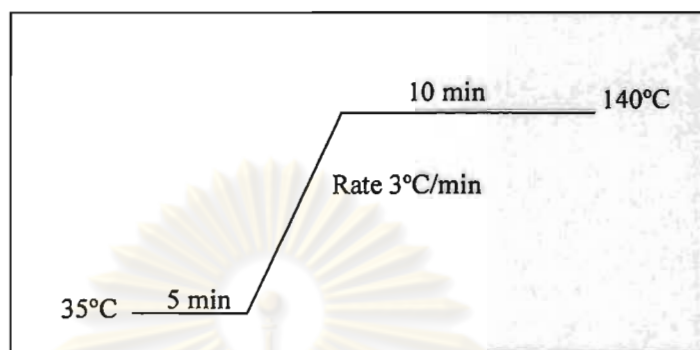
NH₃ TPD

Acid strength of catalysts was determined using the BEL-CAT Japan instrument. The sample weight was near 100 mg and weighted exactly pretreatment at 400°C for 20 min before each measurement.

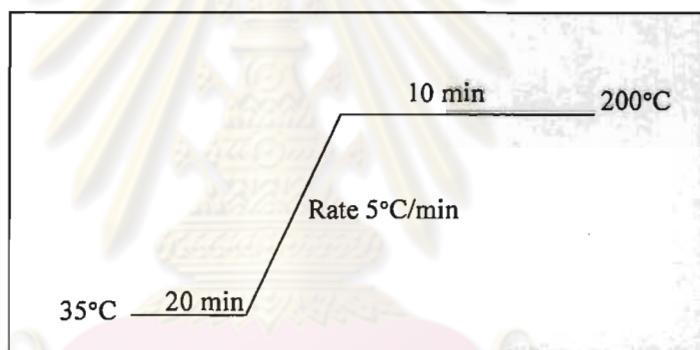
Gas Chromatograph

Hydrocarbon gases were analyzed using a Varian CP-3800 gas chromatograph equipped with a 50-m long and 0.53-mm inner diameter Alumina-PLOT column. Liquid samples were analyzed using a Varian CP-3800 gas chromatograph equipped

with a 30-m long and 0.25-mm inner diameter CP-sil 5 (0.25 μm film thickness) column. All GC detectors are flame ionization detectors (FID). The GC heating programs for 3.00- μl gas and 1.00- μl liquid analysis are shown in Schemes 3.1 and 3.2, respectively.



Scheme 3.1 The GC heating program for gas analysis



Scheme 3.2 The GC heating program for liquid analysis

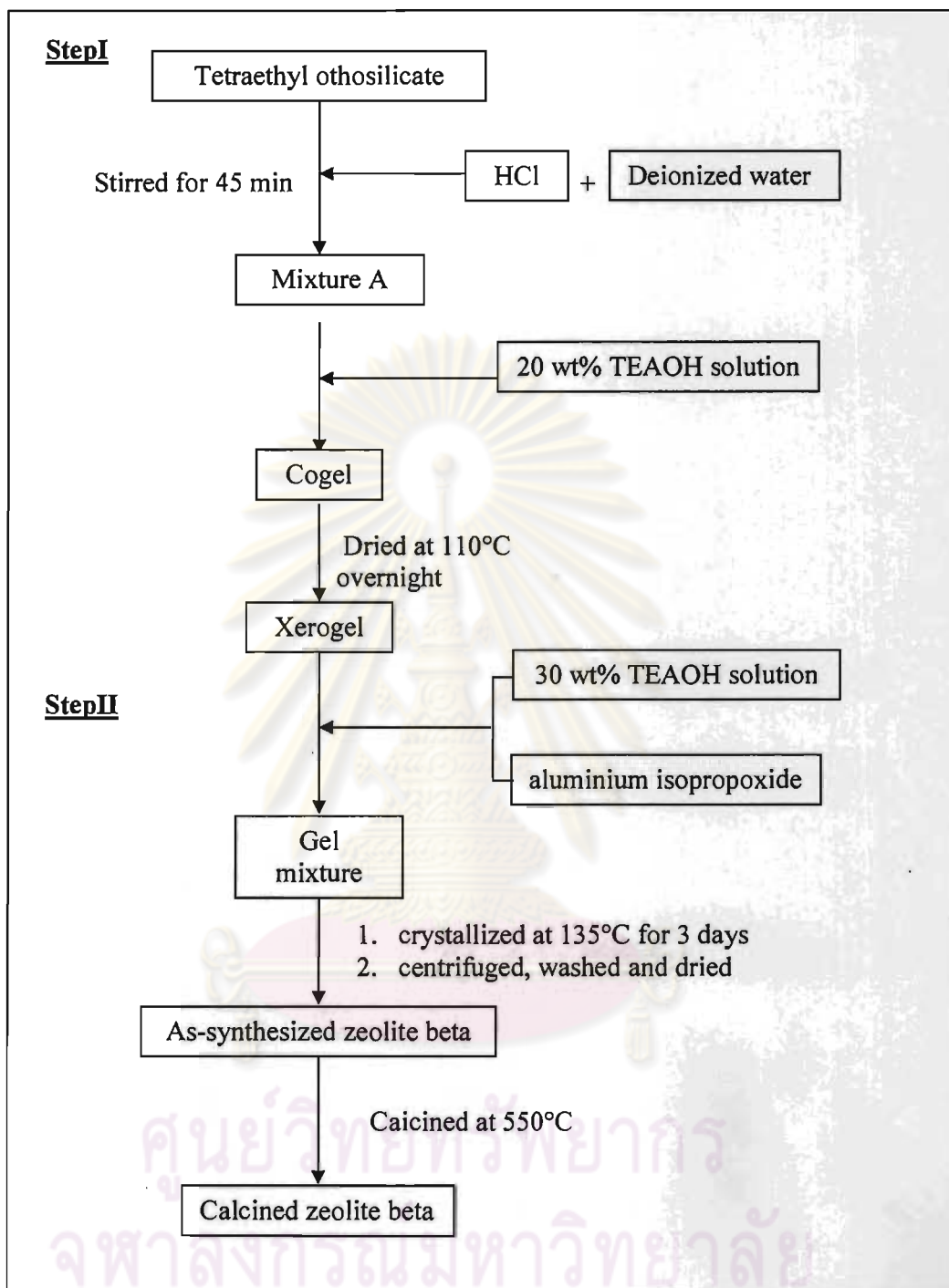
3.2 Chemicals and Gases

1. Tetraethylammonium hydroxide, TEAOH (Fluka, 40 wt %)
2. Tetraethylorthosilicate, TEOS (Aldrich, 98 wt %)
3. Aluminum isopropoxide, AIP (Aldrich)
4. Hydrochloric acid, HCl (Fluka, 37 wt %)
5. Standard liquid mixture (Restek)
6. Standard gas mixture for GC analysis were kindly obtained from PTT Chemical Public Company Limited.
7. Nitrogen gas, N_2 (Thai Industrial Gases (TIG), highly pure grade)
8. Ammonia gas, NH_3 (Linde Gas Thailand, highly pure grade)

3.3 Preparation Methods of Zeolite Beta

The synthesis of zeolite beta was carried out from an amorphous xerogel by a wetness impregnation procedure reported in the literature [29]. This material was prepared by two-step sol-gel method. In the first step, the amorphous xerogel was prepared by hydrolysis of 239.26 g of tetraethyl orthosilicate (TEOS) with a mixture 83.68 g of 0.05 M aqueous HCl and 103.36 g of deionized water in ice-water bath and the mixture was stirred vigorously for 45 min. After two-phase system became monophasic, 17.18 g of 20 wt% TEAOH aqueous solution was dropwise added to the previous mixture until the gel point and the cogel so obtained was dried at 110°C overnight. In the second step, the mixture of 3.9096 g of aluminium isopropoxide and 200.34 g of 30 wt% aqueous TEAOH solution was dropwise added to a 500 cm³ 4-necked round bottom flask containing the xerogel from the first step with stirring under nitrogen atmosphere. Then the mixture with the molar ratio of 0.73(TEA)₂O : SiO₂ : 0.0083Al₂O₃ : 19H₂O was aged by stirring under nitrogen atmosphere for 12 h. The gel was transferred into a stainless-steel autoclave containing Teflon cup and kept in an oven at 135°C for 72 h. After the reaction was quenched, white solid sample was separated by centrifugation, washed with deionized water and dried in the oven at 110°C overnight. The sample is denoted as Beta60-72h. The white solid product was characterized using XRD and SEM. The schematic diagram of this procedure is shown in Scheme 3.3.

ศูนย์วิทยทรัพยากร
จุฬาลงกรณ์มหาวิทยาลัย



Scheme 3.3 Diagram of the synthesis procedure for zeolite beta

3.4 Preparation of Zeolite Beta with Ultrasound Irradiation

Gel mixture of zeolite beta was prepared using exactly the same reagents and method to that described in Section 3.3. After aging of gel mixture for 12 h, the gel was introduced in 4 autoclaves equally into which a high power ultrasonic probe was inserted through the bottom of the autoclaves. The gel was subjected to ultrasound irradiation for 30, 60, 90, and 120 min, respectively. Then the autoclaves were heated in an oven at 135°C for 72 h. After the autoclave was quenched, the solid products were separated by centrifugation, washed with deionized water, dried at 110°C overnight. Sample notation is Beta60-US x -72h, when x is the ultrasound irradiation periods. All zeolite beta samples were characterized by XRD. The optimal ultrasound irradiation period was then selected for synthetic condition.

3.5 Preparation of Zeolite Beta with Various Crystallization Time

In order to study effects of ultrasound irradiation during gel formation process on formation of zeolite beta, Both Beta60 and Beta60-US30 samples were synthesized in same way as described in Section 3.3 and 3.4, respectively with various crystallization time of 8, 12, 16, 20, 24, 48, 72, and 96 h. For zeolite beta synthesized with ultrasound irradiation, gel mixture was subjected to ultrasound irradiation for 30 min prior to crystallization. Sample notation is Beta60-yh and Beta60-US30-yh, when y is the crystallization time. All zeolite beta samples were characterized by XRD. The optimal crystallization time was then selected for synthetic condition.

3.6 Preparation of Zeolite Beta with Various Si/Al Ratios

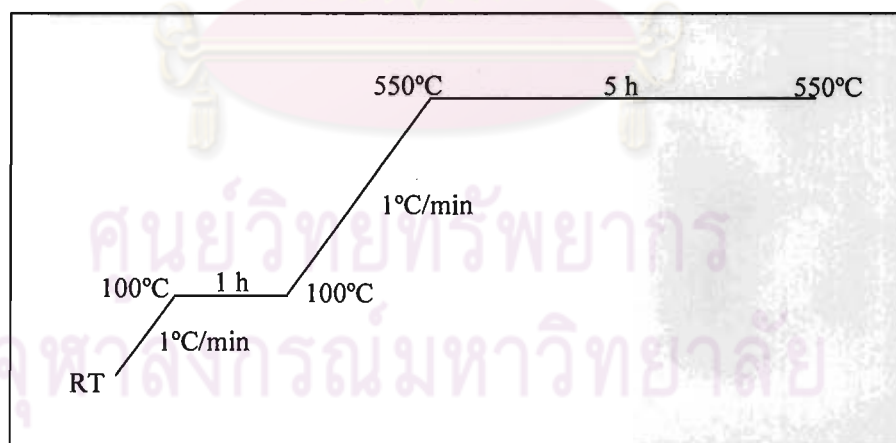
The Beta-24h and Beta-US30-24h samples with various Si/Al ratios in gel of 10, 20, 40, 60 and 80 were synthesized using the same method as that described in Section 3.3 and 3.4. Different amounts of aluminum required for each sample were used as indicated in Table 3.1. Si/Al molar ratio in gel was shown after Beta in sample notation. All zeolite beta catalysts were characterized by XRD.

Table 3.1 Required amounts of aluminum isopropoxide in the preparation of zeolite beta samples with various Si/Al ratios in gel of 10, 20, 40, 60 and 80

Sample	Si/Al molar ratio in gel	Amounts of aluminum isopropoxide (g)
Beta10	10	23.4574
Beta20	20	11.7285
Beta40	40	5.8643
Beta60	60	3.9096
Beta80	80	2.9321

3.7 Removal of Organic Template from Zeolite Beta Catalysts

To make pore in the catalyst structure, the organic template must be removed by oxidation to carbon dioxide at elevated temperature. An as-synthesized zeolite beta was calcined in a muffle furnace using the heating program for the template removal as shown in Scheme 3.4. The calcined sample was characterized using XRD, ICP-AES, SEM, ^{27}Al -MAS-NMR, NH_3 -TPD, and nitrogen adsorption-desorption instruments, and kept in a desiccator prior to use.



Scheme 3.4 A heating program for removal of organic template from the pores of zeolite beta

3.8 Elemental Analysis

Elemental analysis was performed to determine Si/Al in catalyst. Aluminum (Al) content was determined by ICP-AES. The content of silica (SiO₂) was obtained by difference of catalyst weight and Al₂O₃ weight calculated from ICP-AES. For sample preparation, 0.0400 g of a calcined catalyst was soaked with 10 cm³ of 6 M HCl. Then 10 cm³ of 48% hydrofluoric acid was dropwise added to the mixture to get rid off silica in the form of volatile SiF₄ species. The sample was heated but not boiled until it was dried on a hot plate. Then the fluoride treatment was repeated twice before 10 cm³ of reverse aqua regia containing 6M HCl: 6M HNO₃ at a ratio of 1:3 was added slowly and warmed until dried again. After that 10 cm³ deionized water was added to and warmed for 5 min. The sample solution was transferred to a 50-cm³ polypropylene volumetric flask. The solution in the flask was brought to the mark with DI water. The flask was capped and shaken before transferred into a plastic bottle. The sample solution was determined by ICP-AES technique. The standard solution of 1000-ppm aluminum in HNO₃ (from BDH) was diluted to 5, 10, 20 and 30 ppm to obtain a calibration curve.

3.9 Activity of Various Zeolite Beta Catalysts in PP Cracking

3.9.1 Effect of Crystallization Time

The zeolite Beta60 catalysts prepared with and without ultrasound irradiation and crystallized for 20, 24 and 72 h were used for finding optimum crystallization periods in this synthesis. All catalysts were freshly calcined at 550°C before catalytic test was performed. Thermal and catalytic cracking activities were carried out in a glass reactor (4.4 cm. i.d. and 37 cm. length) under a continuous nitrogen flow by batch operation as shown in Figure 3.1 and Scheme 3.5. Initially, weights of 0.50 g of catalyst and 5.00 g of the polypropylene waste were loaded into the reactor and mixed thoroughly. Afterward, the reactor was set up, purged with N₂ at flow rate of 20 ml/min to remove the air, and heated with a rate of 20°C/min up to 380°C, keeping it constant for 40 min. This temperature was continually monitored by a programmable temperature controller equipped with a K-type thermocouple in direct contact with the reaction mixture. The gaseous products at the reaction temperature were swept out from the reactor by the nitrogen stream and separated into liquid and gaseous

fractions in a condenser cooled by a chiller. The gas fraction was collected into a Tedlar bag since the start of heating while the liquid fraction was collected in a 10-cm³ graduated cylinder. After completion of the reaction, the reactor was cooled down to room temperature and weighed. The values of plastic conversion were defined as the sum of collected gaseous and liquid products with regard to the initially loaded polypropylene waste. The solid remaining in the reactor was considered as a residue, not being included in the conversion. The values of %conversion and % yield were calculated based on the equations as follows:

$$\% \text{ Conversion} = \frac{(\text{mass of liquid fraction} + \text{mass of gas fraction}) \times 100}{\text{mass of plastic}}$$

mass of gas fraction = mass of the reactor with plastic and catalyst before reaction –
 mass of the reactor with residue and used catalyst after reaction
 – mass of liquid fraction

$$\% \text{ Fraction yield} = \frac{\text{mass of product fraction} \times 100}{\text{mass of plastic}}$$

The degradation products were classified into three groups: gas fraction (products which were not condensed at water cooling temperature), liquid fraction and residue. The gas products were analyzed by a gas chromatography. The liquid fraction was distilled under vacuum as shown in Figure 3.2. The distillate oil was analyzed by a GC. The values of retention time of components in the distillate oil in the GC column were compared to the boiling point range of reference in form of n-paraffins. The value of %coke formed was determined by the weight loss upon calcination of the used catalyst after leaching out of waxes by n-hexane. The heating program for regeneration of the used catalyst is shown in Scheme 3.4.

3.9.2 Effect of Si/Al Ratios in Catalyst

The degradation of PP waste was performed using Beta-24h and Beta-US30-24h catalysts with various Si/Al ratios (20, 40, 60, and 80). The reaction was performed in the same way as what described in Section 3.8.1. The experiments were set up at reaction temperature of 350°C in order to reduce the effect of thermal reaction.

3.9.3 Effect of Temperature

The catalytic cracking of PP waste was carried out using Beta20-US30-24h with different temperature reactions. The reaction was performed using the same method that described in Section 3.8.1. The experiments were set up at reaction temperatures of 350, 380 and 400°C.

3.9.4 Effect of Polypropylene to Catalyst Ratios

The optimum temperature (380°C) from Section 3.9.3 was used in the degradation of PP waste using 5% and 10% Beta20-US30-24h samples of plastic as catalysts. The reaction was performed using the same method that described in Section 3.8.1.

3.10 Activity of Various Zeolite Beta Catalysts in HDPE Cracking

3.10.1 Effect of Si/Al Ratios in Catalyst

The degradation of HDPE waste was carried out using Beta-24h and Beta-US30-24h catalysts with various Si/Al ratios (20, 40, 60, and 80) as catalysts. The reaction was performed in the same way as what described in Section 3.8.1. The experiments were set up at the reaction temperature of 380°C.

3.10.2 Effect of Temperature

The catalytic cracking of HDPE waste was carried out using Beta20-US30-24h catalyst with various temperature reactions. The experiments were set up at the reaction temperatures of 350, 380 and 400°C. The reaction was performed in the same way as what described in Section 3.8.1.

3.10.3 Effect of Polyethylene to Catalyst Ratio

The Beta20-US30-24h sample was used for studying the effect of polyethylene to catalyst ratio on its activity. The amount of polyethylene to catalyst ratio are 5% and 10% catalyst of plastic. The experiments were set up at the reaction temperature of 400°C which is the optimum reaction temperature from Section 3.10.2. The reaction was performed using the same method as that described in Section 3.8.1.

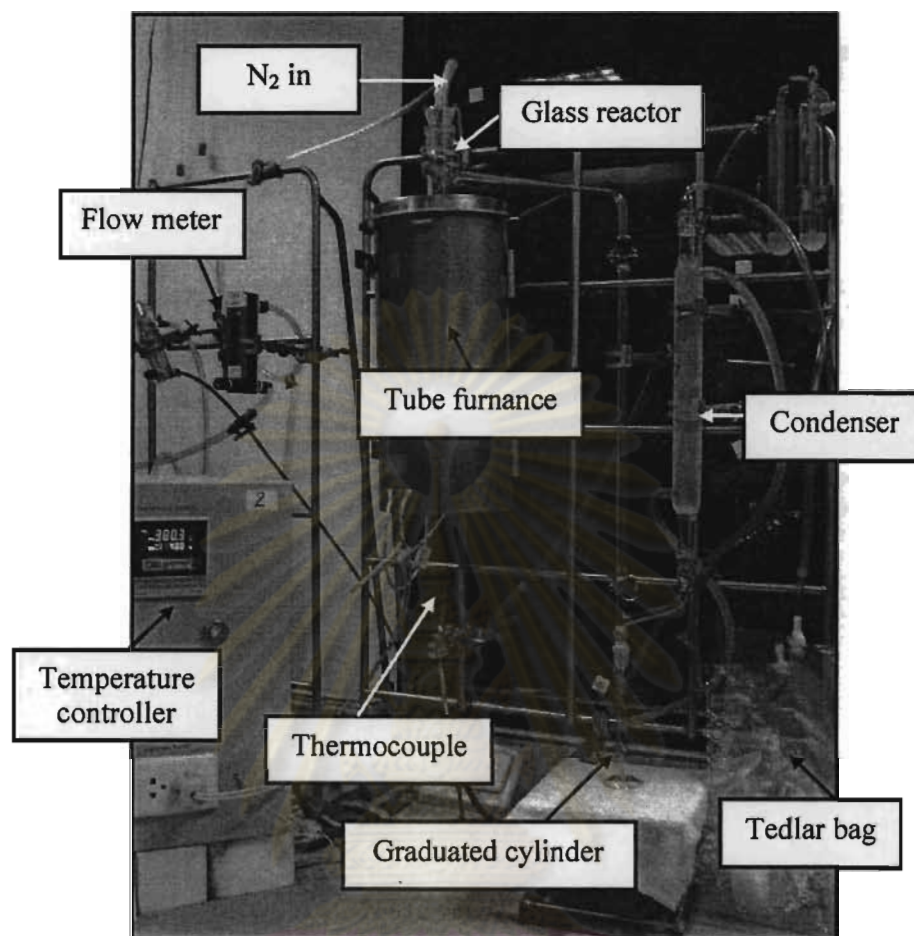


Figure 3.1 Apparatus for catalytic cracking

ศูนย์วิทยทรัพยากร
จุฬาลงกรณ์มหาวิทยาลัย

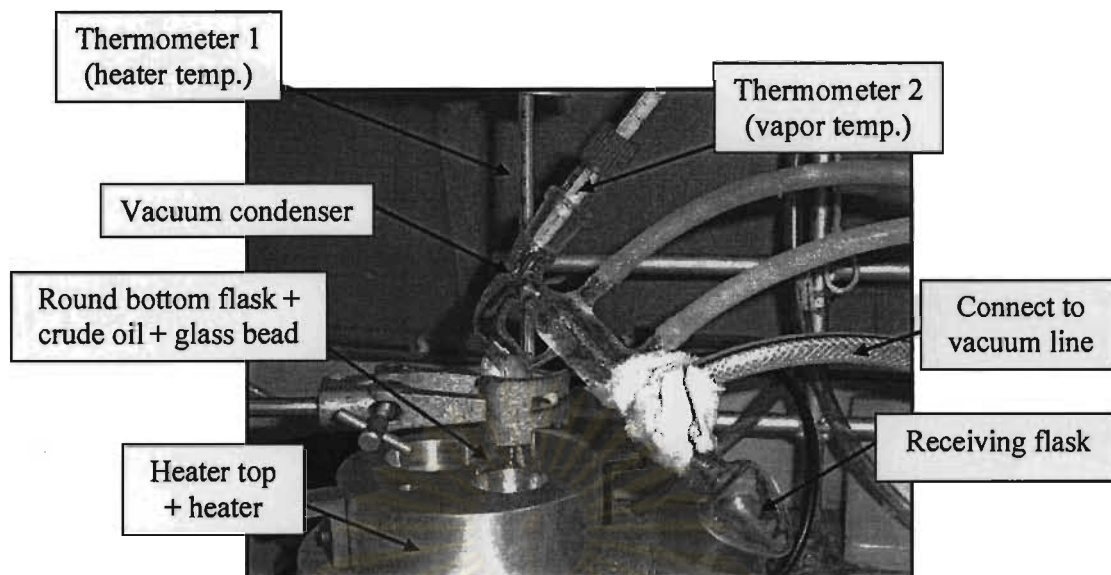
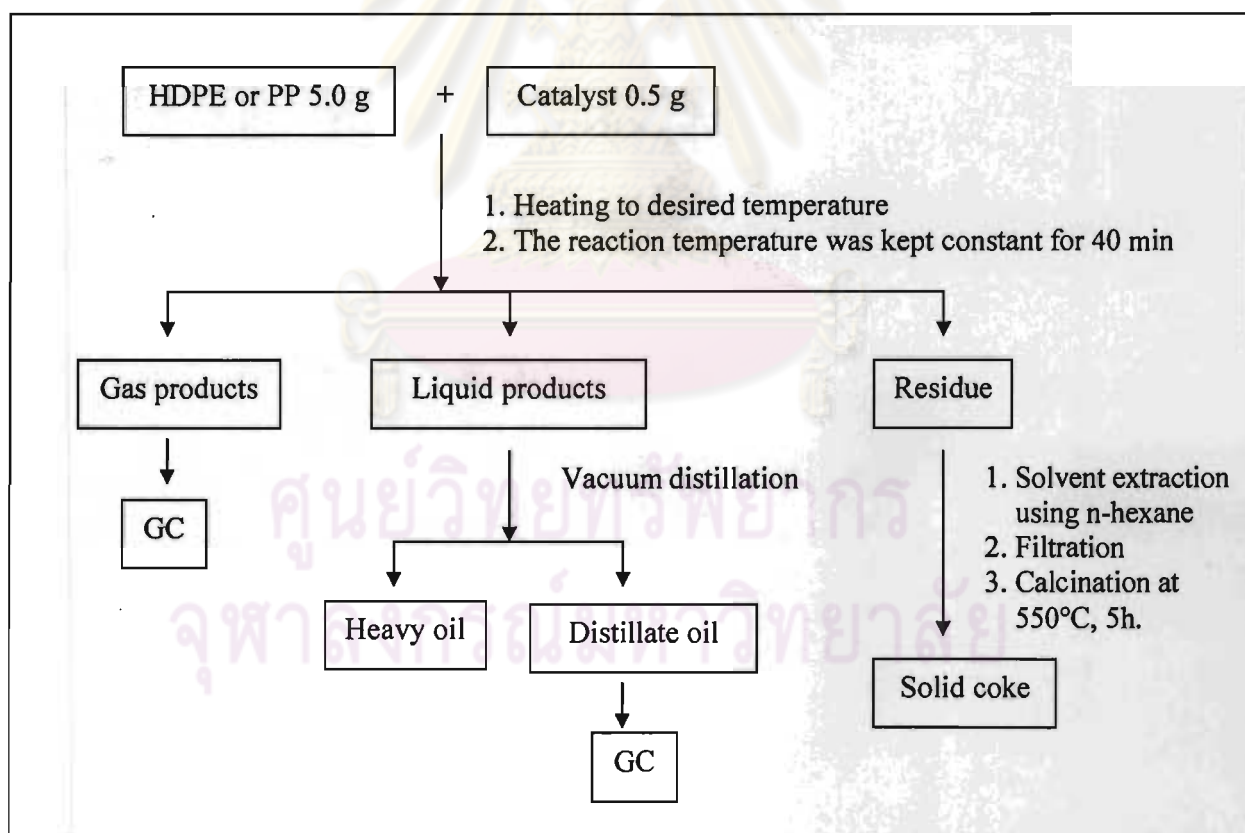


Figure 3.2 Apparatus for vacuum distillation



Scheme 3.5 Catalytic cracking of HDPE and PP using zeolite beta as catalyst.

3.11 Catalyst Regeneration

The spent catalyst (Beta20-US30-24h) from PP cracking at the reaction temperature of 380°C and HDPE cracking at the reaction temperature of 400°C from each cycle was regenerated by calcination in air at 550°C for 5 h. The regenerated catalysts were characterized by XRD, SEM, N₂ adsorption-desorption and test for its activity by catalytic cracking of PP at the reaction temperature of 380°C and HDPE at the reaction temperature of 400°C. The reaction was performed in the same way as what described in Section 3.8.1.



ศูนย์วิจัยทรัพยากร
จุฬาลงกรณ์มหาวิทยาลัย

CHAPTER IV

RESULTS AND DISCUSSION

4.1 Effect of Ultrasound Irradiation Periods on Formation of Zeolite Beta

4.1.1 XRD Results

XRD patterns of as-synthesized samples denoted as -US-, which were synthesized with ultrasound irradiation for various periods are presented in Figure 4.1 in comparison with the one prepared by normal method without ultrasound irradiation before crystallization. All XRD patterns of the samples are similar in intensities of two main characteristic peaks of zeolite beta structure at the Bragg angles, 2θ of 7.7° and 22.5° . They are similar to that reported by Aguado *et al.* [29] and no other crystalline phase was observed. For the calcined samples in Figure 4.2, the intensity of the peak at 2θ of 7.7° becomes much stronger than the peak at 2θ of 22.5° indicating the effect of template removal from the zeolite beta channels, whereas the intensity of the peak at 2θ of 22.5° is extremely decreased showing that dealumination occurs during the calcination process. The XRD patterns of those calcined samples consist of broad features, indicating the co-existence of both polymorphs A and B. This is common for zeolite beta and the two polymorphs are always formed simultaneously and hardly separated. The XRD patterns of calcined Beta60-US30-72h (B), Beta60-US60-72h (C), Beta60-US90-72h (D), and Beta60-US120-72h (E) catalysts are similar to the pattern of zeolite beta (Beta60-72h) synthesized normally without ultrasound irradiation (A). Additionally, the XRD peak intensities of all samples synthesized with ultrasound irradiation are similar to those of Beta60-72h. It can be concluded that applying ultrasound irradiation for 30-120 min during the gel formation step does not affect the structure and the crystallinity of zeolite beta.

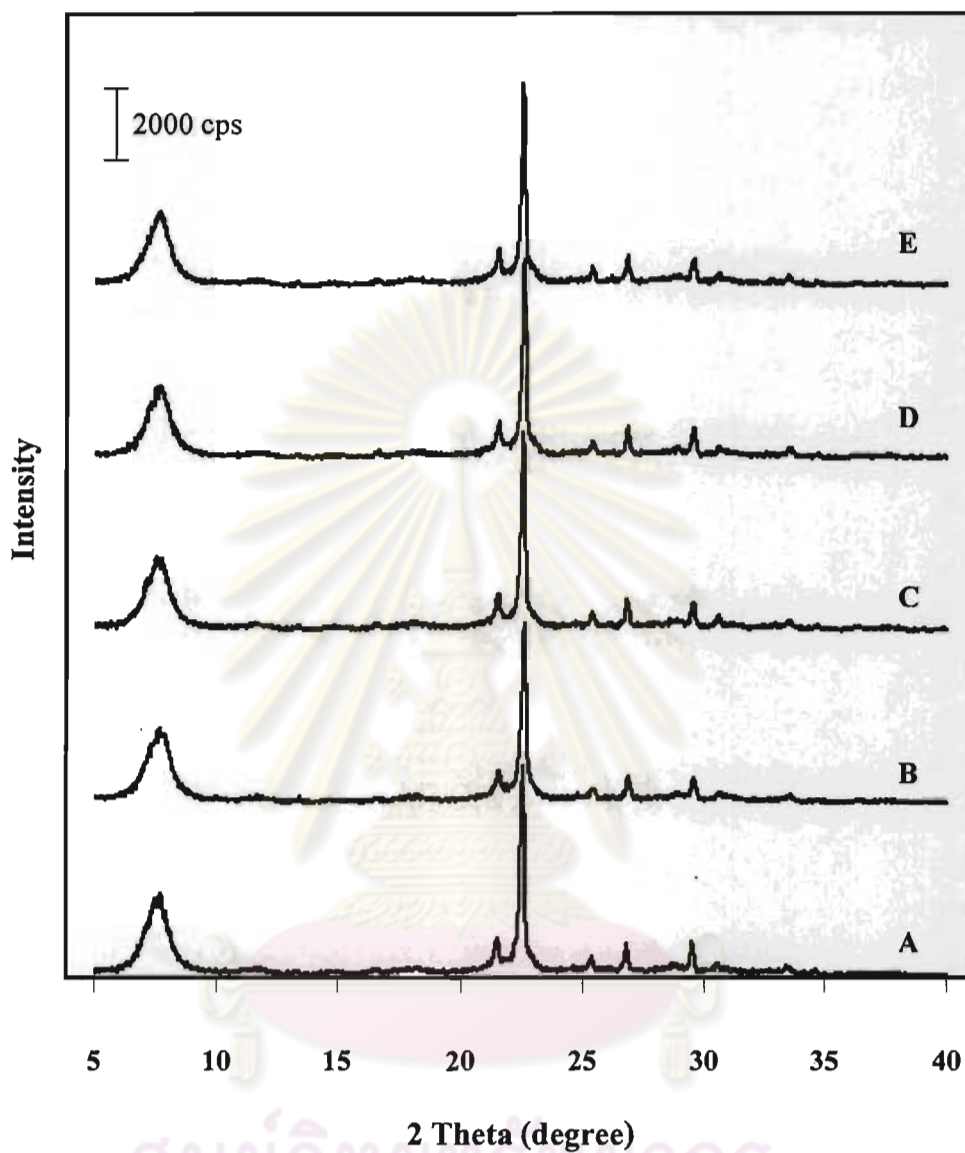


Figure 4.1 XRD patterns of the as-synthesized zeolite beta samples, (A) prepared without ultrasound irradiation; (B), (C), (D), and (E) synthesized with ultrasound irradiation for 30, 60, 90, and 120 min, respectively.

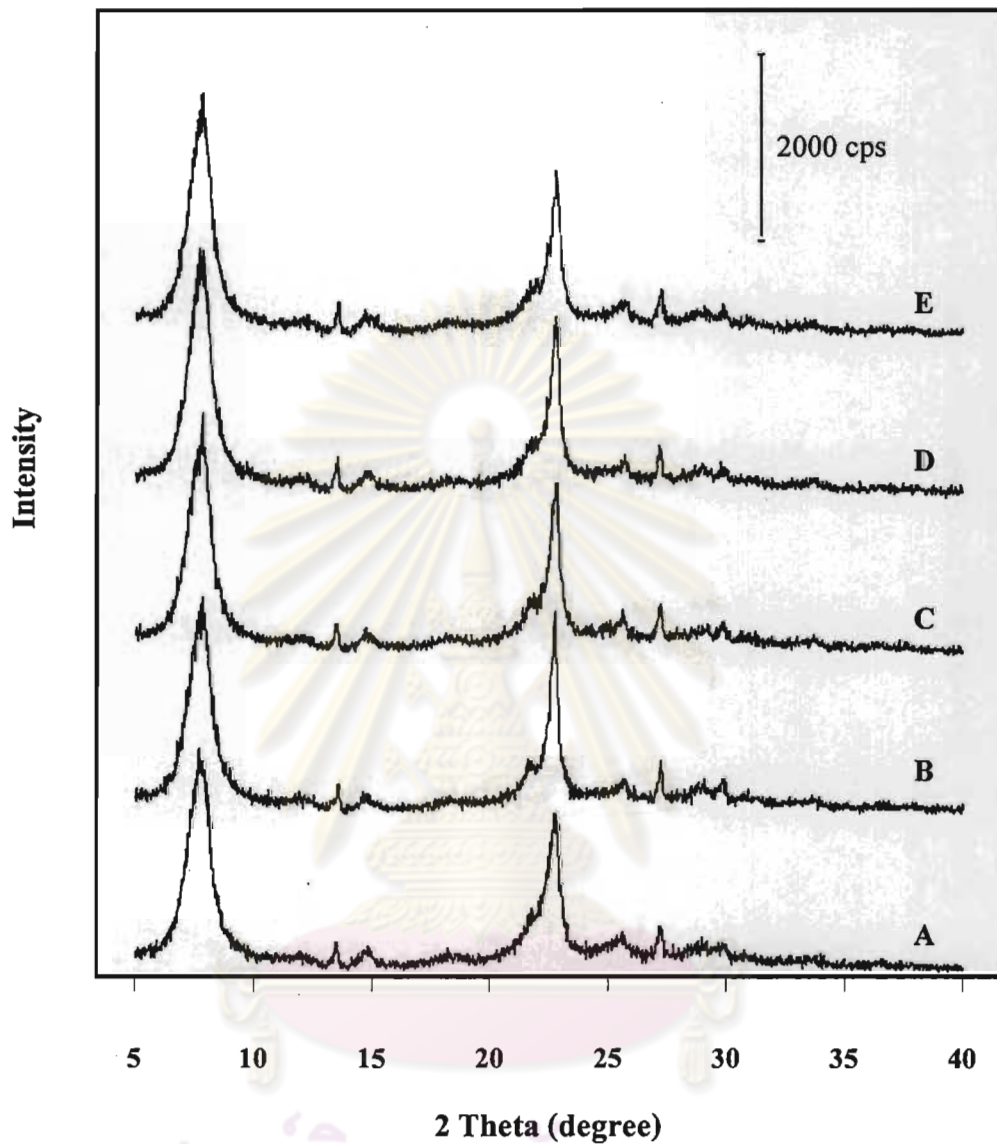


Figure 4.2 XRD patterns of the calcined zeolite beta samples, (A) prepared without ultrasound irradiation; (B), (C), (D), and (E) synthesized with ultrasound irradiation for 30, 60, 90, and 120 min, respectively.

4.1.2 SEM Images

SEM images of calcined zeolite beta synthesized without and with ultrasound irradiation for various periods are shown in Figure 4.3. All SEM images exhibits nano-particles of zeolite beta in uniform round granular shape. The average size of zeolite beta particles synthesized with ultrasound irradiation was about the same with the average size of 185 nm for all samples. Beta60-72h shows relatively smaller size about 170 nm. It is observed in Figure 4.3 that particles of zeolite beta prepared with ultrasound irradiation are slightly larger than the sample synthesized without application of ultrasound irradiation. It can also be illustrated that application of ultrasound irradiation accelerated nucleation and subsequent crystal growth and resulted in slightly larger particles of beta samples. This is in agreement with, Ö. Andaç. *et al.* [60]. Prolongation of irradiation period from 30 to 120 min does not affect the particle size of zeolite beta.



ศูนย์วิทยทรัพยากร
จุฬาลงกรณ์มหาวิทยาลัย

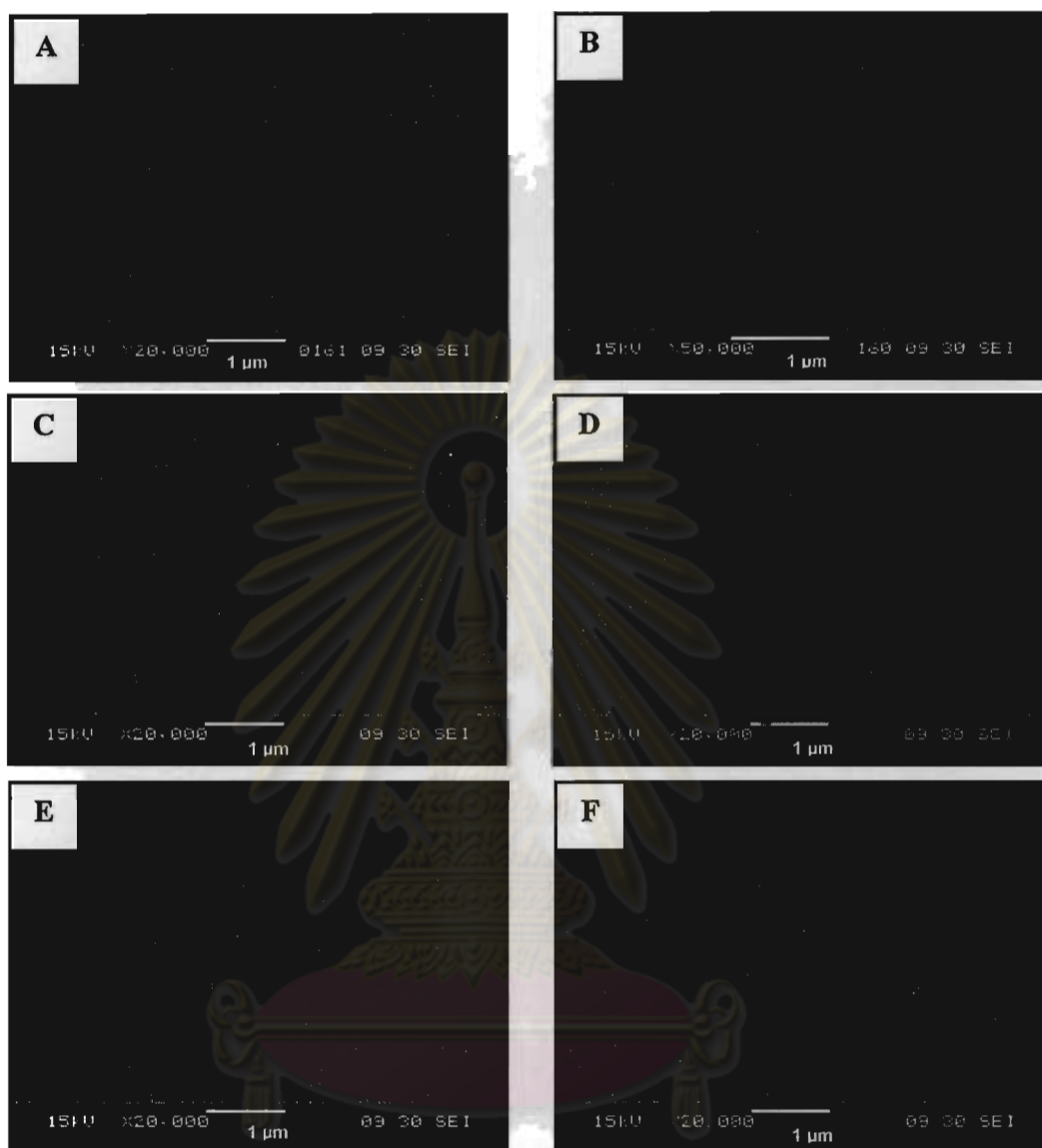


Figure 4.3 SEM images of calcined zeolite beta synthesized without and with ultrasound irradiation for various periods: (A) Beta60, (B) Beta60 with magnification of x 50,000 (C) Beta60-US30 (D) Beta60-US60 (E) Beta60-US90 and (F) Beta60-US120. All images are taken at the same magnification of x 20,000 except for (B).

4.1.3 Nitrogen Adsorption-Desorption

The N₂ adsorption-desorption isotherms of the calcined zeolite beta samples prepared without and with ultrasound irradiation in the gel formation step for various periods are illustrated in Figure 4.4. All samples exhibit a type I isotherm which is typical for microporous materials [52]. Only the isotherm of Beta60-72h is not superimposed with others and the plateau shows larger absorbed amount of nitrogen than other samples while the isotherms of the samples prepared with ultrasound irradiation gives almost the same isotherms. Each isotherm exhibits three different adsorption zones which are typical of nanocrystalline zeolites [78]. The first zone, adsorption at very low pressure corresponds to the nitrogen adsorption in the micropore system. At the medium partial pressure, the second zone is created by the nitrogen adsorption on the external surface. At high relative pressure ($P/P_0 > 0.8$), the third one rises steeply and presents a hysteresis loop indicating the presence of interparticular porosity [78].

Table 4.1 shows textural properties of calcined zeolite beta samples. Among the samples prepared with different period of ultrasound irradiation, they all exhibit the similar textural properties. The BET specific surface area and external surface area of Beta60-72h is higher than all samples prepared with ultrasound irradiation because of the smaller particle size of Beta60-72h. This agrees with the case of zeolite HZSM-5 result that the external surface area of HZSM-5 is increased when the crystal size reduces [78]. Furthermore an increase in ultrasound irradiation periods from 30 to 120 min does not significantly affect the BET surface area. Pore size distribution was obtained from the adsorption data by means of MP method as shown in Figure 4.5. The distribution of micropores is quite narrow and similar for all samples. The pore size distribution peaks of the calcined zeolite beta samples are centered at 0.6 nm.

It is obvious that the properties of zeolite beta samples synthesized with application of ultrasound from 30 to 120 min are not much different in terms of crystallinity, particle size and specific surface area. Therefore, the shortest ultrasound irradiation period (30 min) was chosen to study effect of crystallization time on formation of zeolite beta and the results are subject to be compared with samples prepared without application of ultrasound irradiation.

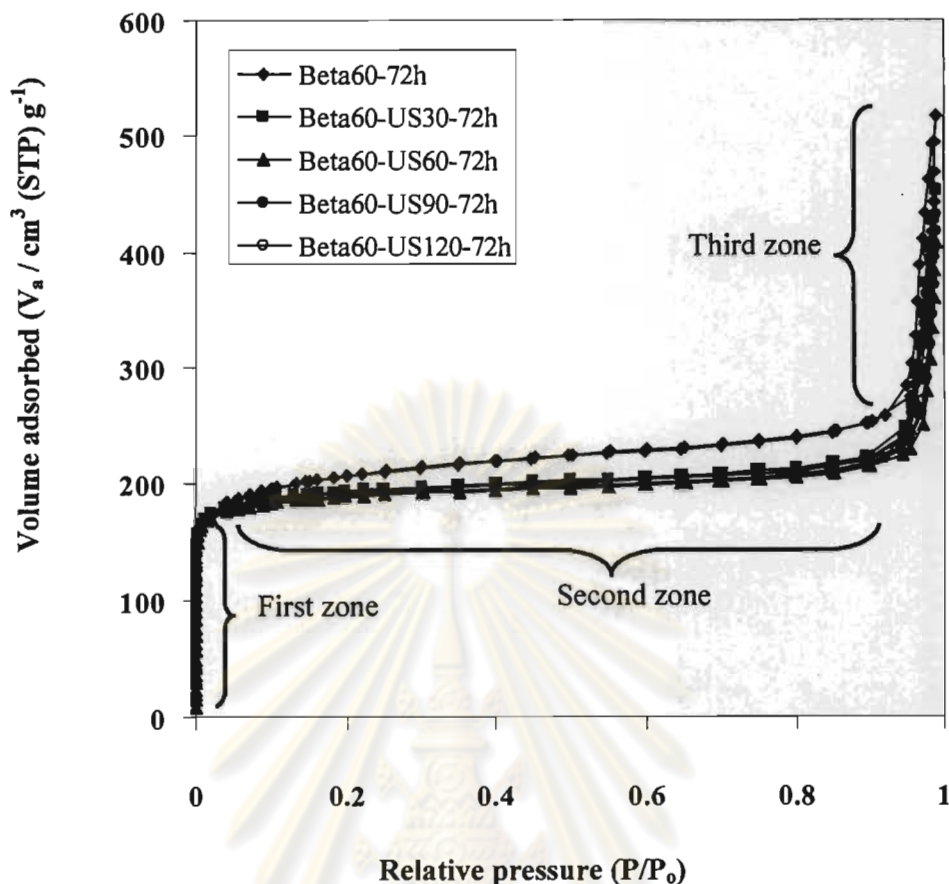


Figure 4.4 N₂ adsorption-desorption isotherms of zeolite beta samples prepared without and with the application of ultrasound irradiation in the gel formation step for various periods

Table 4.1 Textural properties of calcined zeolite beta samples

Sample	particle size ^a (nm)	S_{BET} ^b (m ² /g)	d_p ^c (nm)	S_{ext} ^d (m ² /g)	V_{micro} ^d (cm ³ /g)
Beta60-72h	169	781	0.6	65	0.31
Beta60-US30-72h	190	748	0.6	49	0.28
Beta60-US60-72h	195	729	0.6	43	0.28
Beta60-US90-72h	185	742	0.6	44	0.28
Beta60-US120-72h	181	736	0.6	45	0.28

^a particle size determined by SEM images

^b Specific surface area determined by application of the BET-plot method

^c particle size distribution determined by application of the MP-plot method

^d external surface area and micropore volume determined by application of the t-plot method

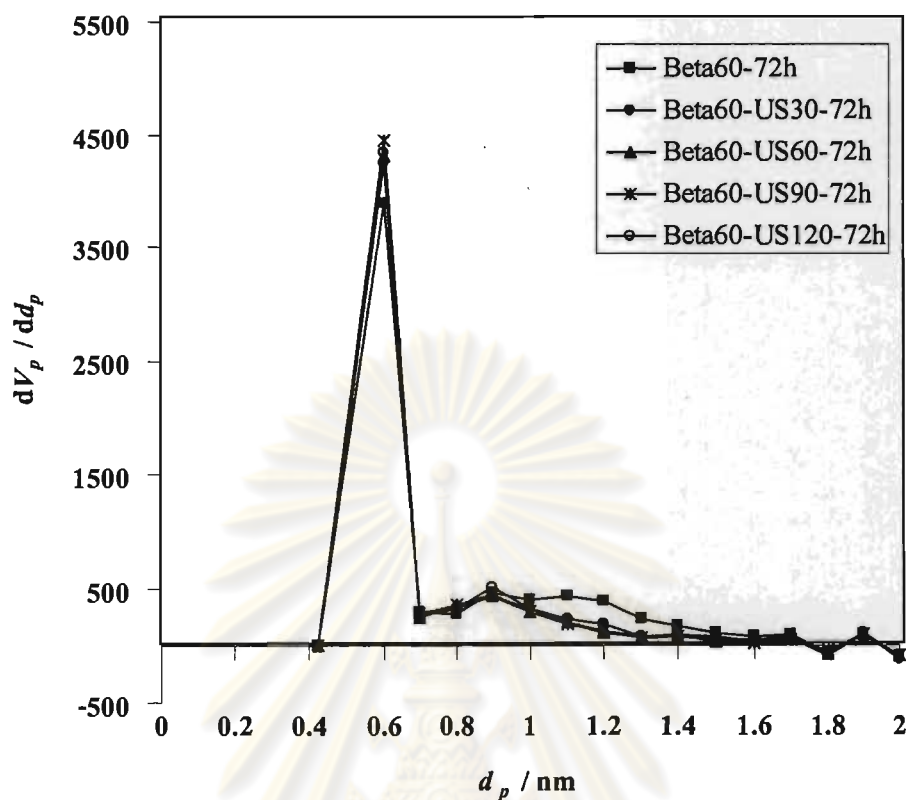


Figure 4.5 MP plots for pore-size distribution of calcined zeolite beta samples

4.2 Effect of Crystallization Time on Formation of Zeolite Beta

4.2.1 XRD Results

The effect of crystallization time from 8 to 96 h on formation of zeolite beta was studied for both methods, with and without employing ultrasound radiation. All XRD patterns of the as-synthesized products for both methods as shown in Figure 4.6 and 4.7 show two intense characteristic peaks of zeolite beta except for the samples crystallized for 8 h and 12 h showing no reflection peak. It indicates that only amorphous product was obtained. As a result, 12 h crystallization is not enough to form zeolite beta crystals. Upon prolongation of crystallization time at 135°C, formation of pure zeolite beta can be achieved after 16 h for both synthesis methods. The characteristic peak at 2θ of 22.5° reaches the maximum intensity after 20 h of crystallization for both synthesis routes. It is interesting that all beta samples prepared with employing ultrasound irradiation have higher peak intensities than those

prepared without ultrasound irradiation, indicating the higher crystallinity of the former.

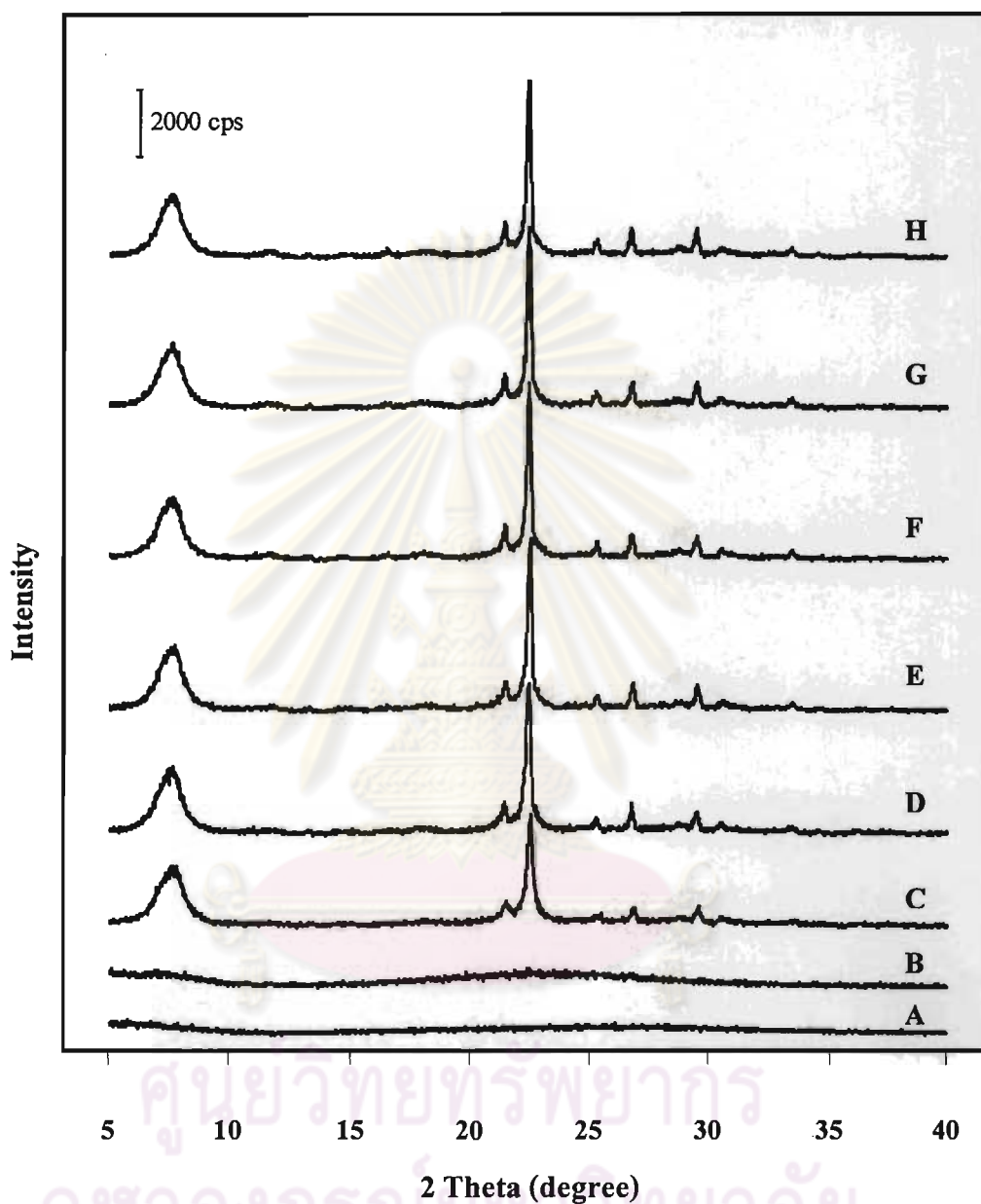


Figure 4.6 XRD patterns of the as-synthesized zeolite beta samples prepared with ultrasound irradiation and crystallized for various periods: (A) 8 h; (B) 12 h; (C) 16 h; (D) 20 h; (E) 24 h; (F) 48 h; (G) 72 h; and (H) 96 h

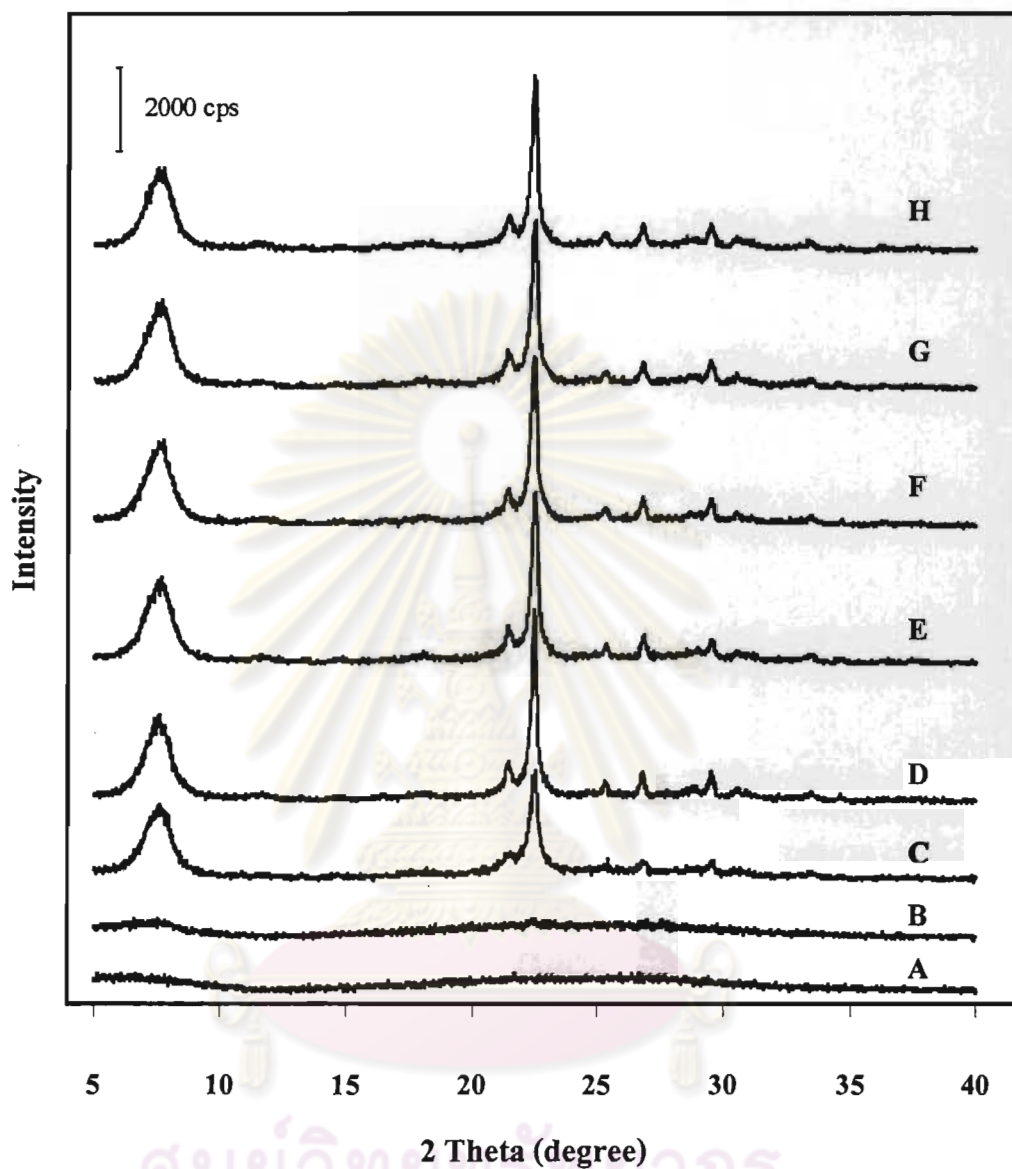


Figure 4.7 XRD patterns of the as-synthesized zeolite beta samples prepared without ultrasound irradiation and crystallized for various periods: (A) 8 h; (B) 12 h; (C) 16 h; (D) 20 h; (E) 24 h; (F) 48 h; (G) 72 h; and (H) 96 h

The XRD patterns of the calcined zeolite beta samples are shown in Figure 4.8 and 4.9. All calcined samples in both Figures show the tremendous increase in intensity of the low angle peak at 2θ of 7.7° due to the removal of the organic template. In general for several zeolites, the high angle peak at 2θ about 22° should maintain unchanged in intensity due to no effect of template removal. Nevertheless, it is always found for zeolite beta to have the significant decrease in intensity of the peak at 2θ of 22.5° after calcination. It implies that there must be some change concerning Si/Al ratio of the zeolite, *i.e.* the migration of aluminum from the framework position to non-framework position. This is also evidenced by the observation of a peak of non-framework aluminum in ^{27}Al -NMR spectra of the calcined samples to be discussed later. Employing ultrasound radiation during the synthesis course, results in less extent of decrease in intensity of this peak. This indicates that applying ultrasound radiation can prevent the migration of aluminum.



ศูนย์วิทยทรัพยากร
จุฬาลงกรณ์มหาวิทยาลัย

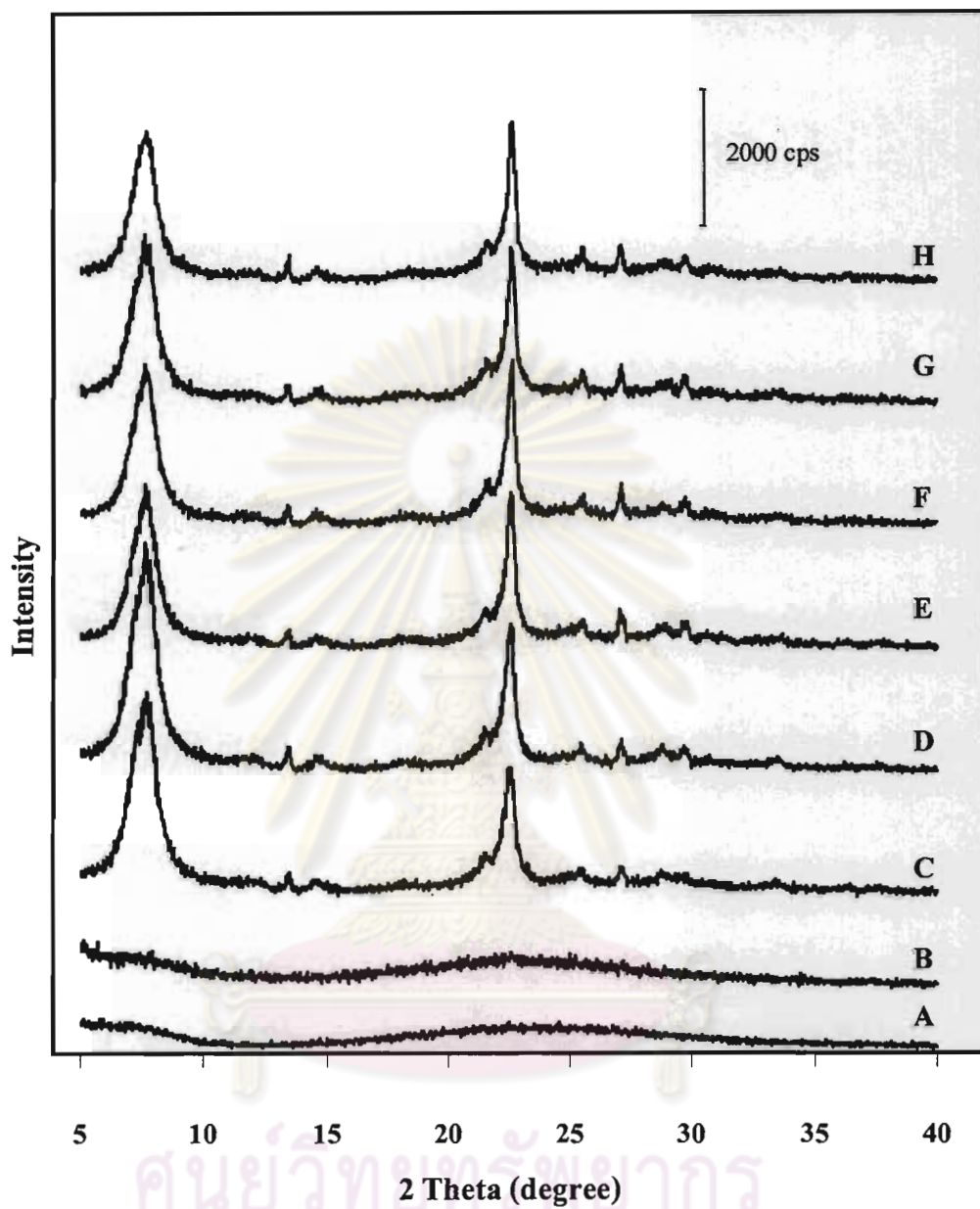


Figure 4.8 XRD patterns of the calcined zeolite beta samples synthesized with ultrasound irradiation and crystallized for various periods: (A) 8 h; (B) 12 h; (C) 16 h; (D) 20 h; (E) 24 h; (F) 48 h; (G) 72 h; and (H) 96 h

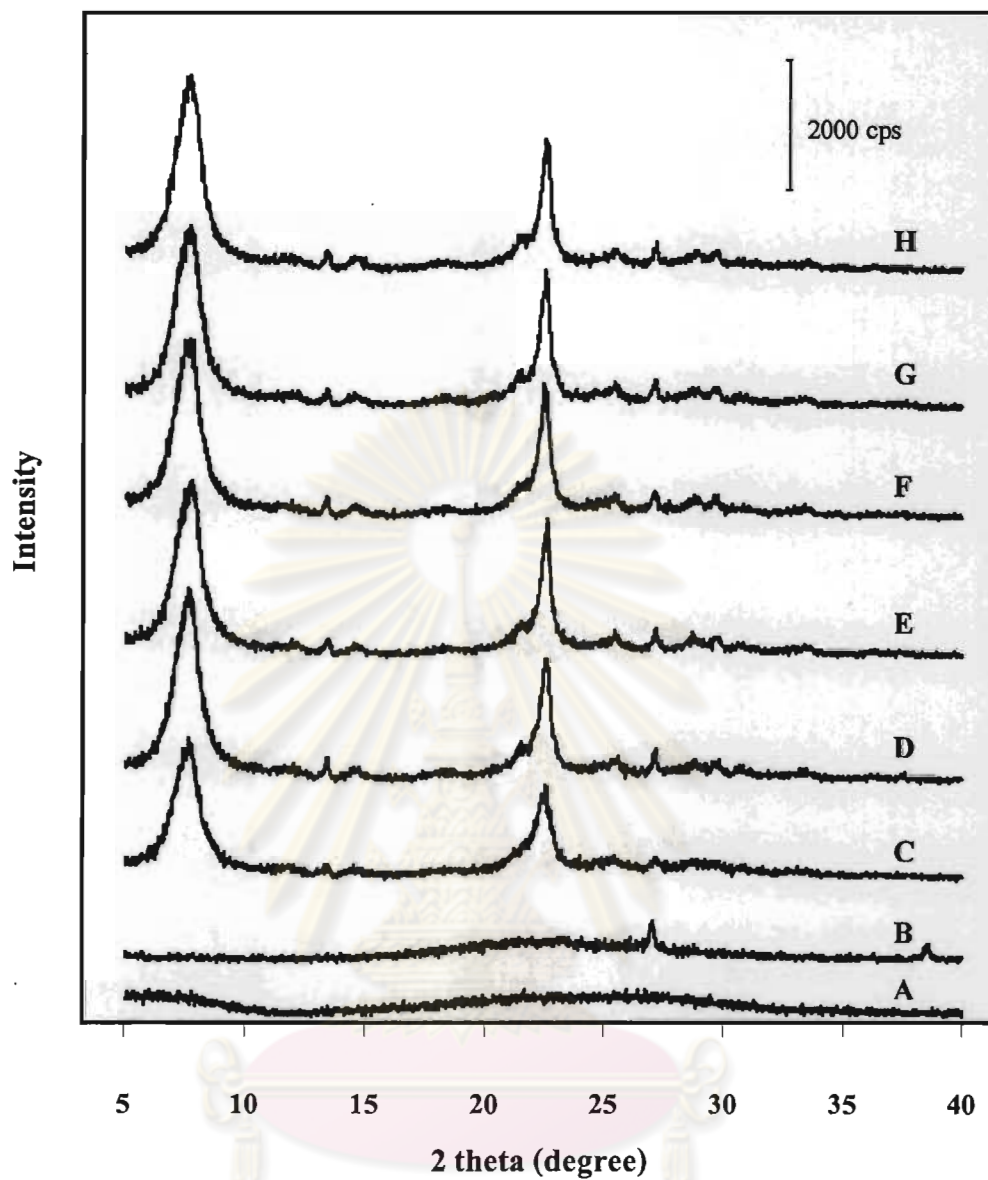


Figure 4.9 XRD patterns of the calcined zeolite beta samples synthesized without ultrasound irradiation and crystallized for various periods: (A) 8 h; (B) 12 h; (C) 16 h; (D) 20 h; (E) 24 h; (F) 48 h; (G) 72 h; and (H) 96 h

4.2.2 SEM Images

SEM images of zeolite beta synthesized without ultrasound irradiation show amorphous phase in chunks of the starting silica gel in Figure 4.10A as well as of the sample crystallized for 12 h as shown in Figure 4.10B. After 16 h or longer crystallization time, chunky particles disappeared while nano-particles in uniform spherical shape of zeolite beta were observed as shown in Figure 4.10C-H. The longer crystallization time, the larger crystal size and particle size of zeolite beta are, but it is not significant after longer than 20 h. The smallest particle size is 165 nm and the largest size is 173 nm. In the case of employing ultrasound irradiation as shown in Figure 4.11, the SEM images show results in the same way but slightly larger particle size than the case without employing ultrasound radiation, *i.e.* the smallest particle size is 190 nm and the largest size is 208 nm when they were crystallized for 24-96 h. It can also be experienced that ultrasound irradiation caused the white reactant slurry turned to homogeneous condensed gel rapidly, resulting in accelerated crystal growth.

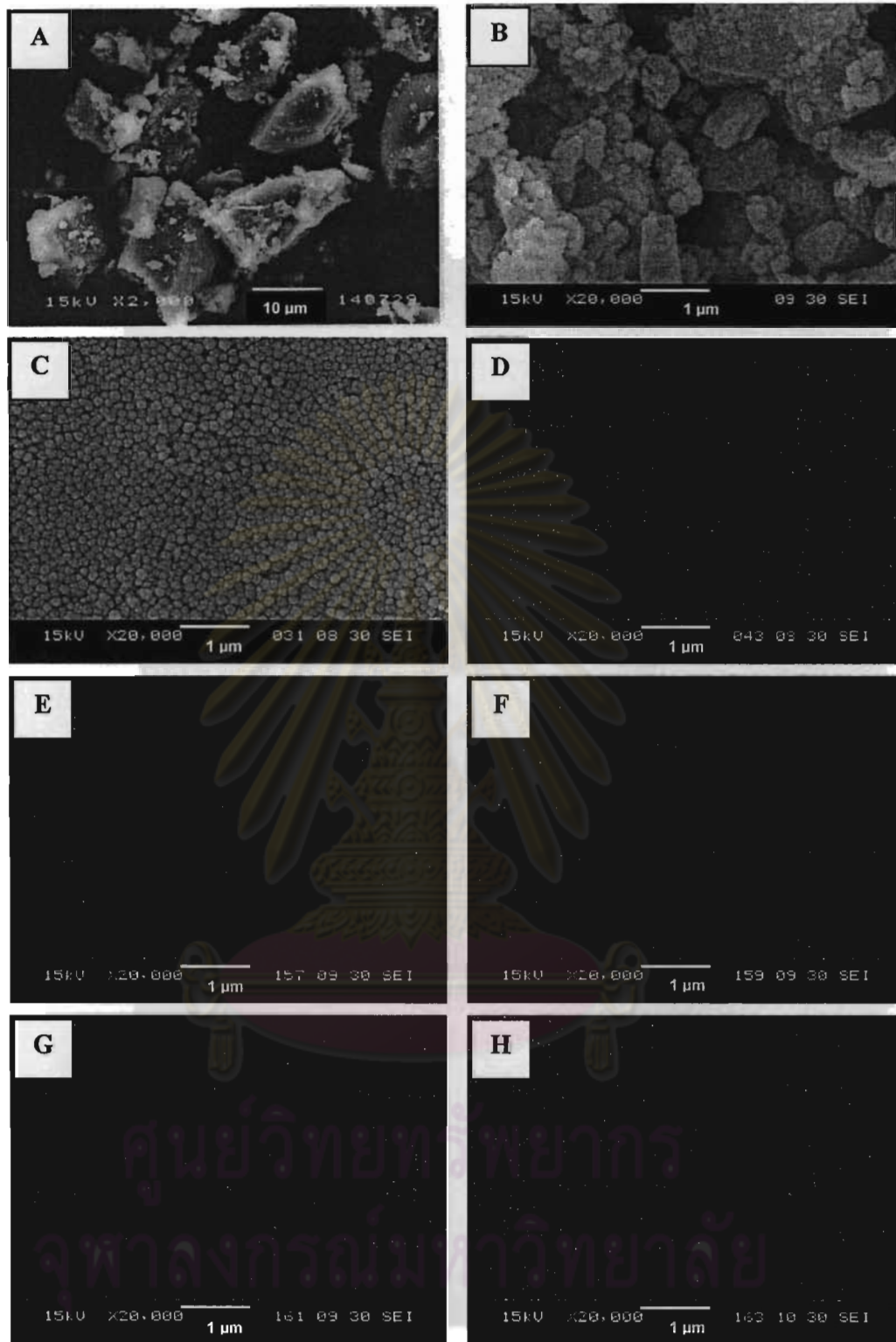


Figure 4.10 SEM images of (A) xerogel and (B-H) Beta60 samples crystallized at 135°C for various periods: (B) 12 h; (C) 16 h; (D) 20 h; (E) 24 h; (F) 48 h; (G) 72 h and (H) 96 h

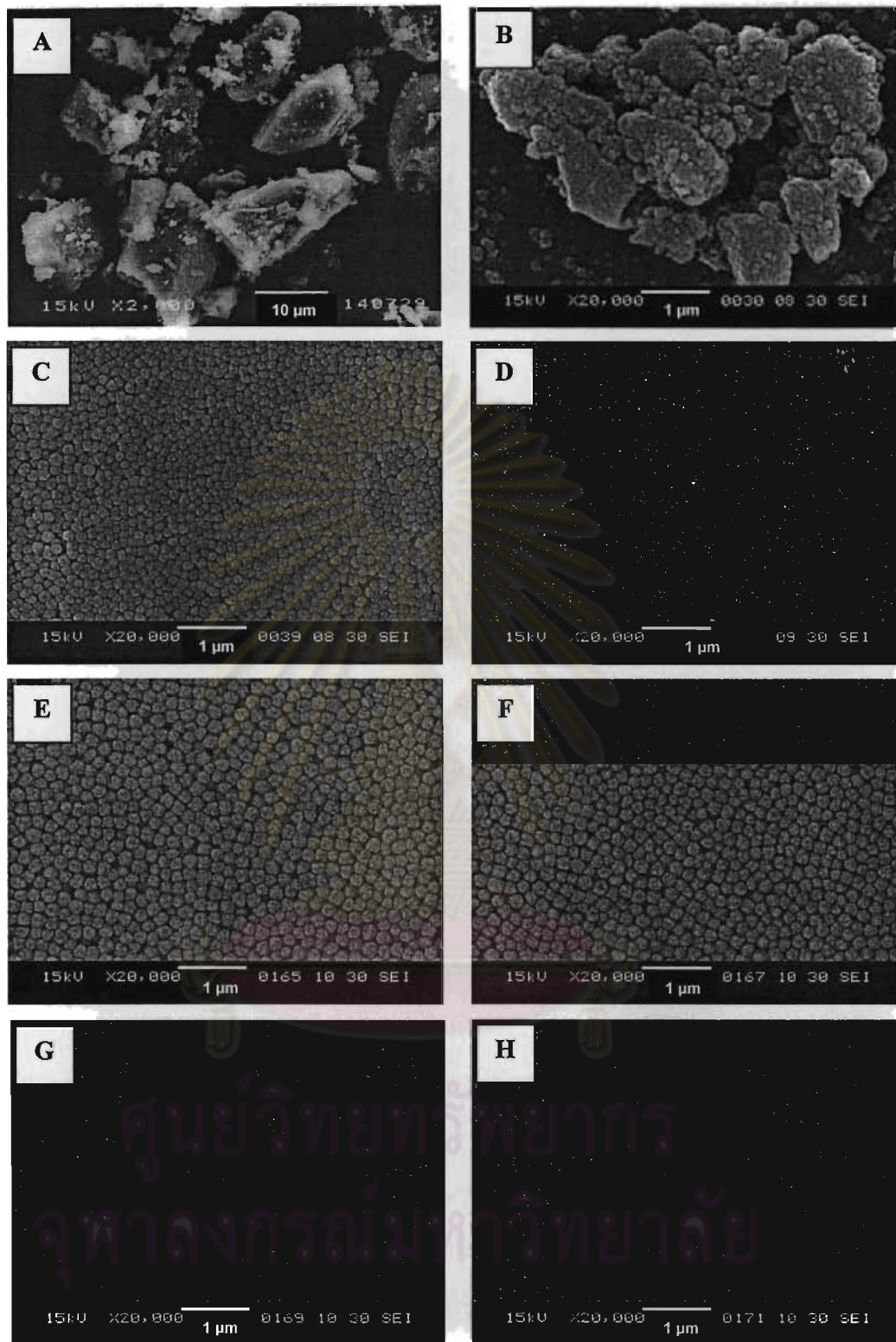


Figure 4.11 SEM images of (A) xerogel and (B-H) Beta60-US30 samples crystallized at 135°C for various periods: (B) 12 h; (C) 16 h; (D) 20 h; (E) 24 h; (F) 48 h; (G) 72 h and (H) 96 h

4.2.3 Nitrogen Adsorption-Desorption

Figure 4.12 shows the adsorption-desorption isotherms of the calcined zeolite beta samples prepared without ultrasound irradiation. In Figure 4.12A, silica xerogel exhibits a type IV adsorption-desorption isotherm which is a characteristic of mesoporous material. After the gel mixture was crystallized for at least 16 h, the steep adsorption was observed at very low relative pressure, giving a so-called type I isotherm which is typical for microporous materials. Figure 4.12B depicts the same adsorption-desorption isotherm of Beta60 crystallized for 24 – 96 h. Considering at extremely high relative pressure ($P/P_0 > 0.8$), each of zeolite samples exhibits the unusual second step of isotherm, indicating the existence of mesoporosity on external surface of the zeolite samples. This observation has been reported for nanoparticle zeolites [11-12]. The smaller the particles, the greater mesoporous volume is. Among the zeolite products, Beta60-16h shows the greatest mesoporous volume as well as the highest external surface area as shown in Table 4.2. Figure 4.13 presents the adsorption-desorption isotherms of calcined zeolite beta samples prepared with ultrasound irradiation. It can be described in the same way.

The textural properties of the samples crystallized for various periods are compiled in Table 4.2 and 4.3. The BET specific surface areas of all zeolite beta samples are higher than silica xerogel. For both methods, the BET specific surface areas reach to maximum value when of zeolite beta samples were crystallized for 24 h. Prolongation of crystallization time from 24 h to 96 h does not significantly change the BET specific surface areas. By comparing the %product yield from the two methods, zeolite beta samples synthesized with ultrasound irradiation gives %product yield higher than those without employing ultrasound radiation, indicating that the ultrasound irradiation increases number of nucleation center resulting the higher yield of zeolite beta. This result is in agreement with literature [60] that the yield of zeolite A enhances due to an effect of ultrasound radiation.

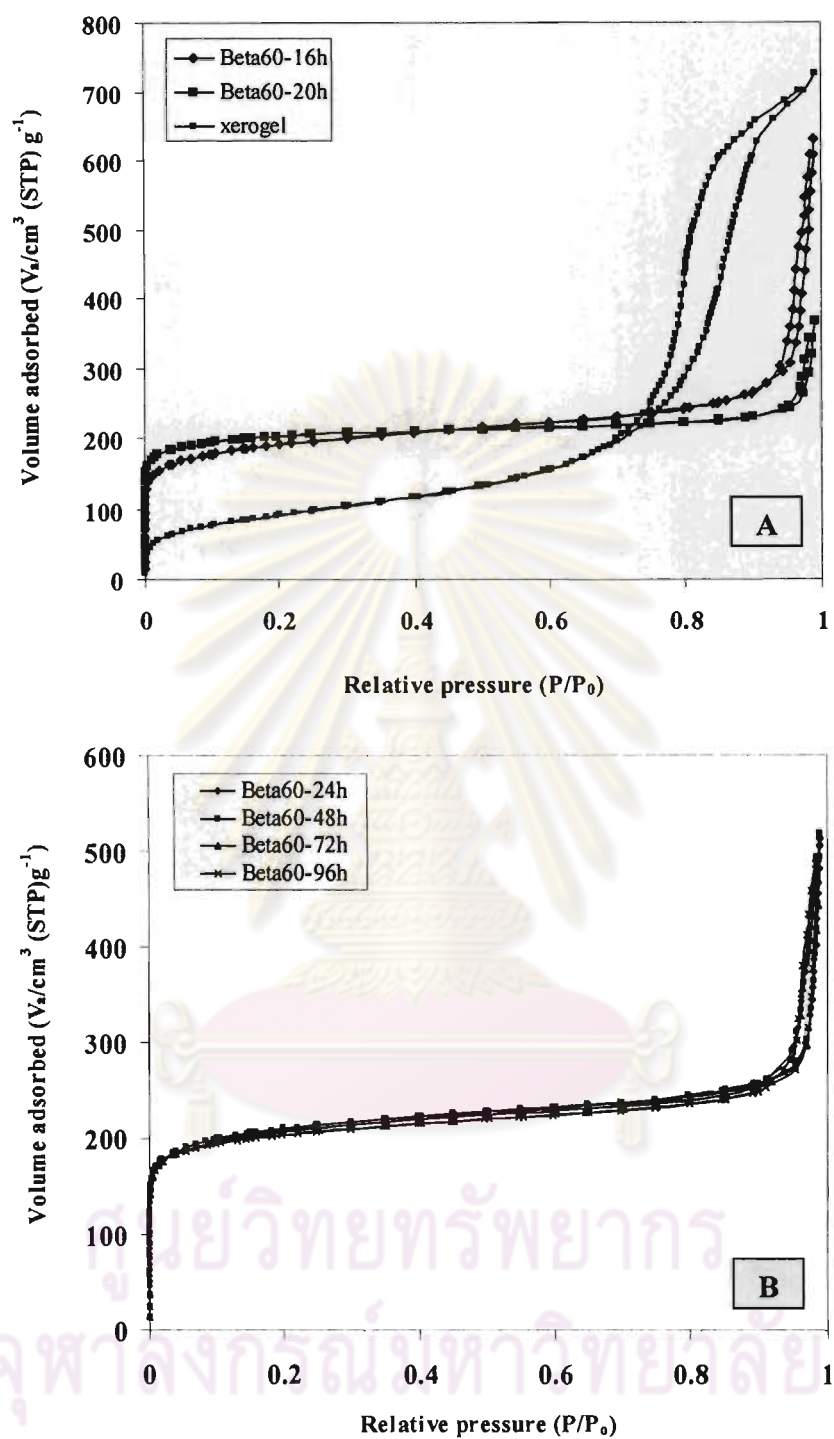


Figure 4.12 N_2 adsorption-desorption isotherms of calcined zeolite beta prepared without ultrasound irradiation: (A) silica xerogel and samples crystallized for 16 and 20 h, (B) samples crystallized for 24 - 96 h

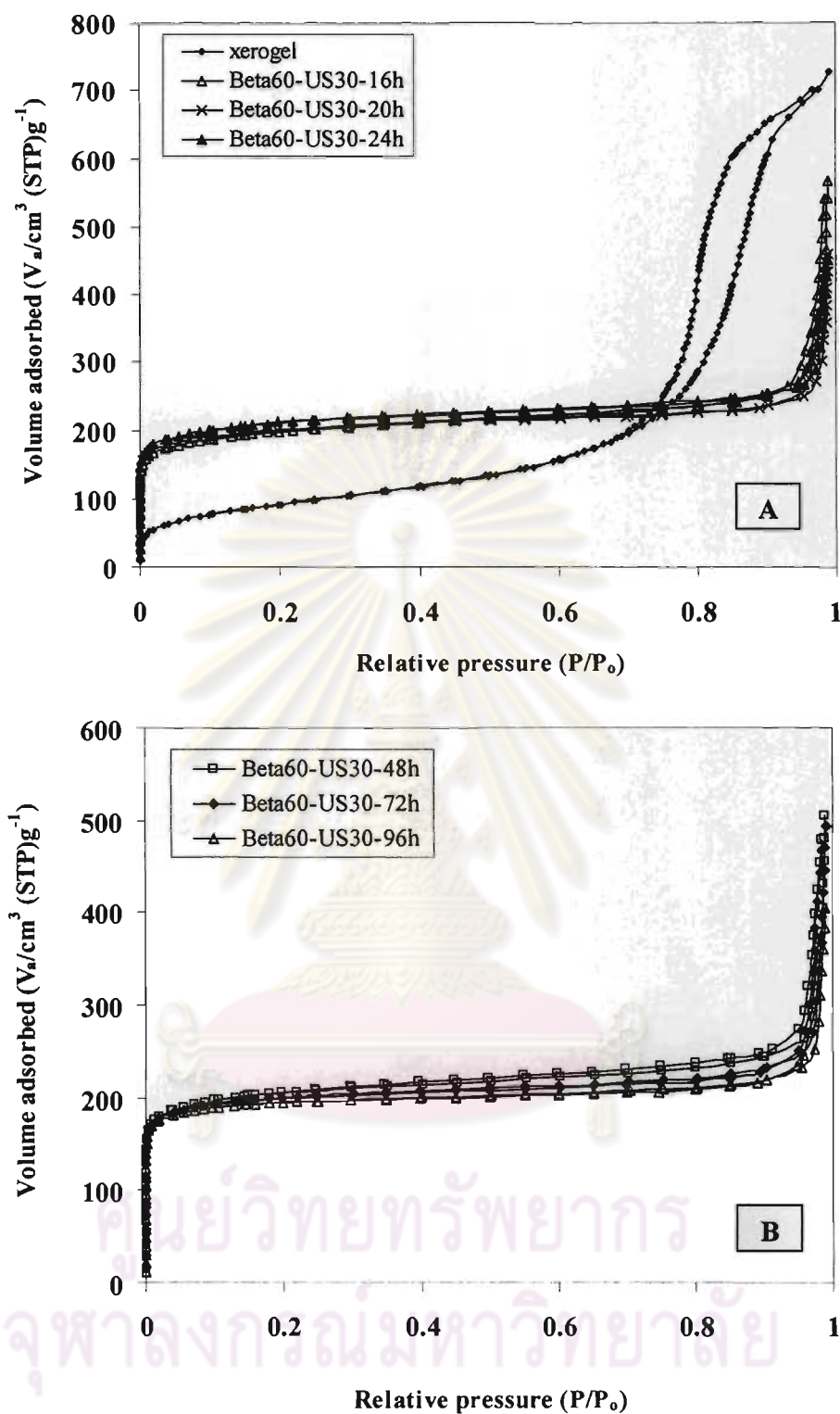


Figure 4.13 N_2 adsorption-desorption isotherms of calcined zeolite beta prepared with the application of ultrasound irradiation and with various periods of crystallization: (A) silica xerogel and samples crystallized for 16 and 24 h, (B) samples crystallized for 48 - 96 h

Table 4.2 Textural properties of calcined zeolite beta samples synthesized without ultrasound irradiation

Sample	particle size ^a (nm)	%yield ^b	S _{BET} ^c (m ² /g)	d _p ^d (nm)	S _{ext} ^e (m ² /g)	Micropore volume ^e (cm ³ /g)
Silica xerogel	10,000	-	333	13.9	313.6	-
Beta60-16h	161	0.7	719	0.6	109.3	0.27
Beta60-20h	196	3.5	712	0.6	44.5	0.28
Beta60-24h	173	5.8	784	0.6	65.9	0.31
Beta60-48h	165	6.7	784	0.6	67.9	0.31
Beta60-72h	169	7.8	781	0.6	64.8	0.31
Beta60-96h	170	8.4	771	0.6	66.9	0.30

^a particle size determined by SEM images

^b Gram of solid per 100g of starting gel

^c Specific surface area determined by application of the BET-plot method

^d particle size distribution determined by application of the MP-plot method

^e external surface area and micropore volume determined by application of the t-plot method

Table 4.3 Textural properties of calcined zeolite beta samples synthesized with ultrasound irradiation

Sample	particle size ^a (nm)	%yield ^b	S _{BET} ^c (m ² /g)	d _p ^d (nm)	S _{ext} ^e (m ² /g)	Micropore volume ^e (cm ³ /g)
Silica xerogel	10,000	-	333	13.9	313.6	-
Beta60-US30-16h	160	1.8	732	0.6	79.3	0.29
Beta60-US30-20h	196	7.8	747	0.6	49.4	0.30
Beta60-US30-24h	190	8.5	784	0.6	62.4	0.31
Beta60-US30-48h	195	9.7	780	0.6	61.6	0.30
Beta60-US30-72h	202	11.1	768	0.6	48.4	0.30
Beta60-US30-96h	208	13.4	754	0.6	39.1	0.29

^a particle size determined by SEM images

^b Gram of solid per 100g of starting gel

^c Specific surface area determined by application of the BET-plot method

^d particle size distribution determined by application of the MP-plot method

^e external surface area and micropore volume determined by application of the t-plot method

Figure 4.14 shows the mesopore distribution of amorphous xerogel obtained from the N_2 adsorption data using the Barrett, Joyner and Halenda (BJH) method. The distribution peak of mesopores is broad and centered at about 13.9 nm. The pore size distributions of Beta60 and Beta60-US30 samples which are obtained from the adsorption data by means of MP method are shown in Figure 4.15 and 4.16, respectively. All zeolite beta samples exhibit the narrow distribution of micropores with the same pore size about 0.6 nm.

From the results shown above, crystallization time of 24 h should be suitable for both synthesis methods, with and without ultrasound irradiation, since it is the shortest time showing the highest BET specific surface area. However, the tests for activities of these zeolite beta samples in the catalytic cracking of PP were carried out to confirm this hypothesis.

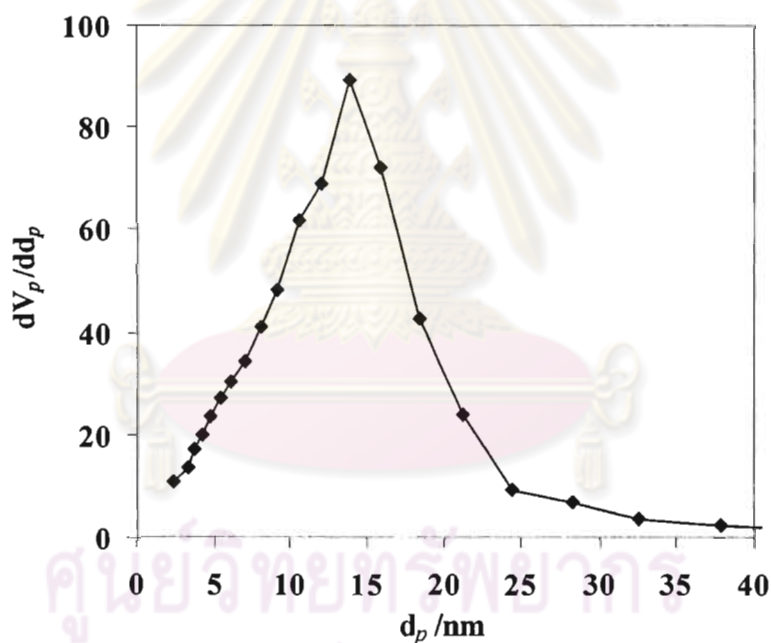


Figure 4.14 BJH pore-size distribution of silica xerogel

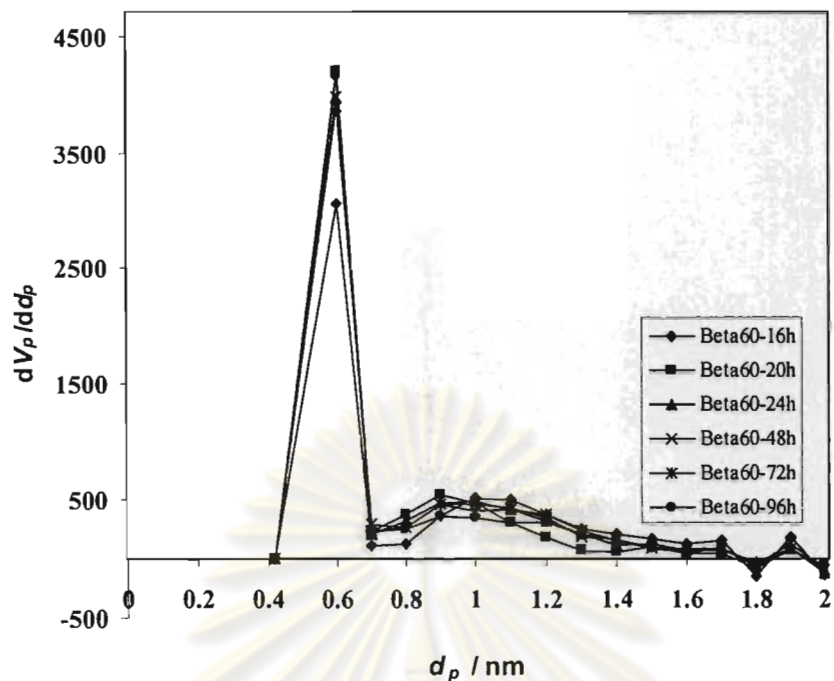


Figure 4.15 MP pore-size distributions of zeolite beta samples synthesized without ultrasound irradiation and with various periods of crystallization

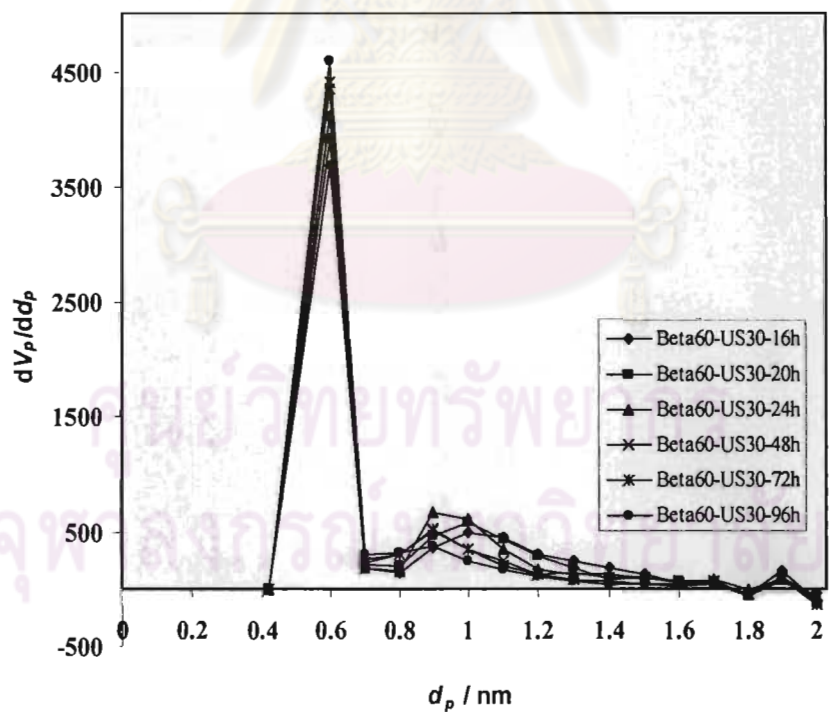


Figure 4.16 MP pore-size distributions of zeolite beta samples synthesized with ultrasound irradiation and with various periods of crystallization

4.3 Effect of the Si/Al Ratios on Formation of Zeolite Beta

4.3.1 Elemental Analysis

Table 4.4 shows the Si/Al mole ratios in gel and in catalyst of the samples prepared with and without employing ultrasound radiation. It was clearly observed that the Si/Al mole ratios in catalyst of all samples prepared in this work were less than the Si/Al ratios in gel which were calculated from reagent quantities. The large aluminum content determined by the ICP-AES technique is total content of both framework and non-framework aluminum species. Only the data from ICP-AES technique can not classify the aluminum species, whether it is located at the tetrahedral framework or octahedral non-framework species. Consequently, supportive data from ^{27}Al -NMR is needed. In addition, there is no significant difference between the Si/Al ratios in catalyst for the analogous samples synthesized from the same Si/Al ratio in gel except for Beta20-24h and Beta20-US30-24h, both of which were prepared from the gel with Si/Al ratio of 20. The Si/Al molar ratio in catalyst of Beta20-US30-24h is lower than Beta20-24h, indicating the larger aluminum content in Beta20-US30-24h.

Table 4.4 Comparison of calcined zeolite beta samples with different Si/Al ratios

Sample	Si/Al molar ratio in gel ^a	Si/Al molar ratio in catalyst ^b
Beta10-24h*	10	-
Beta20-24h	20	15.0
Beta40-24h	40	23.6
Beta60-24h	60	27.7
Beta80-24h	80	27.6
Beta10-US30-24h*	10	-
Beta20-US30-24h	20	11.6
Beta40-US30-24h	40	22.9
Beta60-US30-24h	60	28.2
Beta80-US30-24h	80	26.9

- ^a calculated from reagent quantities.
- ^b Aluminum (Al) was determined by ICP-AES and Si was calculated from the deduction of AlO_2 from the sample weight.
- * XRD patterns present amorphous phase.

4.3.2 XRD Results

XRD patterns of calcined zeolite beta samples with different Si/Al ratios in catalyst are revealed in Figure 4.17 and 4.18. According to the XRD results, zeolite beta with Si/Al ratios in gel of 10 presents no X-ray peak indicating amorphous phase, no matter ultrasound radiation was applied or not. It implies that longer crystallization time is necessary for this case or the methods are not appropriate for preparing zeolite beta with too low Si/Al ratio. With the Si/Al ratios of 20 – 80 in gel, the well-define structure of zeolite beta was found in the XRD patterns of all samples. The samples with the Si/Al ratio in gel of 60 show the highest relative peak intensities for both synthesis methods. The influence of ultrasound irradiation is clearly observed for the samples with Si/Al ratio of 20. In the case of application of ultrasound radiation, the Beta20-US30-24h sample exhibits much lower peak intensity than the one without ultrasound irradiation. This result suggests that ultrasound enhances incorporation of aluminum into structure of the zeolite better than other Si/Al ratios. It is known that the greater amount of aluminum incorporated into a zeolite structure, the less ordered structure and the less resulted crystallinity of the zeolite will be obtained. The exceptional high content of aluminum in the Beta20-US30-24h sample is confirmed by the results of elemental analysis in Table 4.4. However, the crystallinity may not be the most important for cracking of plastics. Other properties such as external surface area must be considered along with the acidity of catalysts.

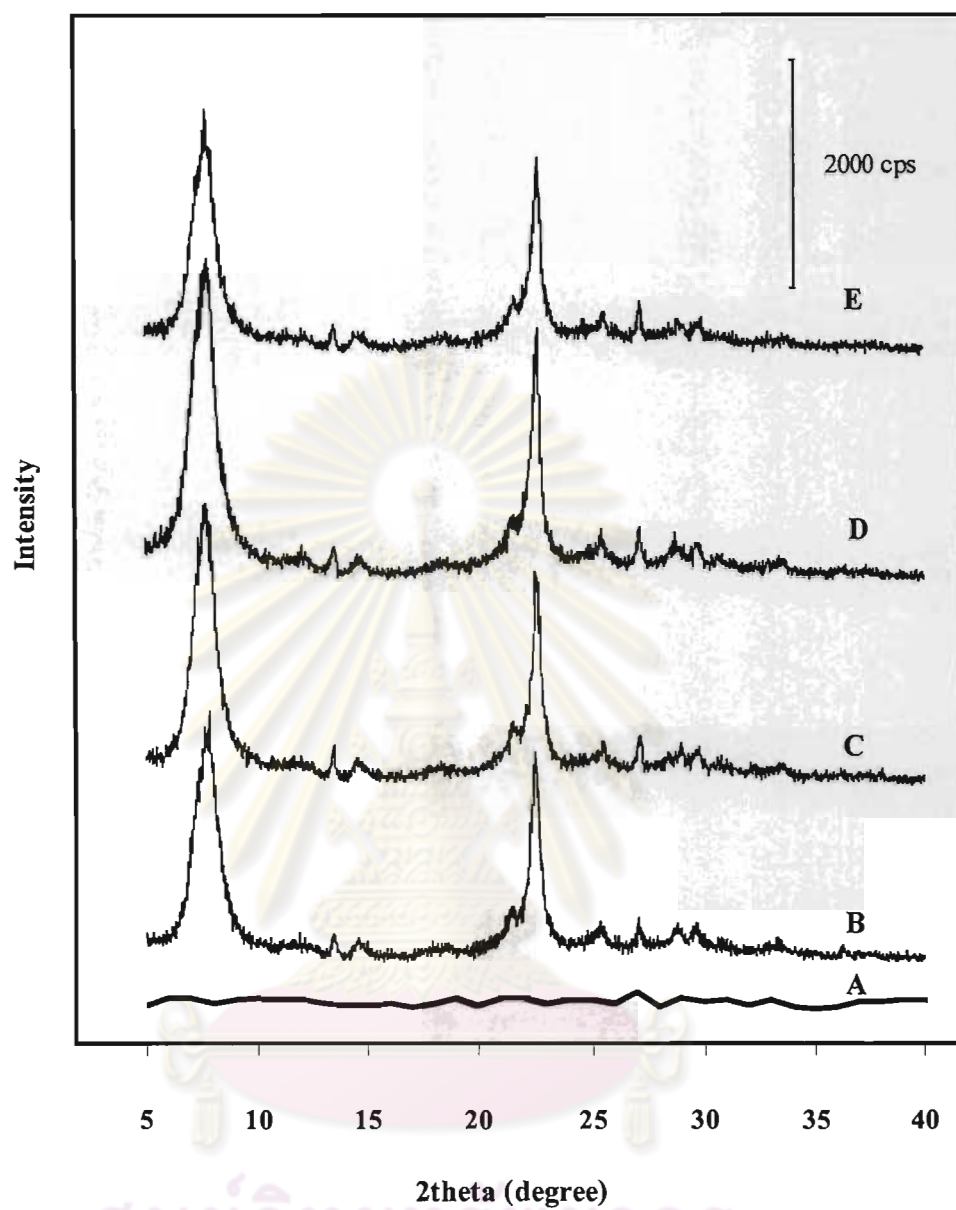


Figure 4.17 XRD patterns of calcined zeolite beta catalysts prepared without ultrasound irradiation and with different Si/Al ratios in gel: (A) 10; (B) 20; (C) 40; (D) 60; and (E) 80

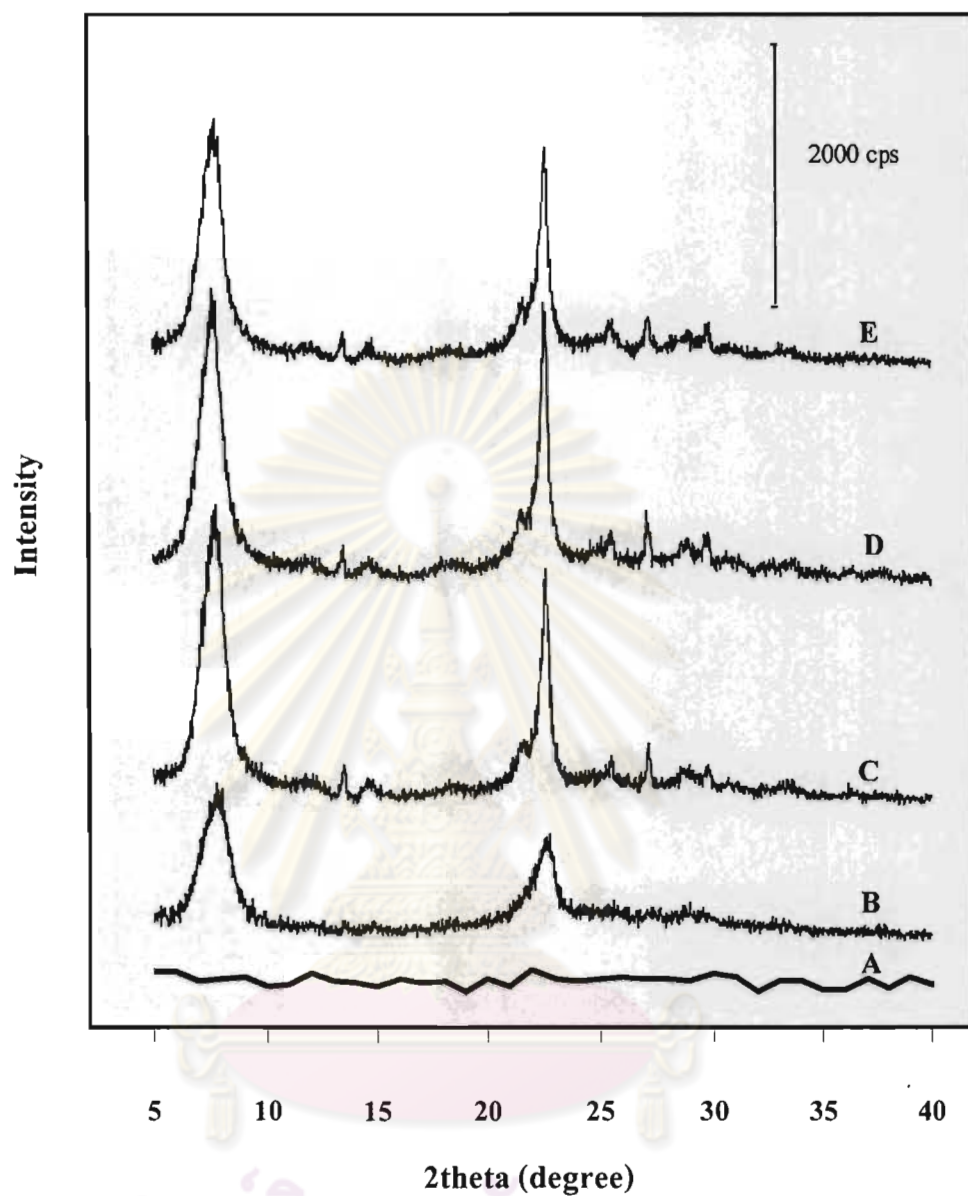


Figure 4.18 XRD patterns of calcined samples synthesized by ultrasound irradiation method with different Si/Al ratios in gel: (A) 10; (B) 20; (C) 40; (D) 60; and (E) 80

4.3.3 ^{27}Al -MAS-NMR Spectra

^{27}Al -MAS-NMR spectra of calcined zeolite samples with different Si/Al ratios are presented in Figure 4.19 and 4.20. The spectra of all calcined samples show the presence of an intense signal centered at around 55 ppm which corresponds to aluminum in tetrahedral (T_d) framework position and a small signal at about 0 ppm that is assigned to octahedral (O_h) non-framework aluminum species [14]. The results indicate that non-framework aluminum species were also generated during the calcination process for the zeolite obtained [13]. The intensity of signal at 55 ppm hardly changes when the aluminum content increases due to the saturation of number of framework site. However, Beta20-US30-24h in Figure 4.20A gives the signal at around 0 ppm with lower intensity than other samples in this work. It demonstrates that application of ultrasound radiation at high aluminum content caused more aluminum incorporate into tetrahedral framework and reduced dealumination from the framework site to the non- framework site. Table 4.5 shows O_h/T_d ratios in calcined zeolite beta samples prepared without ultrasound irradiation compared to those prepared by ultrasound method. The O_h/T_d ratio of Beta20-US30-24h is the lowest, indicating that almost all aluminum atoms incorporated into the tetrahedral framework position. This implies that the acidity of Beta20-US30-24h should be the highest too.

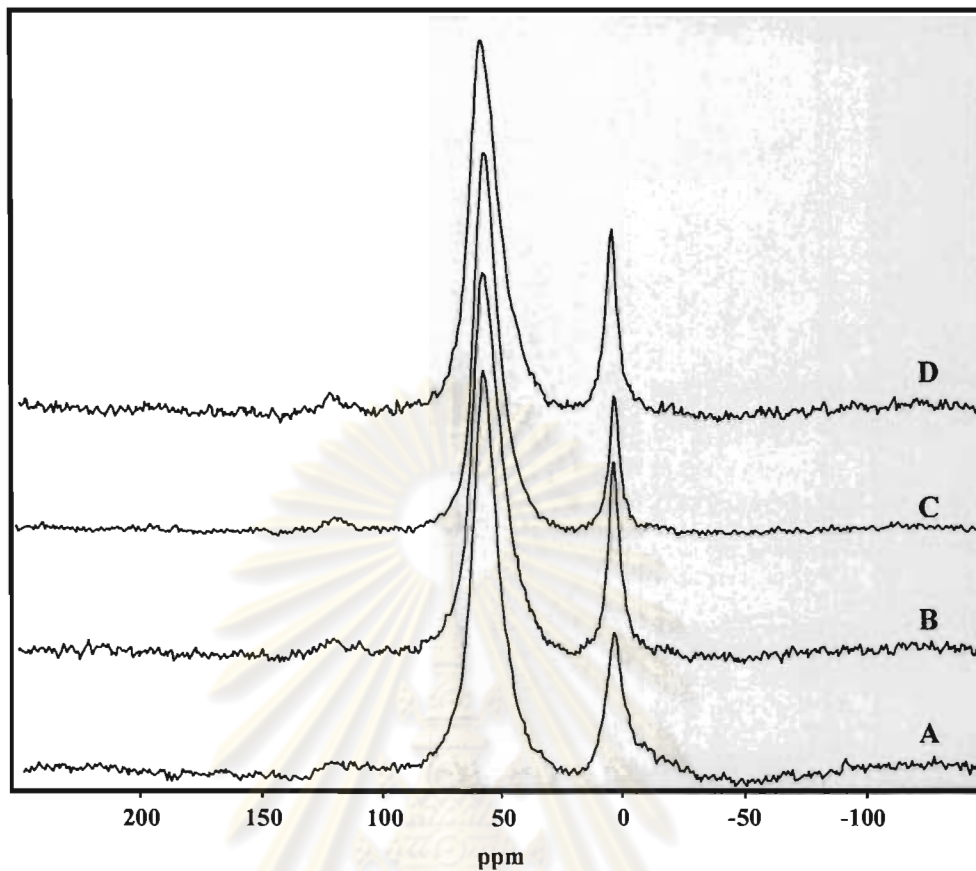


Figure 4.19 ^{27}Al -MAS-NMR spectra of calcined zeolite beta catalysts prepared without ultrasound irradiation and with different Si/Al ratios in catalyst (A) 15.0; (B) 23.6; (C) 27.7 and (D) 27.6

ศูนย์วิทยทรัพยากร
จุฬาลงกรณ์มหาวิทยาลัย

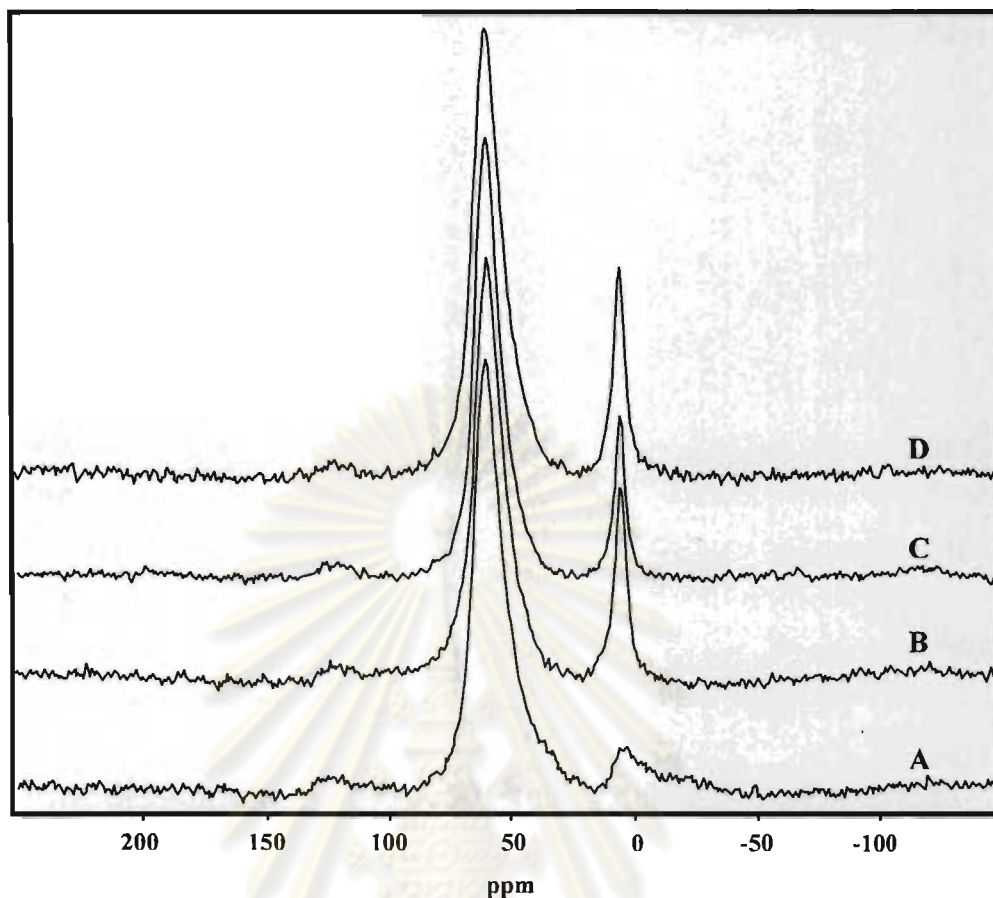


Figure 4.20 ^{27}Al -MAS-NMR spectra of zeolite beta samples synthesized by ultrasound irradiation method and with different Si/Al ratios in catalyst (A) 11.6; (B) 22.9; (C) 28.2 and (D) 26.9

Table 4.5 Comparison of O_h/T_d ratios in the calcined zeolite beta samples with different Si/Al ratios

Samples	% T_d	% O_h	O_h/T_d^*
Beta20-24h	82.64	17.36	0.21
Beta40-24h	83.33	16.67	0.20
Beta60-24h	86.21	13.79	0.16
Beta80-24h	83.33	16.67	0.20
Beta20-US30-24h	92.59	17.41	0.08
Beta40-US30-24h	83.33	16.67	0.20
Beta60-US30-24h	86.21	13.79	0.16
Beta80-US30-24h	83.03	16.97	0.19

* calculated from ratio of peak area of the signal centered at around 0 ppm to peak area of the signal centered at around 55 ppm

4.3.4 SEM Images

SEM images of zeolite beta catalysts synthesized with and without application of ultrasound irradiation and with different Si/Al ratios are shown in Figure 4.21. All images exhibit agglomeration of small crystal to larger sphere like particles. The decrease of Si/Al ratio from 80 to 40 led to slightly change of particle size but the larger particle size was formed when the Si/Al ratio reduces to 20. It is remarkable at the low Si/Al ratio of 20 that the particle size of Beta20-US30-24h is clearly larger than Beta20-24h. This result indicates that application of ultrasound irradiation at the low Si/Al ratio of 20 accelerated formation of nucleation center and enhanced crystal growth, therefore, the large particle was obtained.



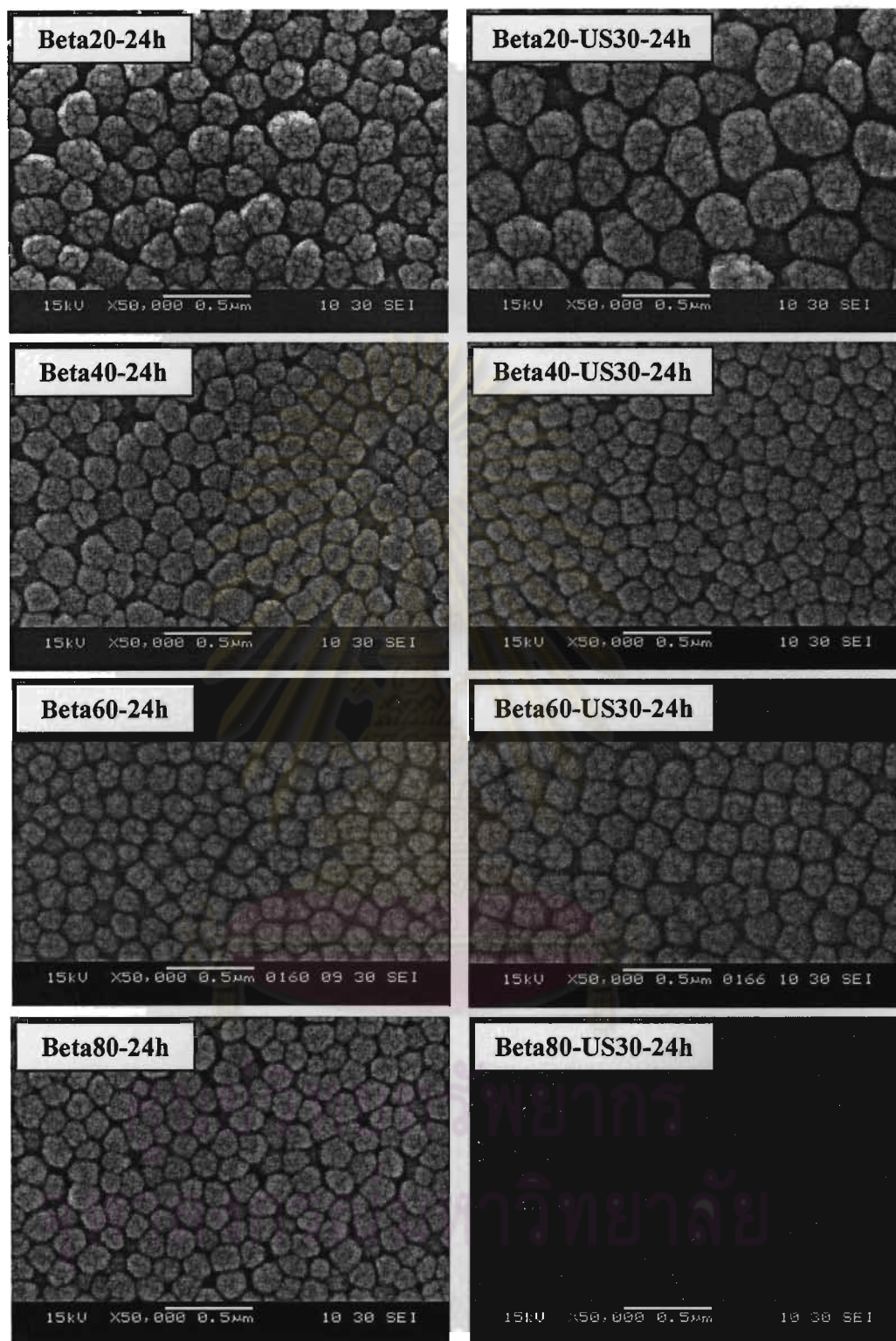


Figure 4.21 SEM images of calcined zeolite beta samples prepared with and without application of ultrasound radiation and with different Si/Al ratios.

4.3.5 Nitrogen Adsorption-Desorption

Figure 4.22 and 4.23 show the adsorption-desorption isotherms of zeolite beta samples prepared with various Si/Al ratios. These Figures show the type I isotherms, typical for microporous materials. The pore size distribution of zeolite beta samples prepared without and with ultrasound irradiation are shown Figure 4.24 and 4.25, respectively. All samples exhibit the narrow distribution of micropore with pore size about 0.6 nm. The textural properties of the zeolite beta samples with various Si/Al ratios are compiled in Table 4.6. The BET specific surface areas of Beta20-24h and Beta20-US30-24h are lower than other samples due to the large particle size, while the increase of Si/Al ratio from 40 to 80 shows small difference in the BET specific surface areas.

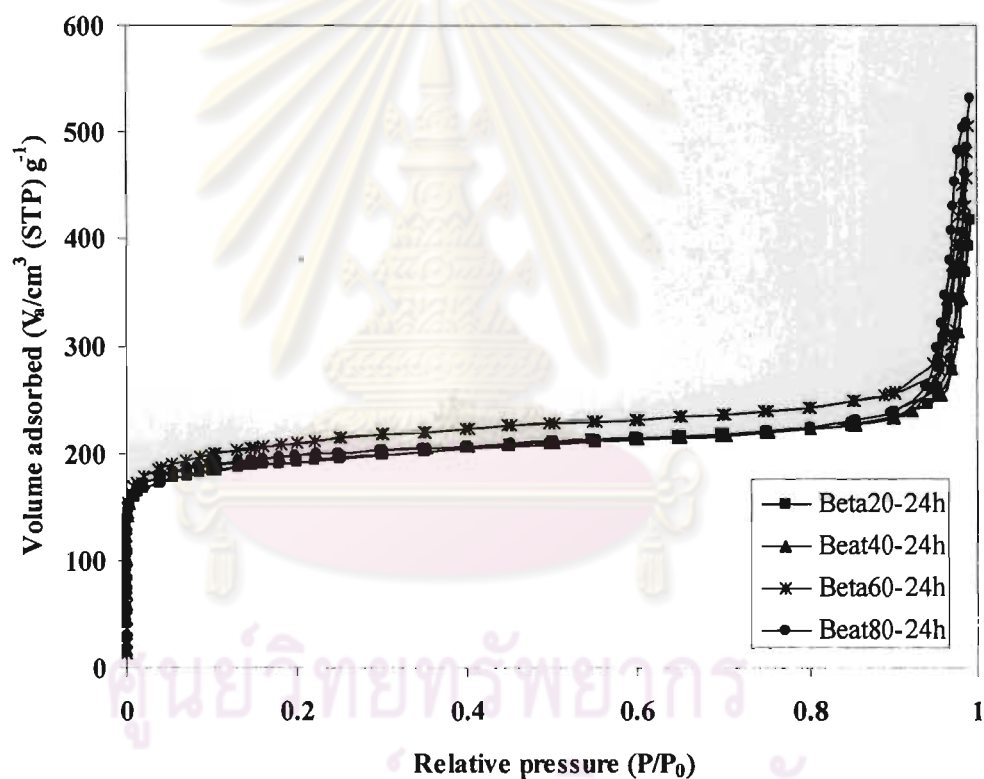


Figure 4.22 N₂ adsorption-desorption isotherms of zeolite beta catalysts prepared without ultrasound irradiation and with various Si/Al ratios in catalyst.

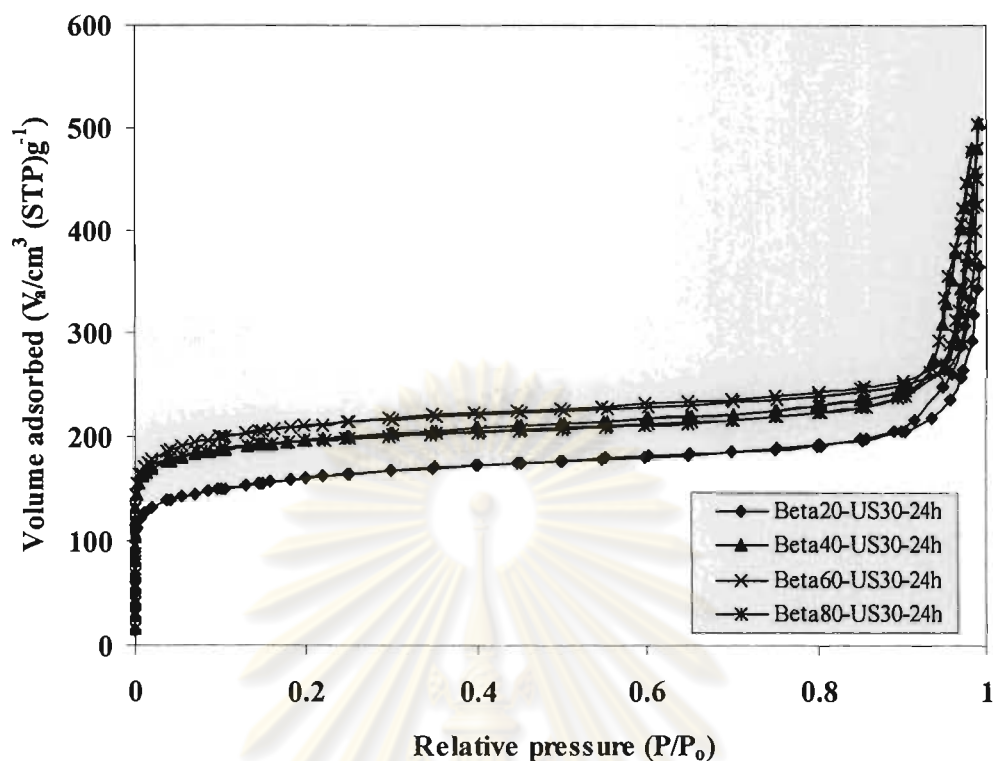


Figure 4.23 N_2 adsorption-desorption isotherms of zeolite beta samples synthesized by ultrasound irradiation method with different Si/Al ratios in catalyst

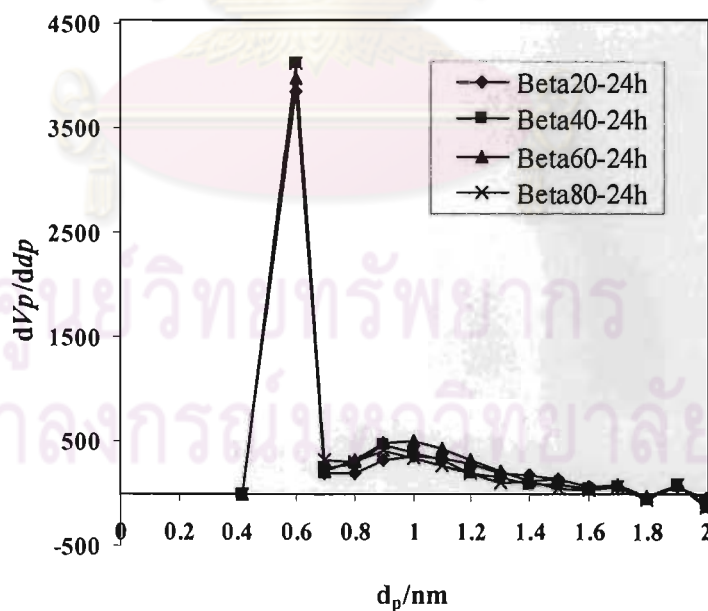


Figure 4.24 MP plots for pore size distribution of calcined zeolite beta samples prepared without ultrasound irradiation and with different Si/Al ratios

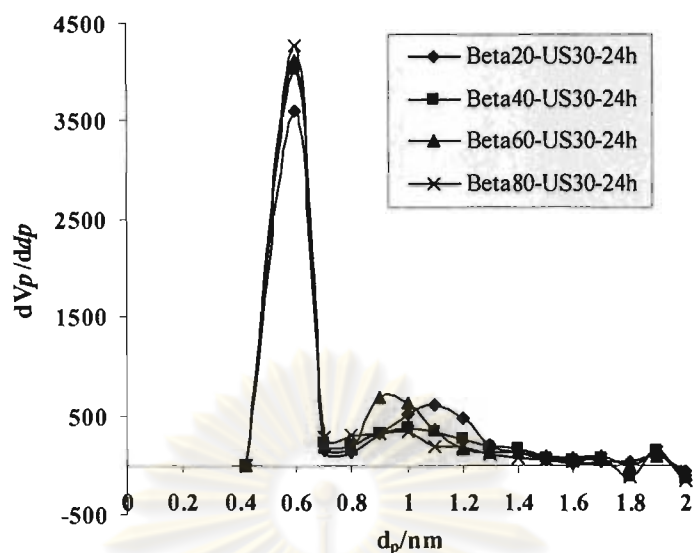


Figure 4.25 MP plots for pore size distribution of calcined zeolite beta samples synthesized by ultrasound irradiation method and with different Si/Al ratios

Table 4.6 Textural properties of calcined zeolite beta with various Si/Al ratios

Sample	particle size ^a (nm)	S_{BET} ^b (m^2/g)	d_p ^c (nm)	S_{ext} ^d (m^2/g)	Micropore volume ^d (cm^3/g)
Beta20-24h	237	726	0.6	50.7	0.30
Beta40-24h	159	768	0.6	52.4	0.29
Beta60-24h	173	784	0.6	65.9	0.30
Beta80-24h	147	752	0.6	62.7	0.29
Beta20-US30-24h	286	703	0.6	45.3	0.30
Beta40-US30-24h	165	766	0.6	65.3	0.29
Beta60-US30-24h	190	784	0.6	62.4	0.30
Beta80-US30-24h	147	749	0.6	65.6	0.30

^a particle size determined by SEM images.

^b Specific surface area determined by application of the BET-plot method.

^c particle size distribution determined by application of the MP-plot method.

^d external surface area and micropore volume determined by application of the t-plot method.

4.3.6 NH₃-TPD Profiles

Figure 4.26 exhibits NH₃-TPD profiles of zeolite beta catalysts prepared without ultrasound irradiation and with different Si/Al ratios. All samples show two NH₃ desorption peaks. The peak position corresponds to acid strength while the peak area corresponds to number of acid site. The peak centered at 170°C is normally assigned to a weaker acid site, and the other one at 430°C is assigned to a stronger acid site. It is obvious that the acid strength is similar for all four samples and only the number of acid sites is different. Table 4.7 shows the number of acid sites in term of acidity (mmol/g). The increase in Si/Al ratio from 40 to 80 does not much change the total acidity because aluminum content of the three ratios determined by ICP-AES are not much different. Considering the Si/Al ratio of 20, the number of weaker acid site of Beta20-24h increases to almost two folds of others ratios, while the number of stronger acid site of Beta20-24h decreases. It can be explained that the increase in aluminum content in catalyst causes the number of weaker acid sites increased. The highest total acidity is also shown in Beta20-24h due to the largest aluminum content conformed by ICP-AES data.

The NH₃-TPD profiles of zeolite beta samples synthesized by ultrasound irradiation method with different Si/Al ratios in Figure 4.27 can be explained in the same way. For the Si/Al ratios in a range from 40 to 80, the total acidity is not much different. For the low Si/Al ratio of 20, the total acidity of Beta20-US30-24h is higher than the total acidity of Beta20-24h because application of ultrasound causes more aluminum content incorporated into the framework structure. This result is conformed by the data from ICP-AES and ²⁷Al-MAS-NMR.

ศูนย์วิทยทรัพยากร
จุฬาลงกรณ์มหาวิทยาลัย

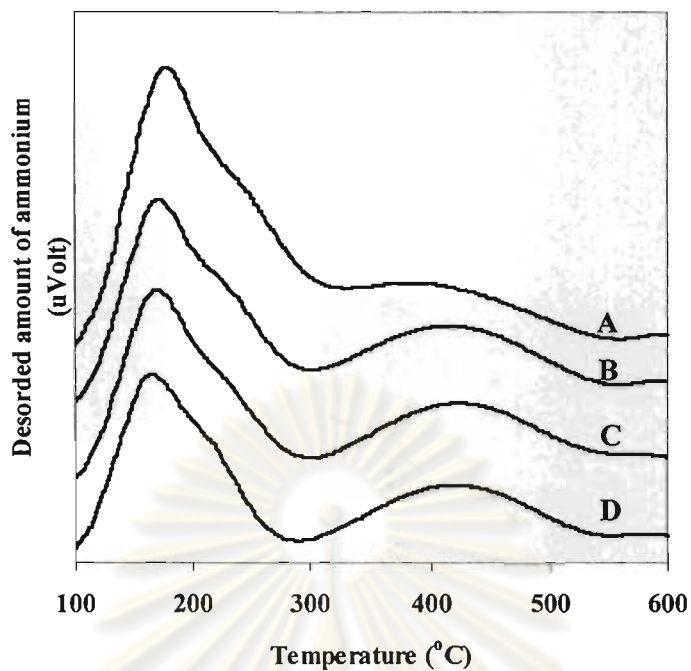


Figure 4.26 NH_3 -TPD profiles of zeolite beta catalysts prepared without ultrasound irradiation and with various Si/Al ratios in catalyst of (A) 15.0; (B) 23.6; (C) 27.7 and (D) 27.6

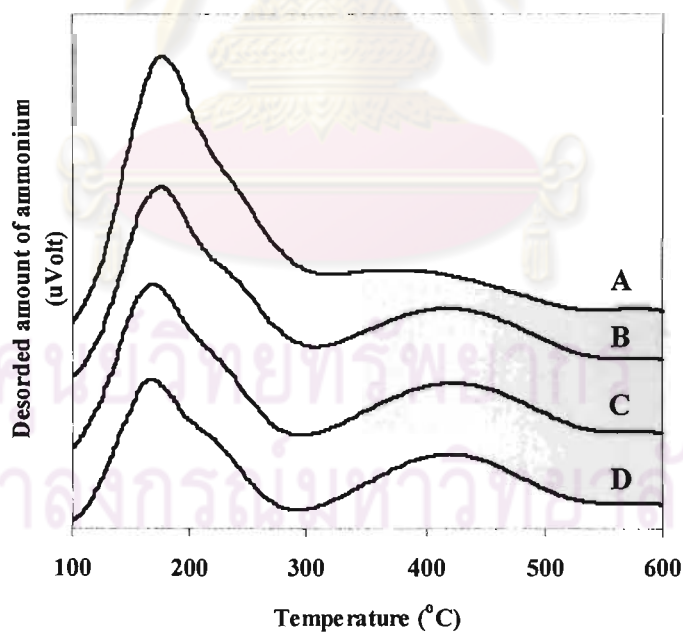


Figure 4.27 NH_3 -TPD profiles of zeolite beta samples synthesized by ultrasound irradiation method with different Si/Al ratios in catalyst of (A) 11.6; (B) 22.9; (C) 28.2 and (D) 26.9

Table 4.7 Acidity of calcined zeolite beta catalysts prepared without ultrasound irradiation and the samples prepared by the ultrasound irradiation method with various Si/Al ratios.

samples	Acidity ^a (mmol/g)		
	Weaker acid site ^b	Stronger acid site ^c	Total ^d
Beta20-24h	1.12	0.36	1.48
Beta40-24h	0.73	0.56	1.29
Beta60-24h	0.68	0.57	1.25
Beta80-24h	0.70	0.53	1.23
Beta20-US30-24h	1.17	0.45	1.62
Beta40-US30-24h	0.77	0.56	1.33
Beta60-US30-24h	0.66	0.59	1.25
Beta80-US30-24h	0.64	0.58	1.22

^a Obtained by NH₃ temperature programmed desorption.

^b Obtained at temperature around 170°C.

^c Obtained at temperature around 430°C.

^d Summation of number of weaker acid site and stronger acid site.

4.4 Activities of Various Zeolite Beta Catalysts in PP Cracking

4.4.1 Effect of Crystallization Time

The degradation of PP waste over various catalysts: Beta60-20h, Beta60-24h, Beta60-72h, Beta60-US30-20h, Beta60-US30-24h, and Beta60-US30-72h were carried out at 380 °C for 40 min, in order to find optimum crystallization periods for zeolite beta synthesis. The thermal cracking without catalyst was tested in comparison. The values of %conversion and product yield for thermal cracking and catalytic cracking of PP waste over zeolite beta samples crystallized for various time at 380°C are shown in Table 4.8.

Table 4.8 Values of %conversion and %yield obtained by thermal cracking and catalytic cracking of PP over Beta60 and Beta60-US30 samples crystallized for various periods at 380°C (Condition: 10 wt% catalyst of plastic, N₂ flow of 20 cm³/min and reaction time of 40 min)

	Thermal	Beta60-20h	Beta60-24h	Beta60-72h	Beta60-US30-20h	Beta60-US30-24h	Beta60-US30-72h
%Conversion*	14.35	95.45	96.47	96.20	94.73	95.73	96.00
%Yield*							
1. gas fraction	8.70	42.35	42.87	42.65	40.73	41.20	41.85
2. liquid fraction	5.65	53.10	53.60	53.55	54.00	54.53	54.15
- % distillate oil	56.00	71.37	76.89	74.58	73.28	78.23	78.38
- % heavy oil	44.00	28.63	23.11	25.42	26.72	21.77	21.62
3. residue	85.65	4.55	3.53	3.80	5.27	4.27	4.00
- wax	85.65	2.55	2.16	2.05	3.94	2.94	2.15
- solid coke	-	2.00	1.37	1.75	1.33	1.32	1.85
Total volume of liquid fraction (cm ³)	0.38	3.80	3.90	3.93	3.90	3.95	3.90
Liquid fraction density (g/cm ³)	0.71	0.70	0.71	0.71	0.71	0.71	0.70

*Deviation within 0.6% for conversion, 0.8% for yield of gas fraction, 0.6% for yield of liquid fraction, and 0.6% for yield of residue

All zeolite beta catalysts exhibit a high performance with the conversion of PP waste over 94% in all reactions with small amount of residue. It is remarkable that conversion and product yield obtained in the catalytic cracking of PP are much higher than those of thermal cracking where conversion is only 14.35% due to the activity enhanced by the acidity and surface area of zeolite. Considering product yields, catalytic cracking of PP over zeolite beta catalysts produced higher yields of liquid fraction than gas fraction. The yields of liquid fraction are around 54% while those of gas fraction are in the range of 40 – 43%.

For the degradation of PP over both Beta60 and Beta60-US30 samples, when the crystallization time increases from 20 h to 72 h, the conversion and product yields of all six catalysts are not different. This result indicates that zeolite beta samples prepared with and without application of ultrasound irradiation become powerful catalysts for PP cracking when they were crystallized for only 20h. However, Beta60-24h and Beta60-US30-24h show a high selectivity to distillate oil and less amounts of

coke deposited on its surface compared to those catalysts crystallized for 20 h and 72 h. Therefore, crystallization time of 24 h is an optimum condition which was chosen for the catalyst synthesis for the rest of studies.

Figure 4.28 illustrates the accumulative volume of liquid fractions in the graduated cylinder and the temperature of the reactor increased as a function of spent time. Although, the initial rates of liquid fraction formation of all six catalysts are quite different, the total volumes of liquid fraction are nearly equal.

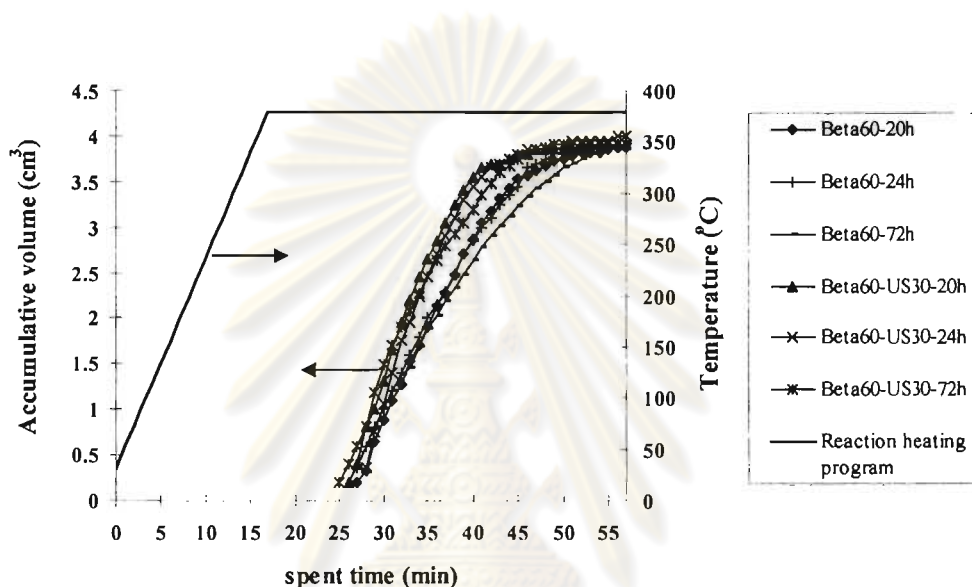


Figure 4.28 Accumulative volume of liquid fractions obtained by catalytic cracking of PP waste over Beta60 samples crystallized for various time at 380°C (Condition: 10 wt% catalyst of plastic, N₂ flow of 20 cm³/min and reaction time of 40 min).

Gas product distribution in thermal cracking and catalytic cracking reactions at 380°C is given in Figure 4.29. The gas fraction obtained by thermal cracking consists of ethane, propene, i-butene, n-pentane, and C₅+ whereas the gas fraction from catalytic cracking contains propene, i-butene and C₅+. In addition, all distribution plots of PP waste cracking over six catalysts exhibit similar gas product distribution, indicating that the distribution of gas products is not affected by variation of crystallization time from 20 h to 72 h.

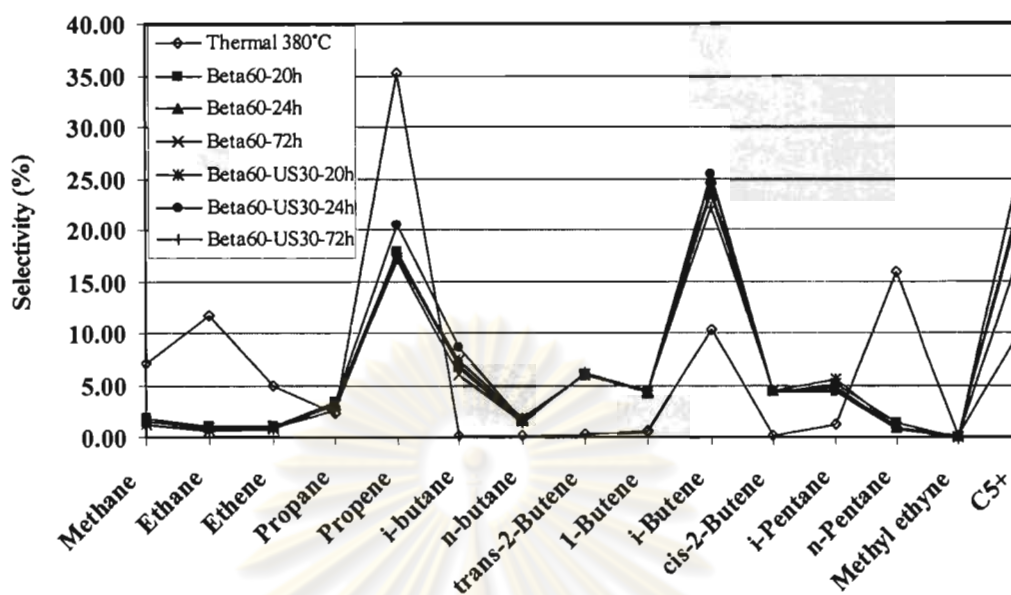


Figure 4.29 Distribution of gas fraction obtained by the thermal cracking and catalytic cracking of PP over Beta60 samples crystallized for various time at 380°C (Condition: 10 wt% catalyst of plastic, N₂ flow of 20 cm³/min and reaction time of 40 min).

Figure 4.30 shows carbon number distribution of distillate oil obtained by thermal cracking and catalytic cracking of PP waste using zeolite beta catalysts synthesized with and without application of ultrasound irradiation and crystallized for various periods. Liquid products are investigated with the C_{np} value which relates to the boiling point of normal-paraffins. For example, the products in the boiling point range of C₆ represent a combination of some aliphatic, alicyclic, and aromatic hydrocarbon which have boiling points between those of n-pentane and n-hexane. For thermal cracking, the main distillate oil component is C₉. In presence of zeolite beta catalysts, the liquid components are mainly in the range of C₆-C₉, showing that zeolite beta catalysts exhibit good catalytic activities for producing light hydrocarbon liquids. All liquid distribution plots obtained by cracking PP waste over Beta60 and Beta60-US30 catalysts crystallized for various time are approximately similar in the range of C₆-C₉ hydrocarbon. There is slightly difference in %selectivity compared among these catalysts; however, this difference is not significant. This result indicates that

not only variations of crystallization time from 20 h to 72 h but ultrasound irradiation route do not affect the distribution of liquid products as well.

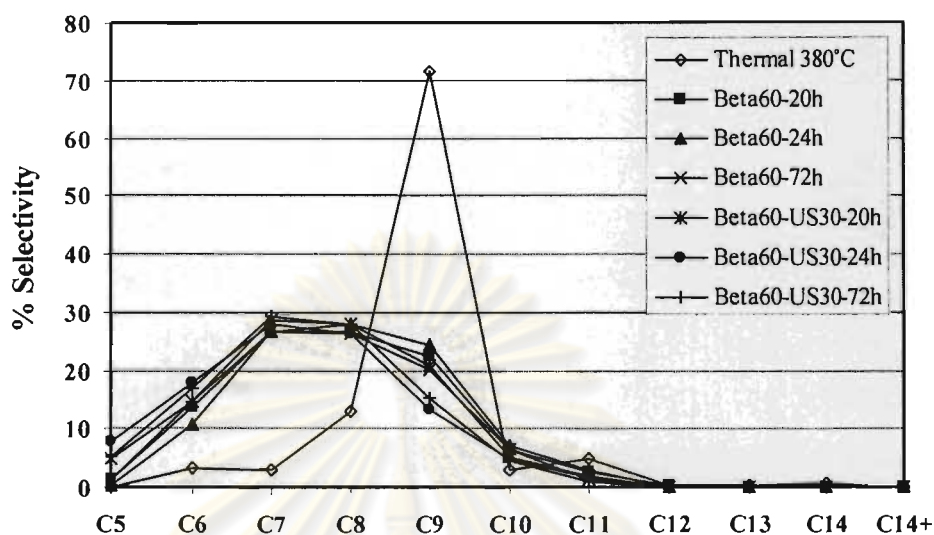


Figure 4.30 Carbon number distribution of liquid fractions from thermal cracking and catalytic cracking of PP over zeolite beta samples crystallized for various time at 380°C (Condition: 10 wt% catalyst of plastic, N₂ flow of 20 cm³/min and reaction time of 40 min).

4.4.2 Effect of Si/Al Ratios in Catalyst

The effect of Si/Al ratios in catalyst was tested in degradation of PP waste at low temperature of 350°C in order to reduce the effect of temperature on catalytic reaction. The values of %conversion and product yield from thermal cracking and catalytic cracking of PP over zeolite beta catalysts prepared with and without application of ultrasound irradiation and with different Si/Al ratios are compared in Table 4.9 and 4.10.

Considering data in Table 4.9 for thermal cracking at 350°C, no liquid fraction was found in the graduated cylinder and %conversion is only 3.6%. The result indicates the difficulty in degradation of PP without catalyst at the low temperature about 350°C. Therefore, the total weight loss of plastic precursor after reaction is dedicated to gas fraction. The white candle wax remained in the reactor after the reaction was included in the residue. For the catalytic cracking over zeolite beta catalysts prepared without application of ultrasound irradiation, the %conversion

increases from 3.6 wt% to about 46 wt% compared with thermal cracking. The result indicated that the waxy residue decomposed into relatively lighter liquid hydrocarbons resulting in higher yield of liquid fractions than the case of thermal cracking. However, there is no difference in %conversion when Si/Al ratio increases from 20 to 80. The specific surface area cannot explicate the activity of those catalysts since their activity do not relate to the change in specific surface area. The number of active site, determined by NH_3 -TPD method, is accounted for their behavior. Beta40-24h, Beta60-24h, and Beta80-24h samples have not much different in term of number of acid sites; consequently, their activities are not different. Considering the catalyst with Si/Al ratio of 20, relatively high aluminum content, the liquid fraction yield for Beta20-24h is slightly larger than the others due to its relatively higher acidity while others seems to have similar acidities independent from the Si/Al ratio.

The results of PP waste degradation over zeolite beta catalysts synthesized with application of ultrasound irradiation are shown in Table 4.10. Similar to the results mentioned above, the increase in Si/Al ratio from 40 to 80 provides no change in %conversion. However, the %conversion for Beta20-US30-24h sample increases as Si/Al ratio decreases. This is in agreement with the increase in acidity of this catalyst as mentioned in Section 4.3.6. In addition, Beta20-US30-24h catalyst presents the highest %liquid fraction yield and largest amount of distillate oil. It can be explained that the higher acidity of Beta20-US30-24h led to the formation of lighter liquid products.

Table 4.9 Values of %conversion and %yield obtained by catalytic cracking of PP over normal zeolite beta catalysts with various Si/Al ratios (Condition: 10 wt% catalyst of plastic, N₂ flow of 20 cm³/min, 350°C, and reaction time of 40 min)

	Thermal 350°C	Beta20- 24h	Beta40- 24h	Beta60- 24h	Beta80- 24h
%Conversion*	3.6	45.67	45.40	46.50	46.20
%Yield*					
1. gas fraction	3.6	25.80	28.10	29.30	29.40
2. liquid fraction	-	19.87	17.30	17.20	16.80
- % distillate oil	-	80.26	78.85	76.33	69.90
- % heavy oil	-	19.74	21.15	23.67	30.40
3. residue	96.4	54.33	54.60	53.50	53.80
Total volume of liquid fraction (cm ³)	-	1.42	1.25	1.25	1.28
Liquid fraction density (g/cm ³)	-	0.71	0.71	0.70	0.69

*Deviation within 0.6% for conversion, 0.8% for yield of gas fraction, 0.4% for yield of liquid fraction, and 0.6% for yield of residue

Table 4.10 Values of %conversion and %yield obtained by catalytic cracking of PP over Beta-US30-24h catalysts with various Si/Al ratios (Condition: 10 wt% catalyst of plastic, N₂ flow of 20 cm³/min, 350°C, and reaction time of 40 min)

	Thermal 350°C	Beta20- US30-24h	Beta40- US30-24h	Beta60- US30-24h	Beta80- US30-24h
%Conversion*	3.6	53.30	46.40	46.40	45.80
%Yield*					
1. gas fraction	3.6	27.00	29.87	30.10	29.40
2. liquid fraction	-	26.30	16.53	16.30	16.40
- % distillate oil	-	82.09	76.81	74.58	64.13
- % heavy oil	-	17.91	23.19	25.42	35.87
3. residue	96.4	46.70	53.60	53.60	54.20
Total volume of liquid fraction (cm ³)	-	1.85	1.20	1.18	1.18
Liquid fraction density (g/cm ³)	-	0.71	0.70	0.70	0.71

*Deviation within 0.6% for conversion, 0.8% for yield of gas fraction, 0.6% for yield of liquid fraction, and 0.6% for yield of residue

Figure 4.31 shows the accumulated volume of liquid fraction obtained by catalytic cracking of PP waste over various zeolite beta catalysts synthesized by the two different methods at 350°C. The overall rate of liquid fraction formation over Beta20-US30-24h is faster than those over other seven beta catalysts due to the effect of the predominant acidity of the Beta20-US30-24h catalyst in contrast to others.

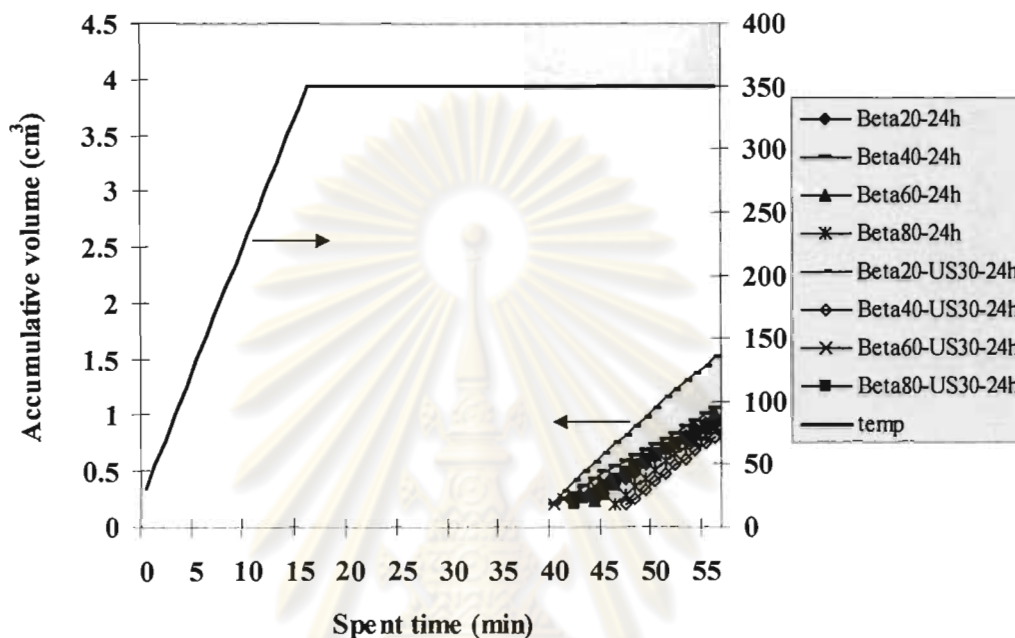


Figure 4.31 Accumulative volume of liquid fractions from catalytic cracking of PP over various zeolite beta catalysts with different Si/Al ratios at 350°C (Condition: 10 wt% catalyst of plastic, N₂ flow of 20 cm³/min and reaction time of 40 min).

Figure 4.32 and 4.33 show distribution of gas fraction obtained by thermal cracking and catalytic cracking of PP over various zeolite beta catalysts prepared without and with application of ultrasound irradiation at 350°C. For thermal cracking, propene and n-pentane are the predominant product. In the presence of any of zeolite beta catalysts, the product distribution in gas fraction is different from that in the absence of catalyst or thermal pyrolysis. The main components in gas fractions from catalytic cracking are i-butene and C₅+. In addition, the product distribution in gas fraction is independent from the Si/Al ratios in the catalyst and the application of ultrasound irradiation.

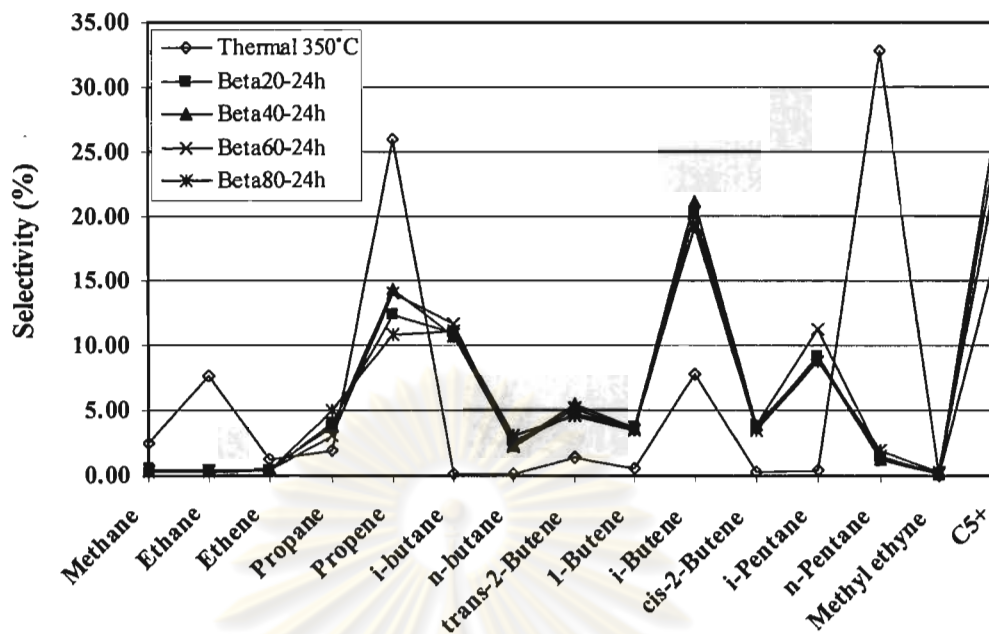


Figure 4.32 Distribution of gas fraction obtained by catalytic cracking of PP over Beta-24h catalysts with various Si/Al ratios at 350°C (Condition: 10 wt% catalyst of plastic, N₂ flow of 20 cm³/min and reaction time of 40 min).

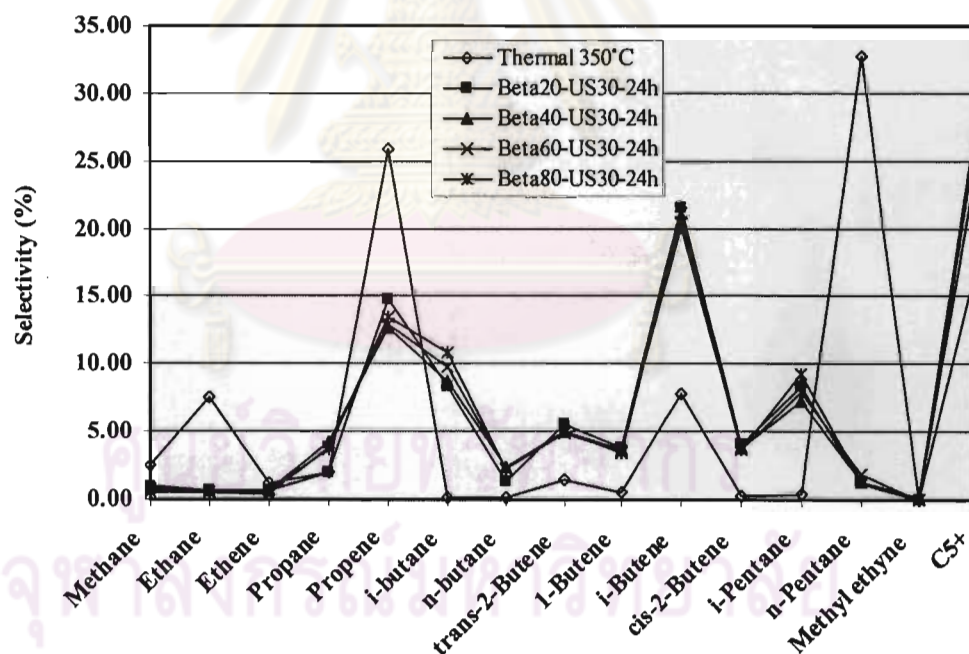


Figure 4.33 Distribution of gas fraction obtained by catalytic cracking of PP over Beta-US30-24h catalysts with different Si/Al ratios at 350°C (Condition: 10 wt% catalyst of plastic, N₂ flow of 20 cm³/min and reaction time of 40 min).

Figure 4.34 and 4.35 show carbon number distribution of distillate oil obtained by catalytic cracking of PP over various zeolite beta catalysts synthesized with and without application of ultrasound irradiation at 350°C. The major liquid products of all Si/Al ratios are distributed in the range of C₇ and C₉. The decrease of Si/Al ratio in catalyst causes the increase in the selectivity to lighter hydrocarbon components. It can be obviously observed for the different liquid product distribution among Beta80 and other Si/Al ratios. The product distribution of SUPELCO standard gasoline fraction is shown in Figure 4.36 and the major components are C₇ and C₈. That is comparable to the distribution of distillate oil obtained in this work based on the boiling point range using n-paraffins as reference. According to the results of Si/Al ratio in catalyst affecting on PP degradation, Beta20-US30-24h is a powerful catalyst selected for the rest of studies in this work due to considerably large amount of liquid fraction was obtained.

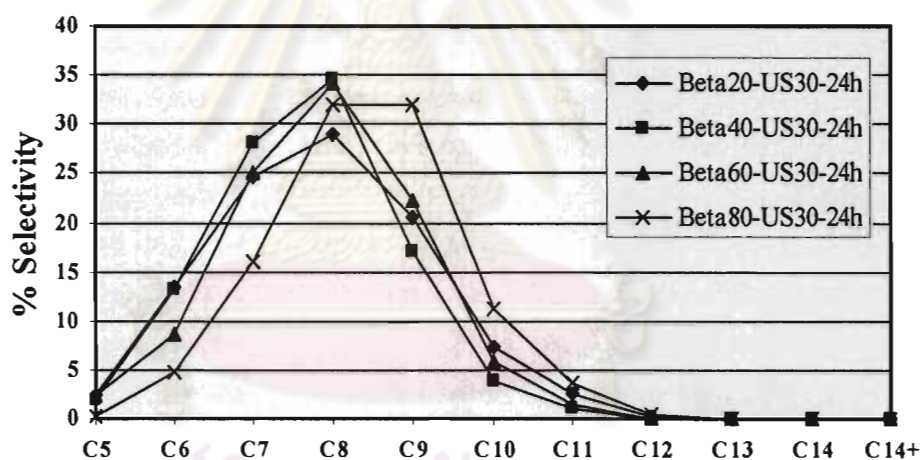


Figure 4.34 Carbon number distribution of distillate oil obtained by catalytic cracking of PP over Beta-US30-24h catalysts with various Si/Al ratios at 350°C (Condition: 10 wt% catalyst of plastic, N₂ flow of 20 cm³/min and reaction time of 40 min).

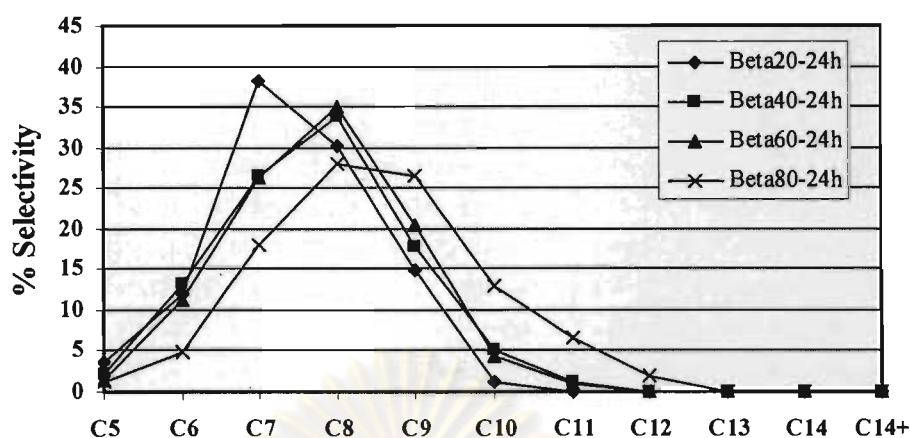


Figure 4.35 Carbon number distribution of distillate oil obtained by catalytic cracking of PP waste over Beta-24h catalysts with various Si/Al ratios at 350°C (Condition: 10 wt% catalyst of plastic, N₂ flow of 20 cm³/min and reaction time of 40 min).

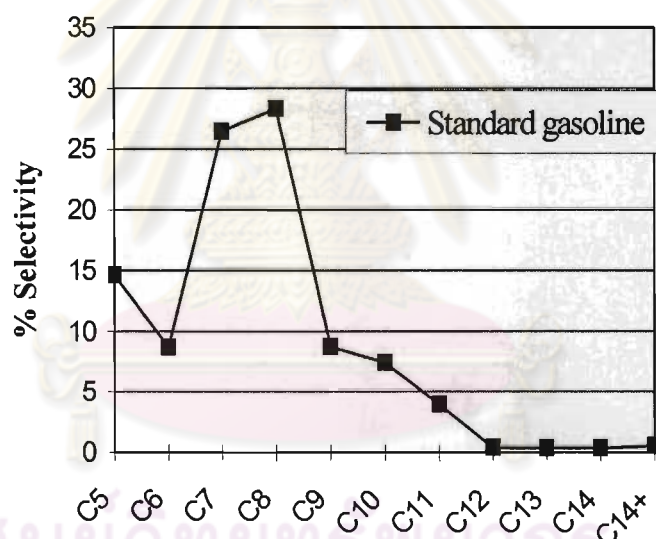


Figure 4.36 Carbon number distribution of commercial SUPELCO standard gasoline fraction.

4.4.3 Effect of Reaction Temperature

Beta20-US30-24h catalyst was used for studying the effect of temperature on its activity and the thermal cracking was tested in comparison. The values of %conversion and the product yields for the thermal cracking and catalytic cracking of PP waste over Beta20-US30-24h catalyst at 350°C, 380°C and 400°C are shown in

Table 4.11. The value of %conversion steeply increases from 53.30% to 97.50% when reaction temperature increases from 350°C to 380°C and that remains constant for 97.40% conversion at 400°C. The yields of both gas and liquid products are affected by temperature. Considering at temperature in range 380°C to 400°C, the products are mainly in liquid fraction at the high yield about 60-62% and the minor products are gas fraction at the yield about 35-37%. The %distillate oil at 380°C is higher than that at 400°C. For thermal cracking at three reaction temperatures, the value of conversion and product yield increase when the reaction temperature increase from 350°C to 400°C. The effect of zeolite beta on PP cracking clearly observes at 380°C that the residue of catalytic cracking dramatically reduces from 85.65% to 2.50% compared with thermal cracking. The liquid fractions have pale yellow color in all three temperatures.

Table 4.11 Values of %conversion and %yield obtained by thermal cracking and catalytic cracking of PP over Beta20-US30-24h catalysts at different temperature (Condition: 10 wt% catalyst of plastic, N₂ flow of 20 cm³/min, and reaction time of 40 min)

	Reaction temperature=350°C		Reaction temperature=380°C		Reaction temperature=400°C	
	Thermal	Beta20-US30-24h	Thermal	Beta20-US30-24h	Thermal	Beta20-US30-24h
%Conversion*	3.60	53.30	14.35	97.50	57.20	97.40
%Yield*						
1. gas fraction	3.60	27.00	8.70	37.30	22.20	35.20
2. liquid fraction	-	26.30	5.65	60.20	35.00	62.20
- % distillate oil	-	82.09	56.00	80.45	51.10	70.97
- % heavy oil	-	17.91	44.00	19.55	48.90	29.03
3. residue	96.40	46.70	85.65	2.50	42.80	2.60
- wax	96.40	-	85.65	1.15	42.80	1.73
- solid coke	-	-	-	1.36	-	0.87
Total volume of liquid fraction (cm ³)	-	1.85	0.38	4.28	2.40	4.40
Liquid fraction density (g/cm ³)	-	0.69	0.71	0.71	0.72	0.71

*Deviation within 0.6% for conversion, 0.8% for yield of gas fraction, 0.4% for yield of liquid fraction, and 0.6% for yield of residue

Figure 4.37 shows the accumulative volume of liquid fractions in the graduated cylinder increased as a function of spent time. When the temperature is increased, the initial rate of liquid fraction formation is much faster in order 400°C, 380°C and 350°C. However, the total volume of liquid fraction was no difference for the 400°C compared to that at 380°C.

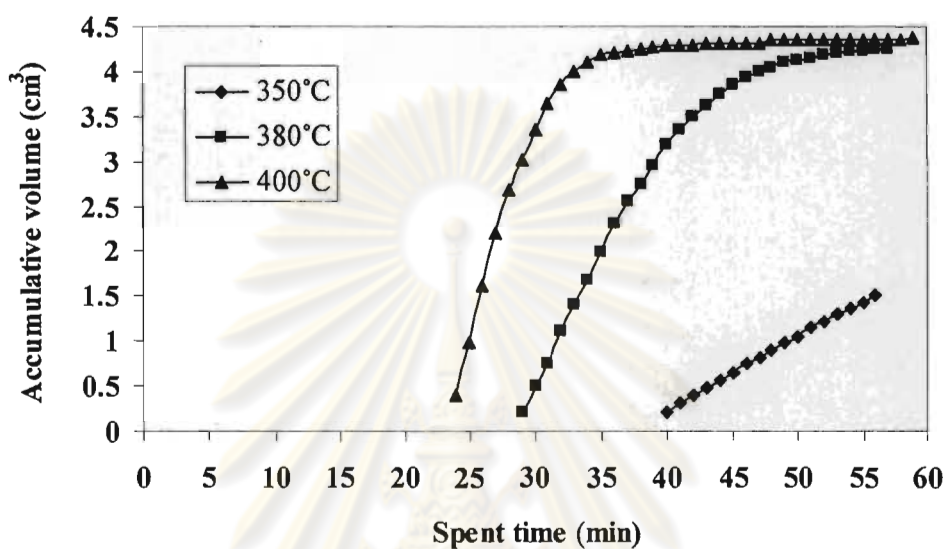


Figure 4.37 Accumulative volume of liquid fractions from catalytic cracking of PP over Beta20-US30-24h catalysts at different temperature (Condition: 10 wt% catalyst of plastic, N₂ flow of 20 cm³/min and reaction time of 40 min).

Figure 4.38 shows distribution of gas fraction obtained by thermal cracking and catalytic cracking of PP over Beta20-US30-24h sample at 350°C, 380°C and 400°C. Considering only gases at ambient condition which are normally C₁ through C₅, the major components for thermal cracking are C₃ (propene) and C₅ (n-pentane) while that for catalytic cracking is C₄ (i-butene) independently from temperature. However, the vapor of C₅⁺ (liquids at ambient condition) which has higher boiling point than that of C₅ (n-pentane) is obviously detected in high amount. For thermal cracking, the reaction temperature effects distribution of gas fraction products. When the reaction temperature increases, the gas fractions of lighter hydrocarbon (ethane and propene) increases, while that of heavier hydrocarbon (n-pentane and C₅⁺) decreases. The growing yield of volatile components as function of temperature could

be caused by the differences in the thermal stability of polymer chain, because hydrocarbons have reducing thermal stability with increasing temperature. Therefore, the C-C bonds were cracked more easily at 400°C than at lower temperature, and it resulted in higher yields of volatile products.

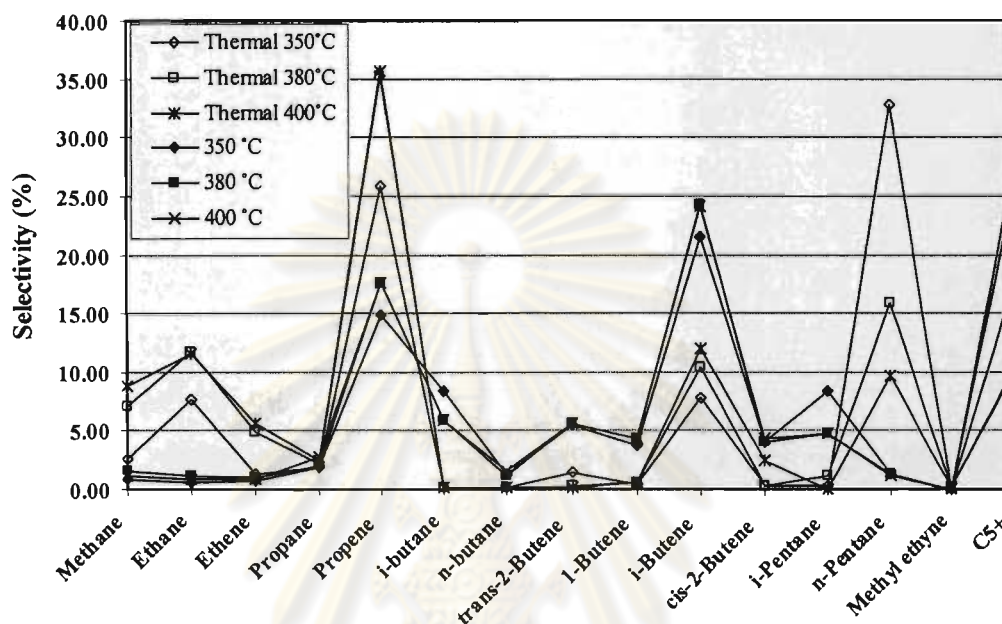


Figure 4.38 Distribution of gas fraction obtained by catalytic cracking of PP over Beta20-US30-24h catalysts at different temperature (Condition: 10 wt% catalyst of plastic, N₂ flow of 20 cm³/min and reaction time of 40 min).

Figure 4.39 shows product distribution of distillate oil obtained by thermal cracking and catalytic cracking of PP over Beta20-US30-24h catalysts at 350°C, 380°C and 400°C. For thermal cracking at 380°C, the liquid fraction is rich of C₉. For the thermal cracking at 400°C, the liquid hydrocarbon fractions are distributed in a wide range of equivalent hydrocarbons from C₆ to C₉. It is well known that thermal cracking occurs by the random scissoring of the long polymeric chain and products of cracking are distributed in a wide range of molecular weights. For catalytic cracking, the distillate oil components are mainly in the range of C₇ to C₉. When the reaction temperature increases to 400°C, the liquid fractions of lighter hydrocarbon (C₆-C₇) increases while that of heavier hydrocarbon (C₉-C₁₀) decreases. This result indicates that liquid product distribution depends on temperature. According to the results of

temperature effect on PP cracking, the large amount of liquid fractions obtained at the temperature of 380°C and 400°C are not different. Moreover, the higher quantity of distillate oil was obtained at the temperature of 380°C. As a result the temperature of 380°C is selected to be the best condition for further studies in this work.

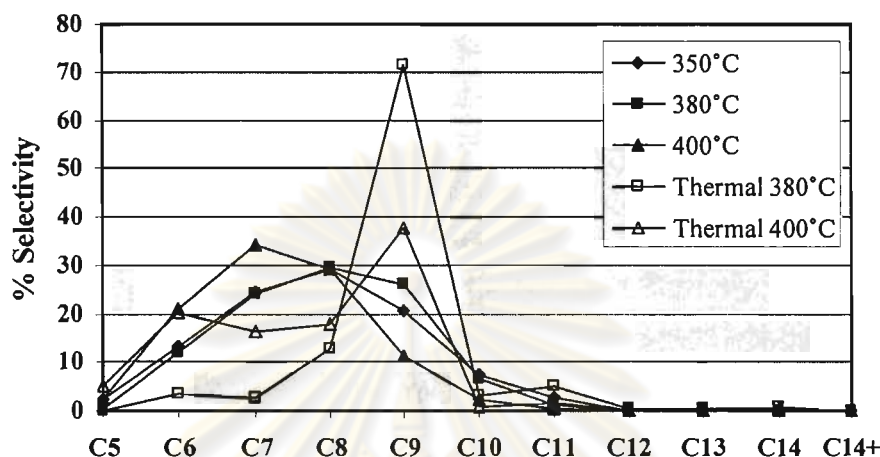


Figure 4.39 Carbon number distribution of distillate oil obtained by catalytic cracking of PP over Beta20-US30-24h catalysts at different temperature (Condition: 10 wt% catalyst of plastic, N₂ flow of 20 cm³/min and reaction time of 40 min).

4.4.4 Effect of Polypropylene to Catalyst Ratio

Value of conversion and product yield obtained by catalytic cracking of PP waste at 380°C over Beta20-US30-24h catalysts with different catalyst amounts of 5 wt%, and 10 wt% to PP are shown in Table 4.12. The high conversion value of 97.50% is obtained when using 10wt% catalyst amount. Reducing of catalyst amount to 5wt% leads the %conversion drop to 87.60%, indicating that the conversion strongly depends on the catalyst content. Considering to %product yield, the gas fraction yield decreases when the amount of catalyst reduces. Basically, the less catalyst amount, the less acidity resulting in the less gas fraction yield. However, there is no difference in liquid fraction yield. The amount of residue and the conversion are inversely related. The residue produced by using 5% catalyst amount contains mainly wax due to lower activity compared to using 10% catalyst. The lower acidity, the higher wax and residue is found.

The selectivity to light oil and heavy oil in liquid fraction is affected by the catalyst content. The PP cracking using 5% beta catalyst provides low selectivity to light oil because of the less acidity. From the results mentioned above, the optimum catalyst amount is the 10 wt% catalyst to PP due to the greatest %conversion and high light liquid hydrocarbon.

Table 4.12 Conversion and product yield obtained by catalytic cracking of PP over Beta20-US30-24h catalysts with different catalyst amounts at 380°C (Condition: N₂ flow of 20 cm³/min, and reaction time of 40 min)

	Catalyst amount to PP	
	5 wt%	10 wt%
%Conversion*	87.60	97.50
%Yield*		
1. gas fraction	26.60	37.30
2. liquid fraction	61.00	60.20
- % distillate oil	59.79	80.45
- % heavy oil	40.21	19.55
3. residue	12.4	2.50
- wax	11.97	1.15
- solid coke	0.43	1.36
Total volume of liquid fraction (cm ³)	4.42	4.28
Liquid fraction density (g/cm ³)	0.69	0.71

*Deviation within 0.4% for conversion, 0.6% for yield of gas fraction, 0.4% for yield of liquid fraction, and 0.4% for yield of residue

Figure 4.40 shows the accumulated volume of liquid fraction obtained by catalytic cracking of PP waste over Beta20-US30-24h catalysts with different catalyst amounts at 380°C. The initial rates of liquid fraction formation in the reaction using 10wt% catalyst content is slower than that over using 5wt% catalyst amount, indicating the predominant competitive rate of dissociation of liquid molecules to gas molecules compared to the rate of liquid formation. However, the total liquid volumes of both cases are not different.

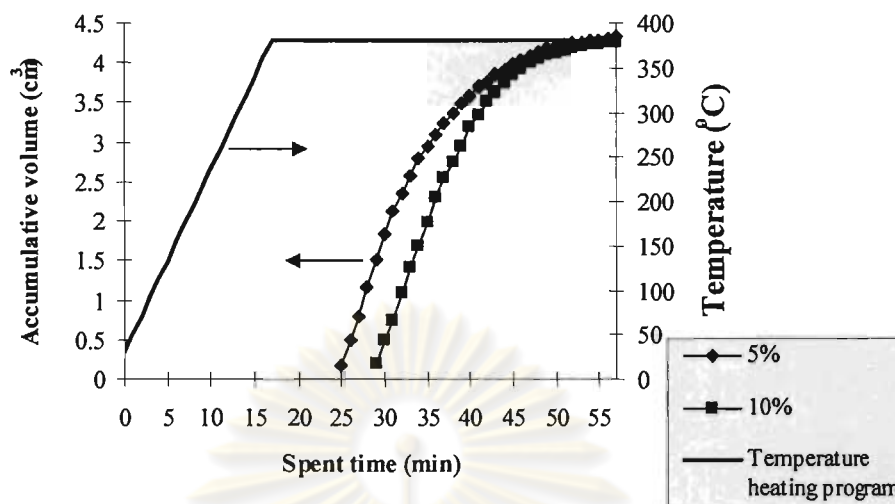


Figure 4.40 Accumulative volume of liquid fractions from catalytic cracking of PP over Beta20-US30-24h catalysts with different catalyst amounts at 380°C (Condition: N₂ flow of 20 cm³/min and reaction time of 40 min)

Figure 4.41 shows distribution plots of gas fraction obtained by catalytic cracking of PP over Beta20-US30-24h catalysts with various catalyst amounts at 380°C. The mainly gas fraction from PP cracking are propene, i-butene and C₅₊ and the product distribution in gaseous phase for 5% and 10% catalyst amounts are similar. It can be concluded that polypropylene to catalyst ratios does not affect gas product distribution.

The product distributions of light oil obtained by catalytic cracking of PP over Beta20-US30-24h catalysts with various catalyst amounts at 380°C are shown in Figure 4.42. The product distribution in liquid phase for 5% and 10% catalyst amounts are slightly different. For 10% catalyst content, the major products are in the range of C₆ and C₁₀. When catalyst amount is reduced, the liquid products distributed in the range of C₆ and C₇ increases while the selectivity to C₉ and C₁₀ components decrease. It indicates that lighter liquid hydrocarbon was obtained in case of 5% catalyst amount. In this work, using 10% catalyst amount is the best condition according to the highest %conversion and distillate oil fraction.

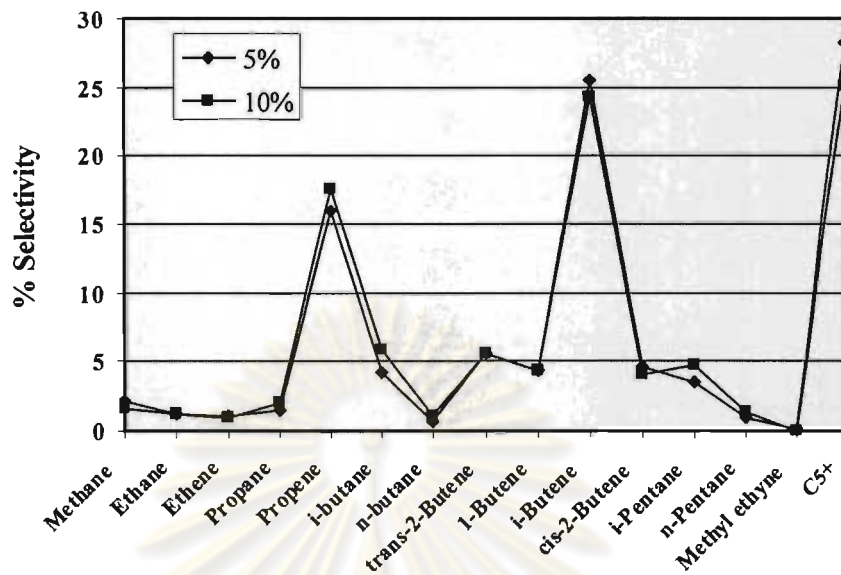


Figure 4.41 Distribution of gas fraction obtained by catalytic cracking of PP over Beta20-US30-24h catalysts with different catalyst amounts at 380°C (Condition: N₂ flow of 20 cm³/min and reaction time of 40 min).

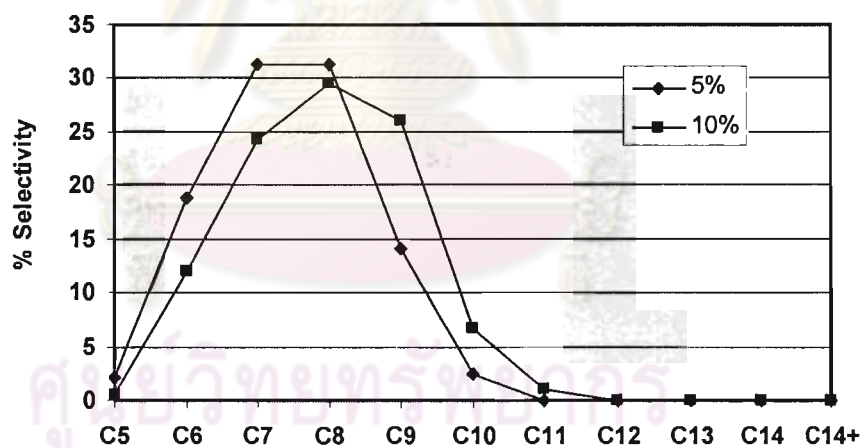


Figure 4.42 Carbon number distribution of distillate oil obtained by catalytic cracking of PP over Beta20-US30-24h catalysts with different catalyst amounts at 380°C (Condition: 10 wt% catalyst of plastic, N₂ flow of 20 cm³/min and reaction time of 40 min).

4.4.5 Catalyst Regeneration

4.4.5.1 XRD Results

The used Beta20-US30-24h catalysts became black owing to coke deposit on the surface and in the pores. However, it easily turned to white after regeneration by calcination in a muffle furnace at 550°C for 5 h. Figure 4.43 shows XRD patterns of the calcined unused and the regenerated Beta20-US30-24h catalysts. After catalytic run, the structure of zeolite beta was still remained for the 1st regenerated Beta20-US30-24h and the 2nd regenerated Beta20-US30-24h catalysts with almost the same crystallinity as the unused catalyst.

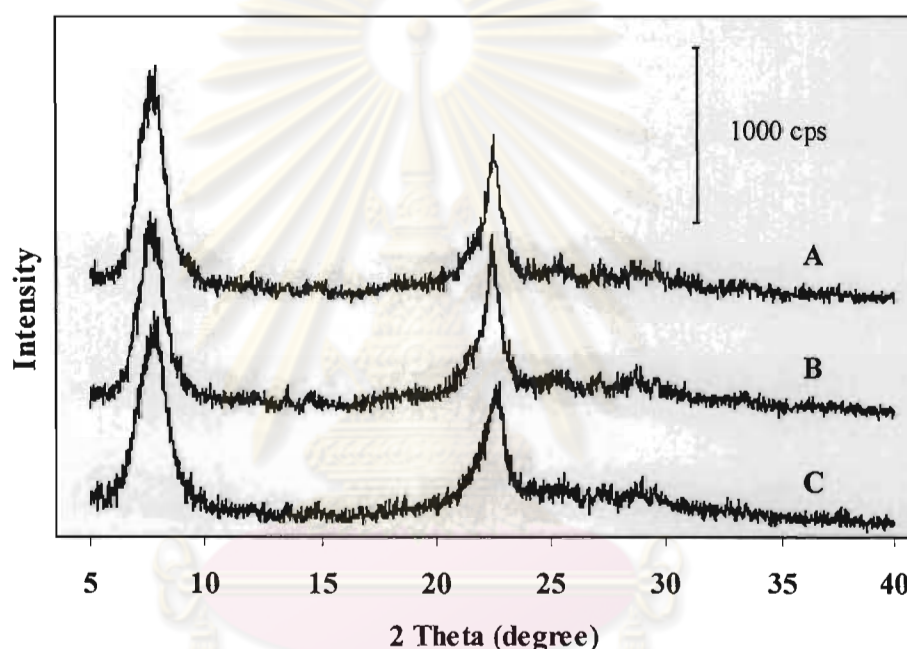


Figure 4.43 XRD patterns of (A) the calcined unused (B) the 1st regenerated Beta20-US30-24h and (C) the 2nd regenerated Beta20-US30-24h catalysts

4.4.5.2 SEM Images

Figure 4.44 shows SEM images of the 3rd regenerated Beta20-US30-24h sample with different magnification. After the third catalytic run, it is obvious that the regenerated catalyst particles have sphere like shape with similar particle size compared to the fresh catalyst SEM image of which has been shown in Figure 4.21.

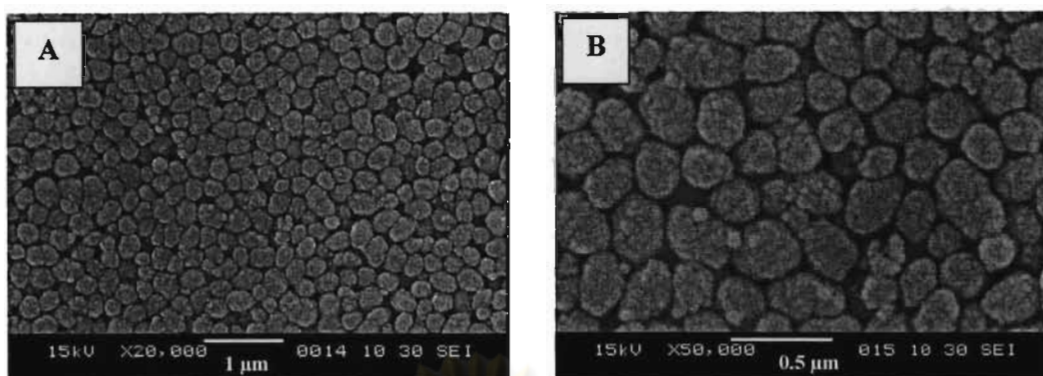


Figure 4.44 SEM images of the 3rd regenerated Beta20-US30-24h sample with different magnification (A) x20,000 and (B) x50,000 times

4.4.5.3 Nitrogen Adsorption-Desorption

The adsorption-desorption isotherms of fresh catalyst and regenerated catalyst are present in Figure 4.45. The 1st and 2nd regenerated catalyst show the characteristic isotherm of microporous materials with the specific surface area of 552 and 534 m²/g, respectively. It was sharply decreased compared with the fresh catalyst (703 m²/g).

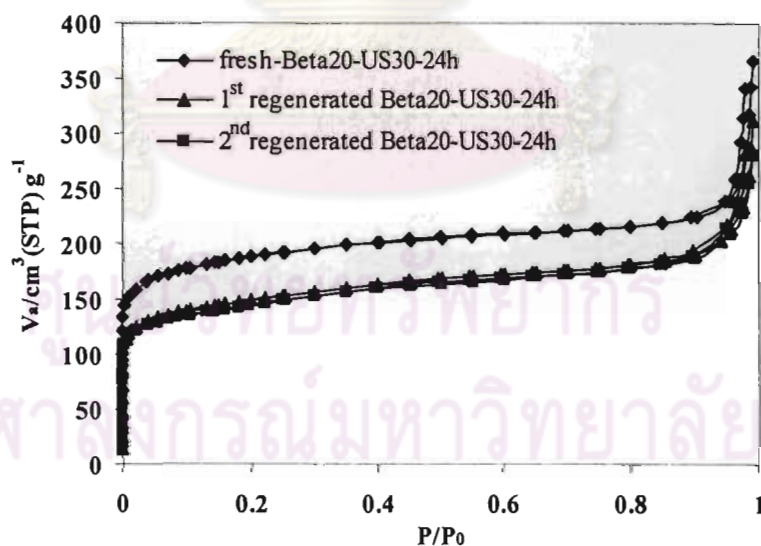


Figure 4.45 N₂ adsorption-desorption isotherms of the fresh and the regenerated Beta20-US30-24h sample

4.4.5.4 Activity of Regenerated Zeolite Beta in PP Cracking

Values of %conversion and %produce yield obtained by catalytic cracking of PP using the fresh and the regenerated Beta20-US30-24h catalysts at 380°C are shown in Table 4.13. The % conversions and product yields of the regenerated catalysts are not much different from that of fresh catalyst. The significant differences are the yield ratio of distillate oil and heavy oil. The regenerated catalyst provided relatively higher yield of distillate oil and lower yield of heavy oil comparing to the fresh catalyst. This result suggests the regenerated catalysts have less specific surface area than the fresh catalyst.

Table 4.13 Values of %conversion and %yield obtained by catalytic cracking of PP using the fresh and the regenerated catalyst (Condition: 10 wt% catalyst of plastic, N₂ flow of 20 cm³/min, 380 °C, and reaction time of 40 min)

	Fresh Beta20-US30-24h	1°Regenerated Beta20-US30-24h	2°Regenerated Beta20-US30-24h
BET specific surface area (m ² /g)	703	552	534
%Conversion*	97.50	95.57	95.25
%Yield*			
1. gas fraction	37.30	35.67	34.25
2. liquid fraction	60.20	59.90	61.00
- % distillate oil	80.45	67.38	65.97
- % heavy oil	19.55	32.62	34.03
3. residue	2.50	4.43	4.75
- wax	1.36	2.75	3.05
- solid coke	1.15	1.68	1.70
Total volume of liquid fraction (cm ³)	4.28	4.26	4.35
Liquid fraction density (g/cm ³)	0.71	0.70	0.71

*Deviation within 0.5% for conversion, 0.8% for yield of gas fraction, 0.4% for yield of liquid fraction, and 0.5% for yield of residue

Figure 4.46 shows the accumulative volume of liquid fraction in the graduated cylinder. The rates of liquid formation are not significantly different no matter using the fresh or the regenerated catalyst. Moreover, total amounts of liquid

fraction are not different. This shows that the catalysts can be used again at similar efficiency after regeneration.

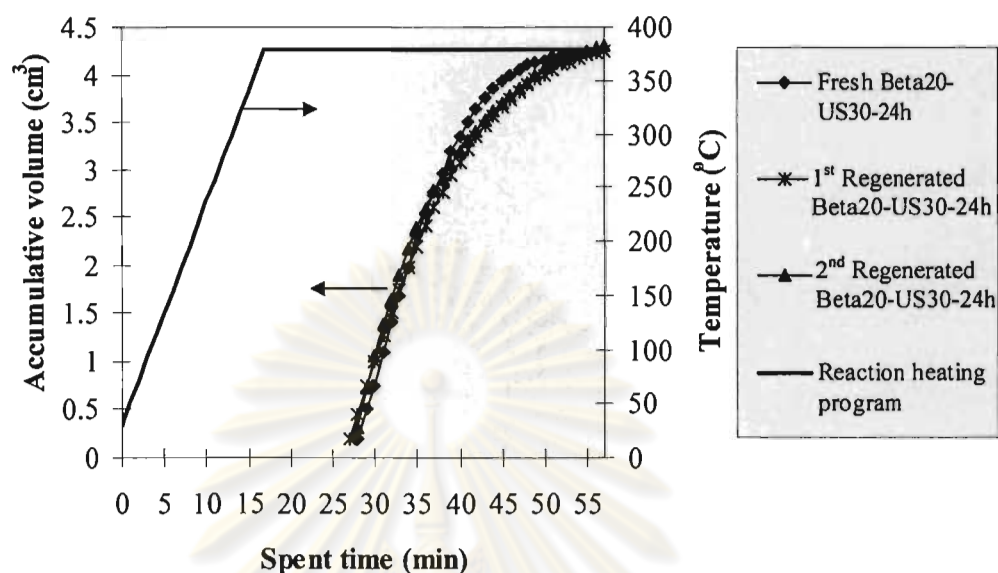


Figure 4.46 Accumulative volume of liquid fraction obtained by catalytic cracking of PP using the fresh and the regenerated Beta20-US30-24h catalysts (Condition: 10 wt% catalyst of plastic, N_2 flow of $20 \text{ cm}^3/\text{min}$, $380 \text{ }^\circ\text{C}$, and reaction time of 40 min).

Figure 4.47 shows distribution of gas fraction obtained by the PP cracking using the fresh and the regenerated Beta20-US30-24h catalysts at 380°C . The gas fraction composes the same product distribution. There is no difference in selectivity in gas fraction between the three catalysts.

Figure 4.48 shows product distribution of the liquid fraction obtained by the PP cracking using the fresh and the regenerated Beta20-US30-24h catalysts 380°C . Both fresh and regenerated catalysts provide mainly C_8 to C_9 range in liquid fraction.

From the results mentioned above, zeolite beta is stable for the use as cracking catalyst and the used catalyst can be regenerated easily in a furnace. Its cracking activity still does not change significantly.

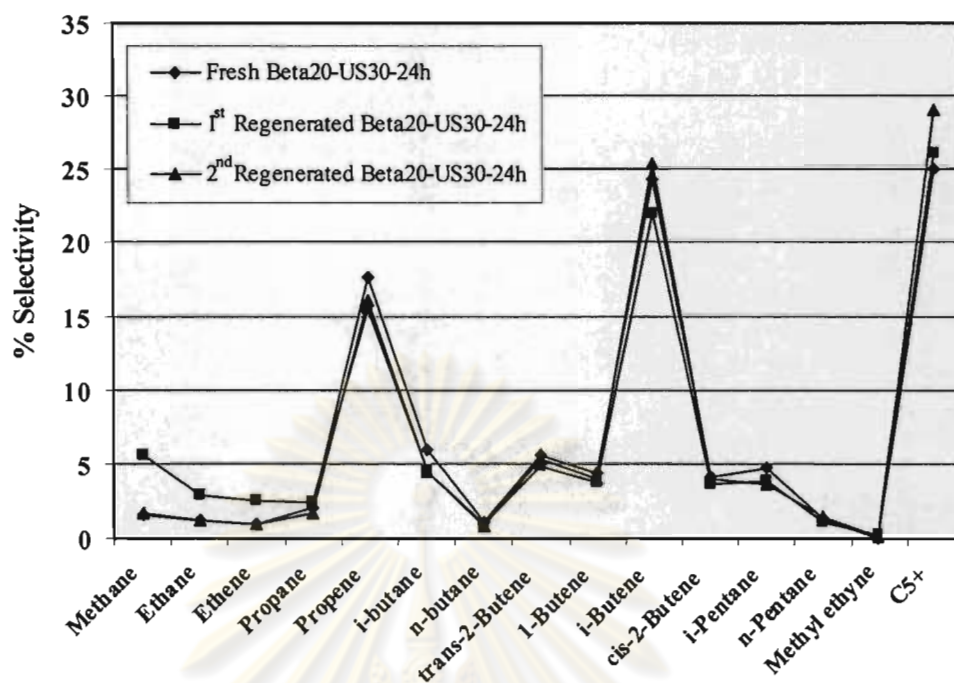


Figure 4.47 Distribution of gas fraction obtained by catalytic cracking of PP using the fresh and the regenerated Beta20-US30-24h catalysts (Condition: 10 wt% catalyst of plastic, N₂ flow of 20 cm³/min, 380 °C, and reaction time of 40 min)

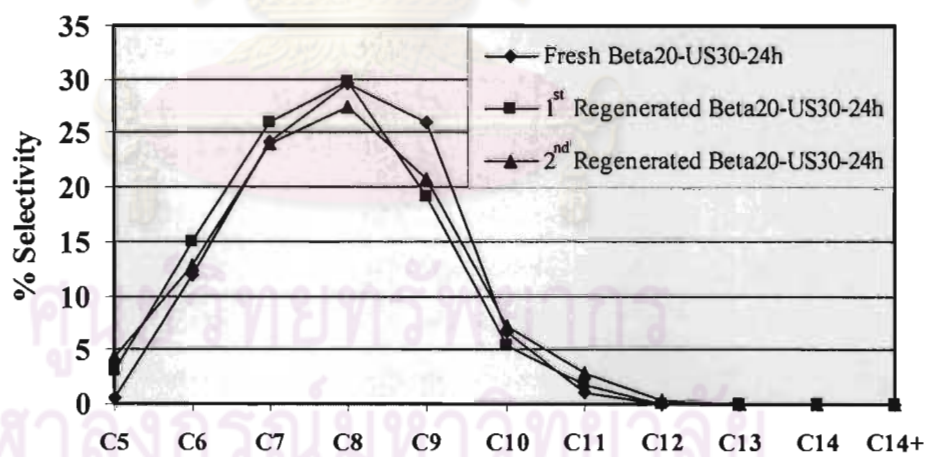


Figure 4.48 Carbon number distributions of liquid fraction obtained by catalytic cracking of PP using the fresh and the regenerated Beta20-US30-24h catalysts (Condition: 10 wt% catalyst of plastic, N₂ flow of 20 cm³/min, 380 °C, and reaction time of 40 min)

4.5 Activity of Various Zeolite Beta Catalysts in HDPE Cracking

4.5.1 Effect of Si/Al Ratios in Catalyst

In order to reduce the influence of temperature on catalytic cracking of HDPE waste over zeolite beta catalysts with different Si/Al ratios, the catalytic reaction was tested at temperature of 380°C where conversion of thermal cracking is only 0.6%. The values of %conversion and %yield obtained by the thermal cracking and catalytic cracking of HDPE waste over various catalysts for both normal and ultrasound irradiation methods with different Si/Al ratios at 380°C are shown in Table 4.14 and 4.15, respectively. The %conversion for catalytic cracking is extremely higher than thermal cracking. The result indicates that the degradation of HDPE at the low temperature of 380°C hardly occur without presence of catalyst. For catalytic cracking, the yield of liquid fraction was higher than that of gas fraction. The high activity and high liquid product yield of nanocrystalline zeolite beta can be elucidate by considering the rapid cracking of HDPE over the acid sites on external surface and fast mass transfer of cracked fragments in the pore of nanocrystalline zeolite beta. The reduced intracrystalline residence period of cracked fragments leads to less cracking reactions, resulting in high liquid products yield [30]. The %conversion and %yield are not significantly affected by the change in Si/Al ratios in the range 40 to 60. However, the change in Si/Al ratio of 20 provides the highest conversion as well as liquid fraction yield for both methods even if the Si/Al ratio of 20 presents the lowest BET specific surface. This result indicates that the acidity of those catalysts is more dominant than its specific surface area. Considering at the Si/Al ratio of 20, Beta20-US30-24h catalyst shows the higher %liquid fraction yield and the less %residue than Beta20-24h because of the higher acidity of Beta20-US30-24h as mention in Section 4.3.6.

Conversion obtained in the catalytic cracking of HDPE is lower than that of PP (Table 4.8) at the same temperature owing to the enhanced reactivity associated to the structure of these polymers. HDPE is formed by linear macromolecule, whereas PP is characterized by a certain degree of branching. The presence of tertiary carbon in the PP molecules provides favorable positions for the initiation of the polymer chain cracking since their activation requires weaker conditions than the secondary carbon activation does [78].

Table 4.14 Values of %conversion and %yield obtained by thermal cracking and catalytic cracking of HDPE over normal zeolite beta catalysts with various Si/Al ratios (Condition: 10 wt% catalyst of plastic, N₂ flow of 20 cm³/min, 380°C, and reaction time of 40 min)

	Thermal 380°C	Beta20- 24h	Beta40- 24h	Beta60- 24h	Beta80- 24h
%Conversion*	0.60	90.20	87.20	88.20	85.50
%Yield*					
1. gas fraction	0.60	37.60	38.00	40.60	38.40
2. liquid fraction	-	52.60	49.20	47.60	47.10
- % distillate oil	-	69.27	67.52	68.52	67.46
- % heavy oil	-	30.73	32.48	31.48	32.54
3. residue	99.40	9.80	12.80	11.80	14.50
- wax	99.40	8.09	11.03	9.86	12.88
- solid coke	-	1.71	1.77	1.94	1.62
Total volume of liquid fraction (cm ³)	-	3.70	3.42	3.35	3.30
Liquid fraction density (g/cm ³)	-	0.70	0.69	0.71	0.70

*Deviation within 0.5% for conversion, 0.7% for yield of gas fraction, 0.6% for yield of liquid fraction, and 0.5% for yield of residue

ศูนย์วิทยทรัพยากร
จุฬาลงกรณ์มหาวิทยาลัย

Table 4.15 Values of %conversion and %yield obtained by thermal cracking and catalytic cracking of HDPE over zeolite beta prepared by ultrasound method and with various Si/Al ratios (Condition: 10 wt% catalyst of plastic, N₂ flow of 20 cm³/min, 380°C, and reaction time of 40 min)

	Thermal 380°C	Beta20- US30-24h	Beta40- US30-24h	Beta60- US30-24h	Beta80- US30-24h
%Conversion*	0.60	93.53	89.40	89.90	86.60
%Yield*					
1. gas fraction	0.60	38.93	40.00	42.63	38.00
2. liquid fraction	-	54.60	49.40	47.27	48.60
- % distillate oil	-	70.77	69.16	70.30	69.48
- % heavy oil	-	29.23	30.84	29.70	30.52
3. residue	99.40	6.47	10.60	10.10	13.40
- wax	99.40	4.95	9.05	8.44	11.56
- solid coke	-	1.52	1.55	1.66	1.84
Total volume of liquid fraction (cm ³)	-	3.82	3.48	3.30	3.40
Liquid fraction density (g/ cm ³)	-	0.70	0.71	0.70	0.71

*Deviation within 0.6% for conversion, 0.8% for yield of gas fraction, 0.5% for yield of liquid fraction, and 0.6% for yield of residue

Figure 4.49 shows accumulative volume of liquid fraction in the graduated cylinder in case of normal zeolite beta with different Si/Al ratio. The initial rate of zeolite beta ratio of 20 and 40 are slightly faster than those of zeolite beta ratio of 60 and 80. The highest overall rate is Beta20-24h.

Figure 4.50 shows accumulative volume of liquid fraction in the graduated cylinder in case of samples synthesized by ultrasound irradiation method. The rate of liquid fraction formation for HDPE cracking over zeolite beta with different Si/Al ratios are quite different and Beta20-US30-24h is faster than that over the others. That confirms the acidity effect of aluminum incorporated in the zeolite beta structure can play important role on activity of the catalysts in cracking of HDPE.

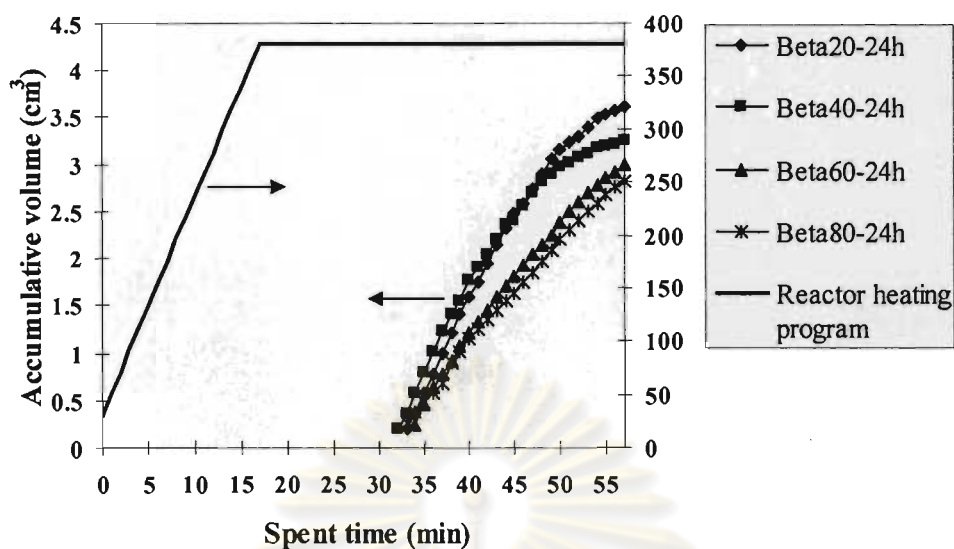


Figure 4.49 Accumulative volume of liquid fraction obtained by catalytic cracking of HDPE using normal zeolite beta with different Si/Al ratios (Condition: 10 wt% catalyst of plastic, N_2 flow of $20 \text{ cm}^3/\text{min}$, $380 \text{ }^\circ\text{C}$, and reaction time of 40 min).

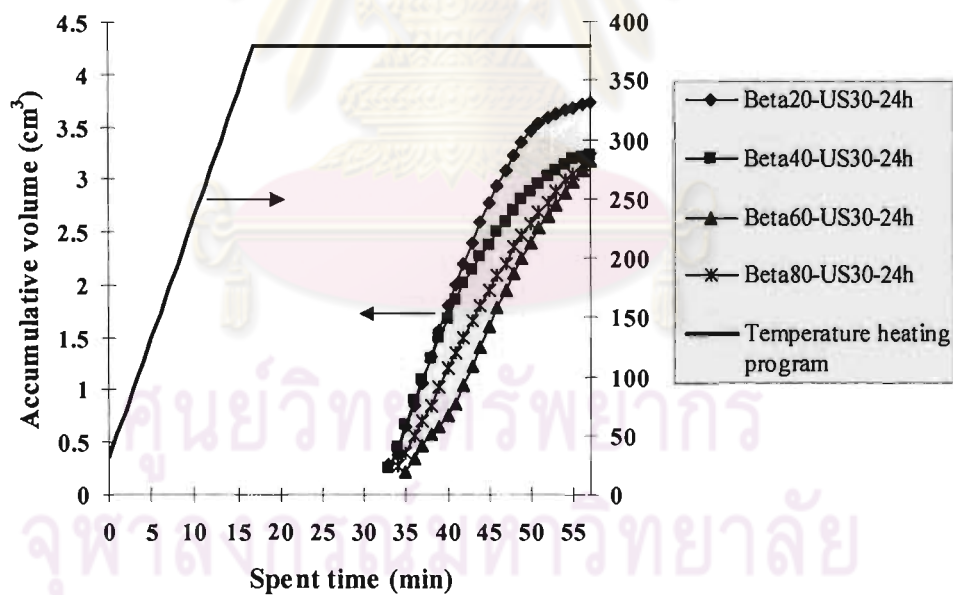


Figure 4.50 Accumulative volume of liquid fraction obtained by catalytic cracking of HDPE using zeolite beta prepared by ultrasound method and with different Si/Al ratios (Condition: 10 wt% catalyst of plastic, N_2 flow of $20 \text{ cm}^3/\text{min}$, $380 \text{ }^\circ\text{C}$, and reaction time of 40 min)

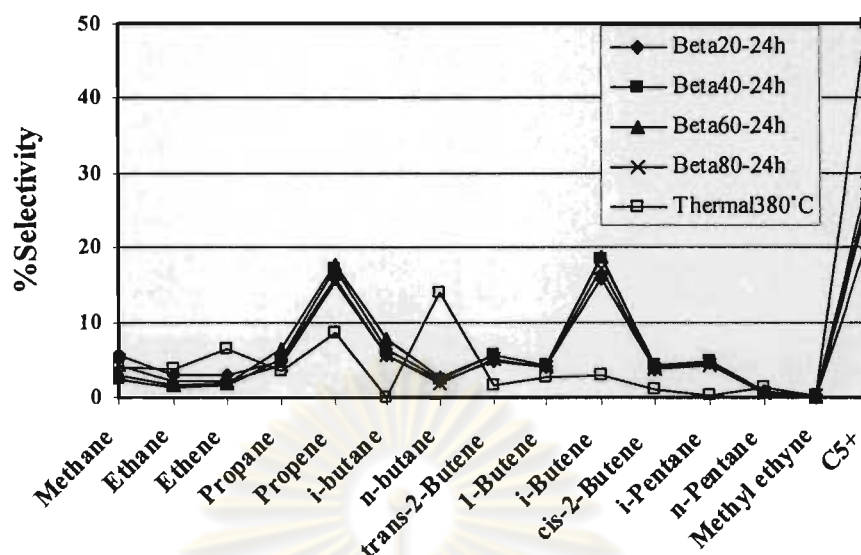


Figure 4.51 Distribution of gas fraction obtained by thermal cracking and catalytic cracking of HDPE using normal zeolite beta with various Si/Al ratios (Condition: 10 wt% catalyst of plastic, N_2 flow of $20 \text{ cm}^3/\text{min}$, $380 \text{ }^\circ\text{C}$, and reaction time of 40 min)

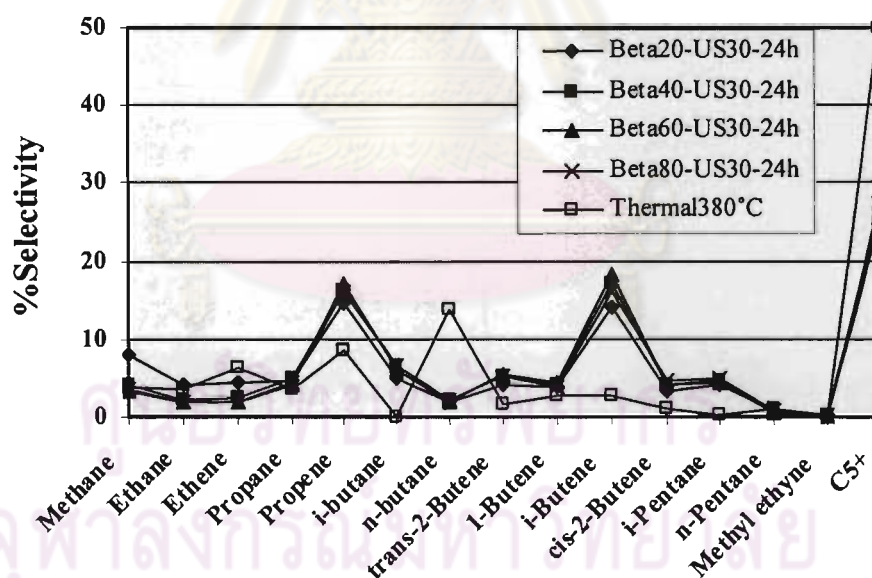


Figure 4.52 Distribution of gas fraction obtained by thermal cracking and catalytic cracking of HDPE using zeolite beta synthesized by ultrasound method and with different Si/Al ratios (Condition: 10 wt% catalyst of plastic, N_2 flow of $20 \text{ cm}^3/\text{min}$, $380 \text{ }^\circ\text{C}$, and reaction time of 40 min)

Figure 4.51 and Figure 4.52 show distribution plots of gas fraction obtained by thermal cracking and catalytic cracking of HDPE over zeolite beta synthesized without and with ultrasound irradiation and with various Si/Al ratios at 380°C. For thermal cracking, ethane, propene, n-butane and C_5^+ are main products and C_5^+ is prominent, whereas gas fractions from catalytic cracking consist of mainly propene, i-butene and C_5^+ . The product distribution in gaseous phase is not different upon changing the Si/Al ratios in the catalyst for both synthesis methods.

Figure 4.53 and Figure 4.54 shows product distribution of distillate oil obtained by the catalytic cracking of HDPE over zeolite beta prepared by normal and ultrasound irradiation methods, respectively. For the HDPE cracking over all catalysts, the liquid fraction is rich of C_7 and C_8 . That is very similar to a commercial SUPELCO standard gasoline (Figure 4.36). When Si/Al ratios decrease, the component C_7 increases in case of catalysts synthesized with application of ultrasound irradiation (Figure 4.54). It can be explicated that the higher acidity provides the formation of lighter liquid fraction. For catalytic cracking over normal catalysts, the liquid product distribution are not significant different.

Comparison between synthesis with and without application of ultrasound irradiation, ultrasound irradiation causes the C_7 and C_8 components increase of about 5%, whereas the C_6 and C_9 components is reduced. Therefore, application of ultrasound irradiation co-operates to degrade the heavier waxy residue into lighter liquid hydrocarbons fraction. In the rest of this work, Beta20-US30-24h was chosen due to noticeably amount of conversion and liquid fraction.

ศูนย์วิทยทรัพยากร
จุฬาลงกรณ์มหาวิทยาลัย

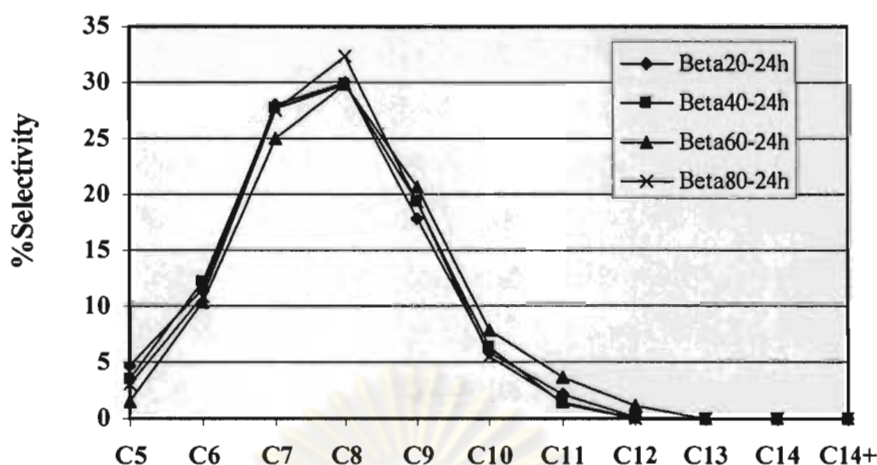


Figure 4.53 Carbon number distribution of liquid fraction from catalytic cracking of HDPE over normal zeolite beta with various Si/Al ratios (Condition: 10 wt% catalyst of plastic, N_2 flow of $20 \text{ cm}^3/\text{min}$ and reaction of 40 min).

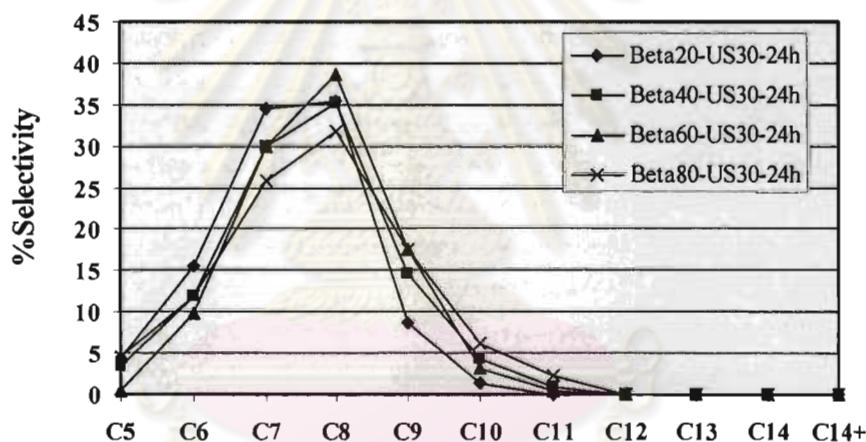


Figure 4.54 Carbon number distribution of liquid fraction from catalytic cracking of HDPE over zeolite beta synthesized by ultrasound irradiation method with various Si/Al ratios (Condition: 10 wt% catalyst of plastic, N_2 flow of $20 \text{ cm}^3/\text{min}$ and reaction of 40 min)

4.5.2 Effect of Reaction Temperature

Table 4.16 summarizes the values of %conversion and %yield obtained in the thermal cracking and catalytic cracking of HDPE over Beta20-US30-24h at 380°C and 400°C . In case of thermal cracking, the increase in reaction temperature from 380°C to 400°C gave the increase in conversion of only 3% and no liquid fraction was

obtained even if the reaction temperature reached to 400°C. The catalytic cracking presents the both conversion and product yield greatly higher than the thermal degradation, because of the high acidity of zeolite beta. Increasing temperature from 380°C and 400°C resulted in significant higher %conversion as well as liquid product yield of HDPE. That indicates both conversion and yield of liquid products are affected by reaction temperature. The increase of product yields (gases, liquids) as function of temperature could be caused by the differences in the thermal stability of polymer chain, since hydrocarbons have reducing thermal stability with increasing temperature.

Table 4.16 Values of %conversion and %yield obtained by thermal cracking and catalytic cracking of HDPE over Beta20-US30-24h at 380°C and 400°C (Condition: 10%wt catalyst of plastic, N₂ flow of 20 cm³/min and reaction of 40 min)

	Reaction temperature=380°C		Reaction temperature=400°C	
	Thermal	Beta20-US30-24h	Thermal	Beta20-US30-24h
%Conversion*	0.60	93.53	3.40	96.00
%Yield*				
1. gas fraction	0.60	38.93	3.40	36.80
2. liquid fraction	-	54.60	-	59.20
- % distillate oil	-	70.77	-	71.83
- % heavy oil	-	29.23	-	28.17
3. residue	99.40	6.47	96.60	4.00
- wax	99.40	4.95	96.60	2.61
- solid coke	-	1.52	-	1.39
Total volume of liquid fraction (cm ³)	-	3.82	-	4.20
Liquid fraction density (g/ cm ³)	-	0.70	-	0.71

*Deviation within 0.4% for conversion, 0.6% for yield of gas fraction, 0.5% for yield of liquid fraction, and 0.4% for yield of residue.

Figure 4.55 exhibits the volume of liquid fraction accumulated in the graduated cylinder along the spent time since heating started. The initial rate of 400°C is much faster than 380°C and the higher total volume of liquid fraction is obtained at the temperature of 400°C, indicating that rate of liquid fraction formation depend on the reaction temperature. Therefore on the purpose of conversion of plastic to liquid fuel, the temperature of 400°C was selected for the rest of work on the catalytic cracking of HDPE.

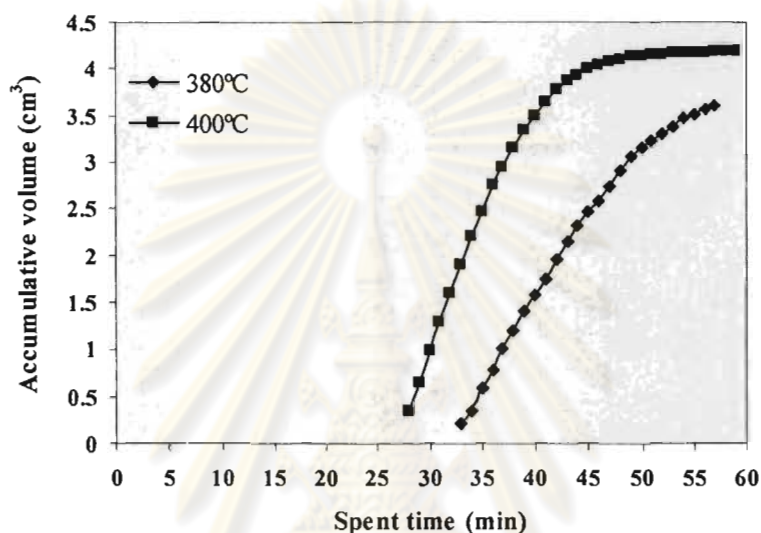


Figure 4.55 Accumulative volume of liquid fraction obtained by catalytic cracking of HDPE using Beta20-US30-24h at 380°C and 400°C (Condition: 10 wt% catalyst of plastic, N₂ flow of 20 cm³/min, and reaction time of 40 min)

The component of gases formed in thermal and catalytic cracking reactions of HDPE using Beta20-US30-24h at 380°C and 400°C are given in Figure 4.56. In thermal cracking, the distribution in gas fraction is mainly propene, n-butane and C₅⁺. In catalytic cracking, the selectivity to propene and i-butene increases and those to n-butane and C₅⁺ decrease, indicating good catalytic activity for producing light hydrocarbon gases. The temperature also affected the composition of gases because the concentration of products of HDPE catalytic cracking (propene and i-butene) increased, while that of C₅⁺ decreased with increasing reaction temperature. Changing of gases component also presents in thermal cracking.

Figure 4.57 shows product distribution of the liquid fraction obtained by catalytic cracking of HDPE using Beta20-US30-24h at 380°C and 400°C. For the catalytic cracking at 380°C, the liquid fraction is mainly C₇ and C₈ components, whereas C₇ component is main liquid fraction for catalytic cracking at 400°C. When the temperature increases, the amount of lighter hydrocarbon of C₅ slightly increases while that of heavier hydrocarbon of C₈ decreases. It can be concluded that not only the presence of catalysts, but also the temperature affects the gases and liquid components.

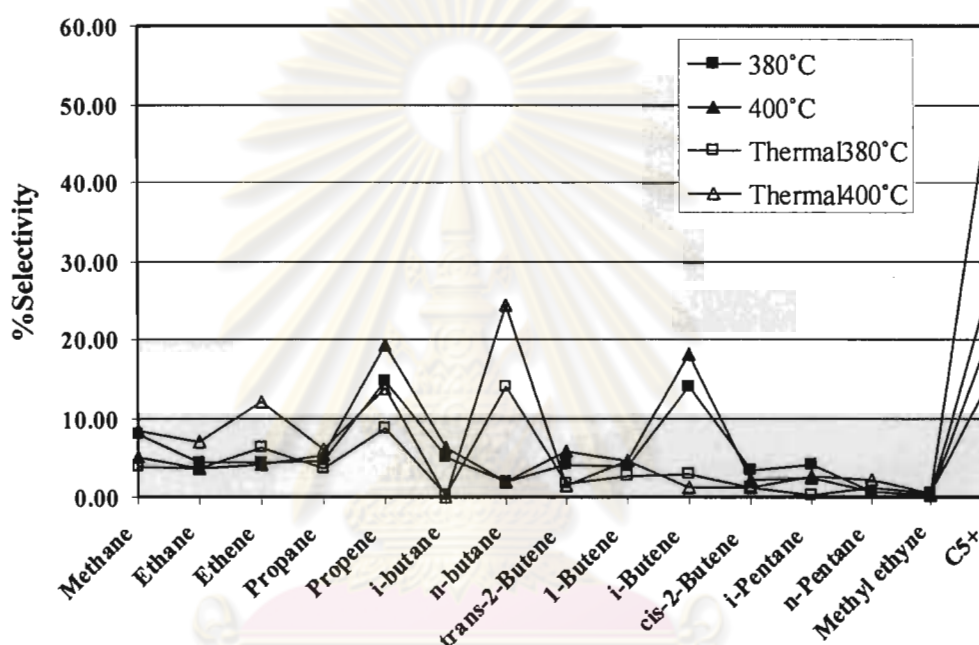


Figure 4.56 Distribution of gas fraction obtained by thermal cracking and catalytic cracking of HDPE using Beta20-US30-24h at 380°C and 400°C (Condition: 10 wt% catalyst of plastic, N₂ flow of 20 cm³/min, and reaction time of 40 min)

จุฬาลงกรณ์มหาวิทยาลัย

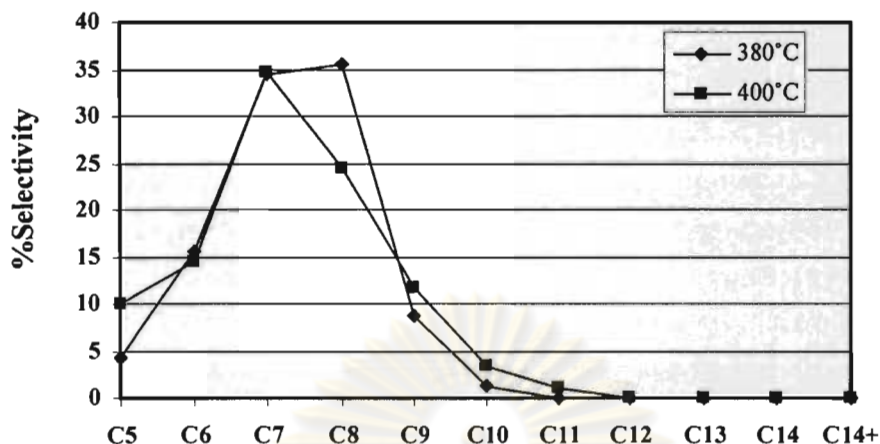


Figure 4.57 Carbon number distribution of liquid fraction from catalytic cracking of HDPE over Beta20-US30-24h at 380°C and 400°C (Condition: 10 wt% catalyst of plastic, N₂ flow of 20 cm³/min and reaction of 40 min)

4.5.3 Effect of HDPE to Catalyst Ratios

The %conversion and product yield obtained by catalytic cracking of HDPE waste at 400°C over Beta20-US30-24h catalysts with different catalyst amounts of 5wt%, and 10wt% to HDPE are given in Table 4.17. The high conversion value of 92.80% is obtained when using 5wt% catalyst amount. Increasing of catalyst amount to 10wt% leads the %conversion slightly increases to 96.00%, indicating that the %conversion slightly depends on the catalyst content. Considering to %product yield, the gas and liquid fraction yields slightly decrease when the amount of catalyst is reduced from 10wt% to 5wt%. The %distillate oil of those conditions is noteworthy. Increasing of catalyst amount to 10wt% leads the %heavy oil reduces by 7%. The residue produced by using 5%wt catalyst amount contains mainly wax due to lower activity compared to using 10%wt catalyst.

Due to the higher %conversion and light liquid hydrocarbon, the optimum catalyst amount is the 10 wt% catalyst to HDPE.

Table 4.17 Conversion and product yield obtained by catalytic cracking of HDPE over Beta20-US30-24h catalysts with different catalyst amounts at 400°C (Condition: N₂ flow of 20 cm³/min, and reaction time of 40 min)

	Catalyst amount to HDPE	
	5 wt%	10 wt%
%Conversion*	92.80	96.00
%Yield*		
1. gas fraction	34.40	36.80
2. liquid fraction	58.40	59.20
- % distillate oil	64.57	71.83
- % heavy oil	35.43	28.17
3. residue	7.20	4.00
- wax	5.78	2.61
- solid coke	1.42	1.39
Total volume of liquid fraction (cm ³)	4.15	4.20
Liquid fraction density (g/cm ³)	0.72	0.71

*Deviation within 0.3% for conversion, 0.5% for yield of gas fraction, 0.5% for yield of liquid fraction, and 0.3% for yield of residue.

The accumulated volume of liquid fraction obtained by catalytic cracking of HDPE waste over Beta20-US30-24h catalyst with different catalyst amounts at 400°C is shown in Figure 4.58. The initial rates of liquid fraction formation in the reaction using 5wt% and 10wt% catalyst content is not significant different, as well as total liquid volumes of both conditions.

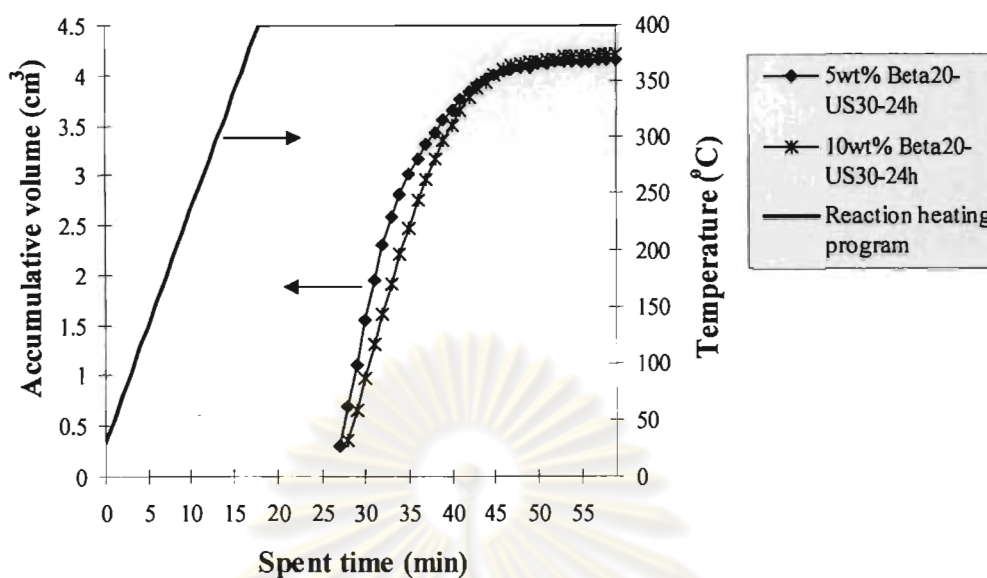


Figure 4.58 Accumulative volume of liquid fractions from catalytic cracking of HDPE over Beta20-US30-24h catalyst with different catalyst amounts at 400°C (Condition: N₂ flow of 20 cm³/min and reaction time of 40 min)

Figure 4.59 shows distribution plots of gas fraction obtained by catalytic cracking of HDPE over Beta20-US30-24h catalyst with various catalyst amounts at 400°C. The mainly gas fraction from HDPE cracking are propene, i-butene and C₅+. Although the product distributions in gaseous phase for 5wt% and 10wt% catalyst amounts are quite similar, there are slightly different in concentration of some hydrocarbon components. Increasing the catalyst amount to 10wt% decreases the heavy hydrocarbon (i-pentane) and increases lighter hydrocarbons (methane, ethane and ethane).

The product distributions of distillate oil obtained by catalytic cracking of HDPE over Beta20-US30-24h catalyst with various catalyst amounts at 400°C are presented in Figure 4.60. The product distribution in liquid phase for 5wt% and 10wt% catalyst amounts are significant different. The C₇ fraction is dominating mainly on the cracking of HDPE using 10wt% catalyst. When catalyst amount is reduced, the C₇ liquid hydrocarbon decreases while the selectivity to C₉ and C₁₀

components increases. It indicates that lighter liquid hydrocarbon was obtained when using 10wt% catalyst amount.

In this work, using 10wt% catalyst amount in HDPE cracking is the best condition according to the highest %conversion and distillate oil fraction.

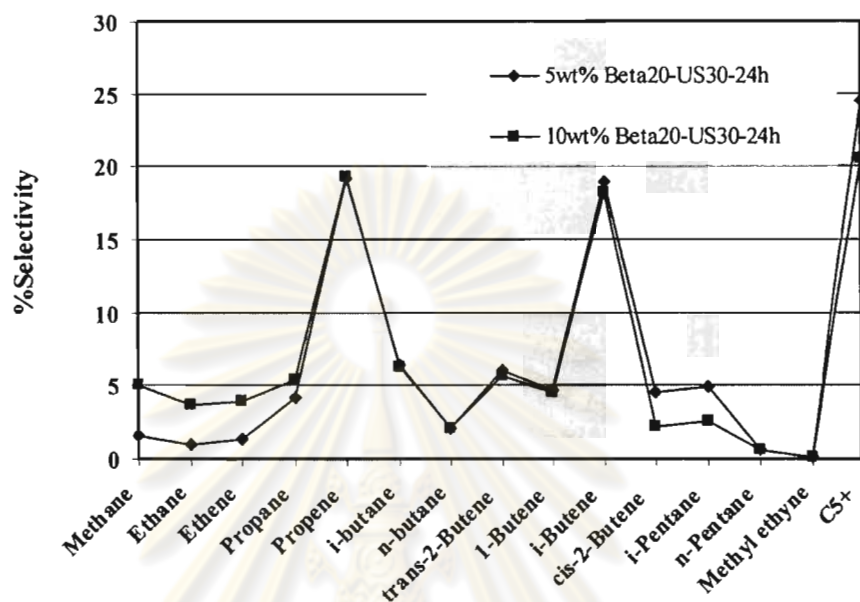


Figure 4.59 Distribution of gas fraction obtained by catalytic cracking of HDPE over Beta20-US30-24h catalyst with different catalyst amounts at 400°C (Condition: N₂ flow of 20 cm³/min and reaction time of 40 min).

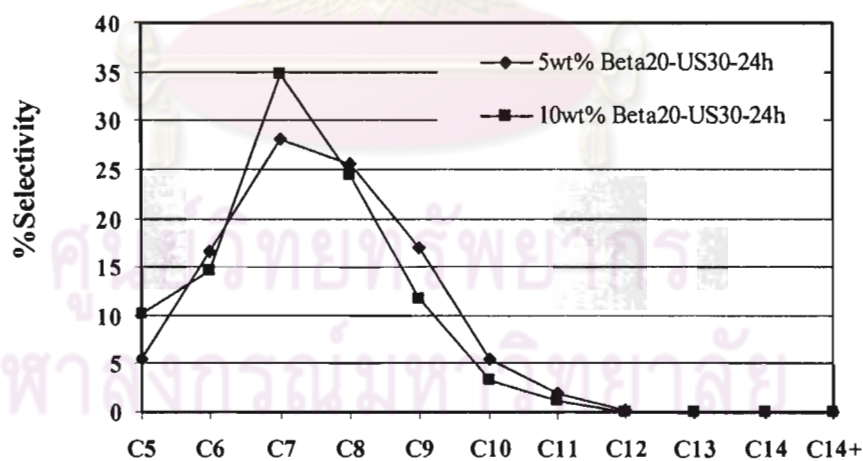


Figure 4.60 Carbon number distribution of distillate oil obtained by catalytic cracking of HDPE over Beta20-US30-24h catalysts with different catalyst amounts at 400°C (Condition: 10 wt% catalyst of plastic, N₂ flow of 20 cm³/min and reaction time of 40 min).

4.5.4 Catalyst Regeneration

4.5.4.1 XRD Results

The used zeolite beta easily turned to white after regeneration by calcination in a muffle furnace at 550°C for 5 h. XRD patterns of the calcined unused and the regenerated catalysts are presented in Figure 4.61. The two characteristic peaks of zeolite beta are still remained with almost the same crystallinity as the unused catalyst, even if catalysts were used in HDPE cracking and regenerated for three times. This indicates the high stability of the zeolite beta structure.

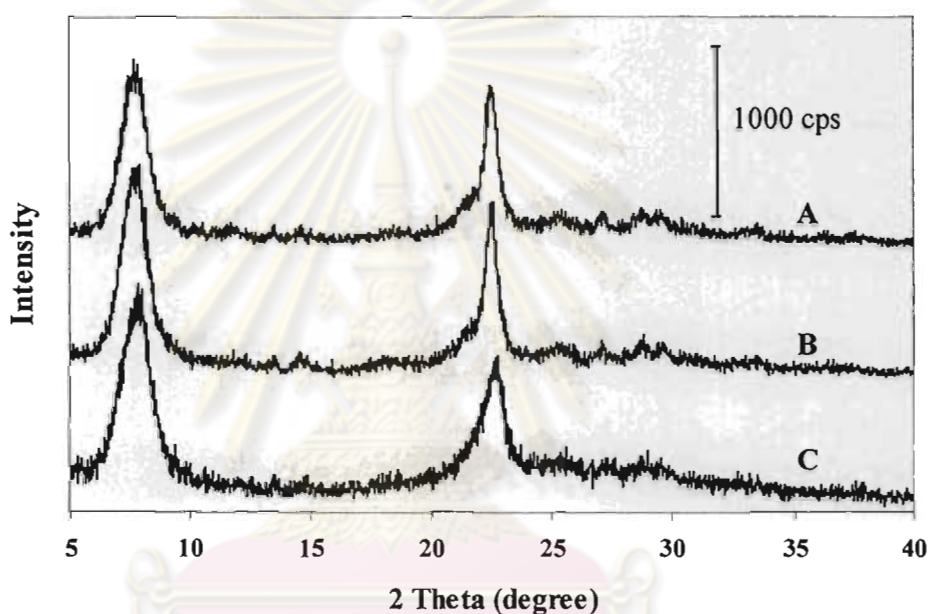


Figure 4.61 XRD patterns of (A) the calcined unused (B) the 1st regenerated Beta20-US30-24h and (C) the 2nd regenerated Beta20-US30-24h catalysts

4.5.4.2 SEM Images

SEM images of the 3rd regenerated Beta20-US30-24h sample with different magnification are shown in Figure 4.62. After the third HDPE cracking, the 3rd regenerated Beta20-US30-24h sample has sphere like shape with un-uniform size compared to the fresh catalyst SEM image of which has been shown in Figure 4.21.

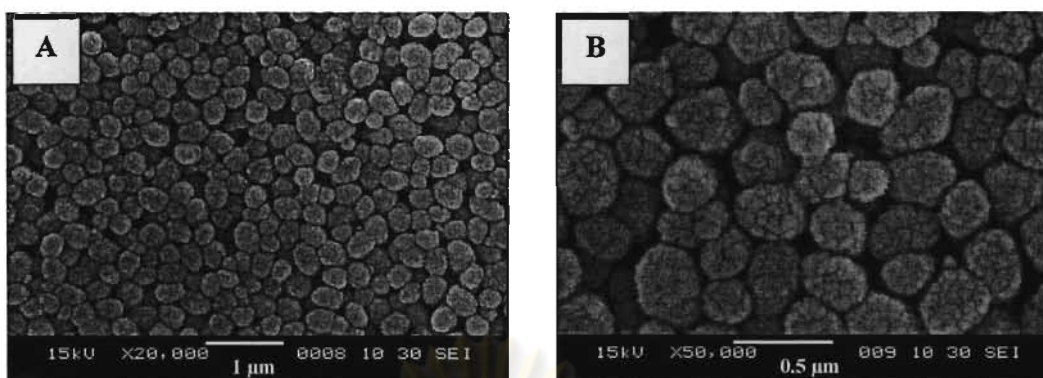


Figure 4.62 SEM images of the 3rd regenerated Beta20-US30-24h sample with different magnification (A) x20,000 and (B) x50,000 times

4.5.4.3 Nitrogen Adsorption-Desorption

Figure 4.63 shows the adsorption-desorption isotherms of fresh catalyst and regenerated catalyst. Both 1st and 2nd regenerated catalyst exhibit the characteristic isotherm of microporous materials with the specific surface area of 636 and 602 m²/g, respectively. It was steeply decreased compared with the fresh catalyst (703 m²/g).

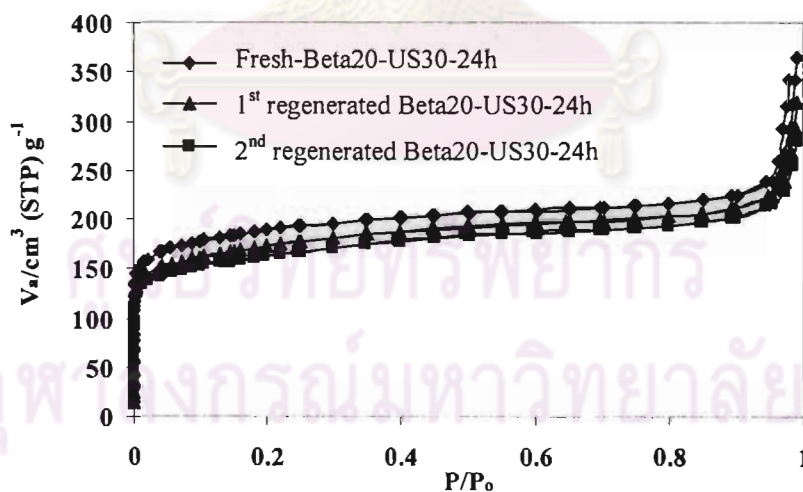


Figure 4.63 N₂ adsorption-desorption isotherms of the fresh and the regenerated Beta20-US30-24h sample

4.5.4.4 Activity of Regenerated Zeolite Beta in HDPE Cracking

Table 4.18 summarized the values of %conversion and %yield obtained by the HDPE cracking using fresh and regenerated Beta20-US30-24h catalyst at 400°C. The values of %conversion obtained in the third cracking are not different from that of fresh catalyst. There are no different between the yield of gas and liquid fraction of fresh and 1st regenerated catalyst, whereas the 2nd regenerated catalyst provided relatively lower yield of gas fraction and higher yield of liquid fraction comparing to the fresh catalyst. Moreover, greatly higher yield of heavy oil and lower yield of distillate oil were obtained for the regenerated catalyst comparing to the fresh catalyst. This result suggests that the regenerated catalyst has less specific surface area than the fresh catalyst. It is illustrious that in the cracking of C-C bonds, the specific surface area of catalysts plays an important role; primary cracking reactions of polymer chain proceed on the macroporous surface of the catalyst, while the smaller fragments are cracked on their micropore surface. The 2nd regenerated catalyst has the lowest specific surface area resulting in lowest gas fraction yield. However the specific surface area is not affect the HDPE conversion.

Table 4.18 Values of %conversion and yield obtained by catalytic cracking of HDPE using the fresh and the regenerated catalyst (Condition: 10 wt% catalyst of plastic, N₂ flow of 20 cm³/min, 400°C, and reaction time of 40 min)

	Fresh Beta20-US30-24h	1 st Regenerated Beta20-US30-24h	2 nd Regenerated Beta20-US30-24h
BET specific surface area (m ² /g)	703	636	602
%Conversion*	96.00	96.40	96.6
%Yield*			
1. gas fraction	36.80	35.00	32.4
2. liquid fraction	59.20	61.40	64.20
- % distillate oil	71.83	58.76	50.49
- % heavy oil	28.17	41.24	49.51
3. residue	4.00	3.60	3.40
- wax	2.61	1.97	1.70
- solid coke	1.39	1.63	1.70
Total volume of liquid fraction (cm ³)	4.20	4.27	4.45
Liquid fraction density (g/cm ³)	0.71	0.72	0.72

*Deviation within 0.6% for conversion, 0.8% for yield of gas fraction, 0.4% for yield of liquid fraction, and 0.6% for yield of residue

Figure 4.64 shows the accumulative volume of liquid fraction in the graduated cylinder. The rates of liquid formation are slightly different when using the fresh and the regenerated catalyst. HDPE cracking using 2nd regenerated catalyst provides the higher total volume of liquid fraction than that using fresh and 1st regenerated catalyst due to the less specific surface area mentioned above.

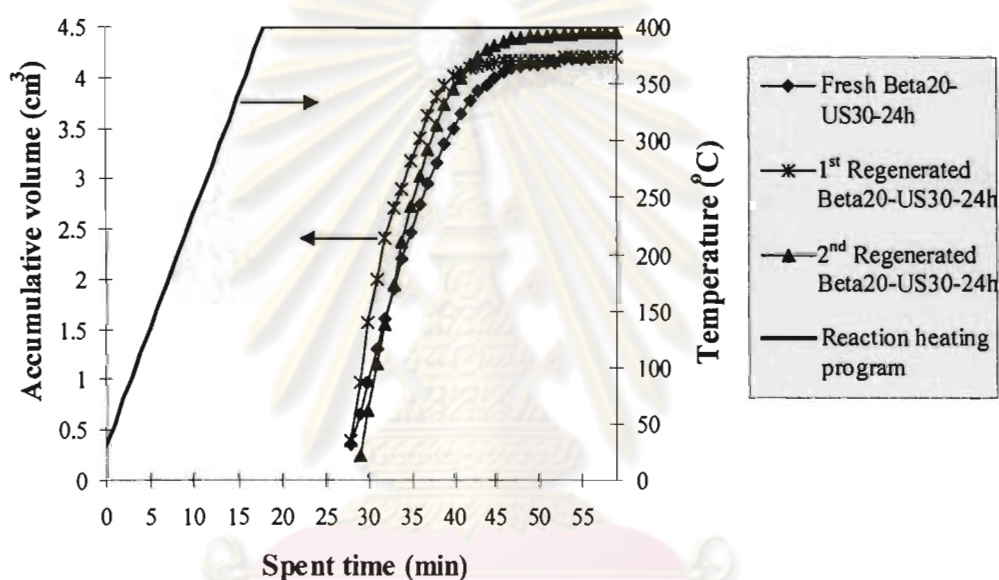


Figure 4.64 Accumulative volume of liquid fraction obtained by catalytic cracking of HDPE waste using the fresh and the regenerated Beta20-US30-24h catalyst (Condition: 10 wt% catalyst of plastic, N₂ flow of 20 cm³/min, 400°C, and reaction time of 40 min).

The distribution of gases component formed in HDPE cracking over the fresh and the regenerated Beta20-US30-24h catalyst at 400°C is given in Figure 4.65. The gas fraction composes the same product distribution but there are slightly differences in selectivity of gas fraction between the three catalysts. The mainly gas fraction from HDPE cracking are propene, i-butene and C₅+. In case of regenerated catalysts, the heavy hydrocarbon (i-pentane and C₅+) is increased, while the lighter

hydrocarbons (methane, ethane and ethane) are decreased due to the effect of specific surface area.

Figure 4.66 shows product distribution of the liquid fraction obtained by the HDPE cracking using the fresh and the regenerated Beta20-US30-24h catalyst 400°C. Both fresh and regenerated catalysts provide mainly C₇ to C₈ range in liquid fraction. For using fresh catalyst, the liquid fraction is mainly C₇ components. For using regenerated catalyst, the liquid fraction is mainly C₈ components.

This shows that zeolite beta is stable for the use as cracking catalyst and the used catalyst can be regenerated easily in a furnace. Its cracking activity still does not change significantly.

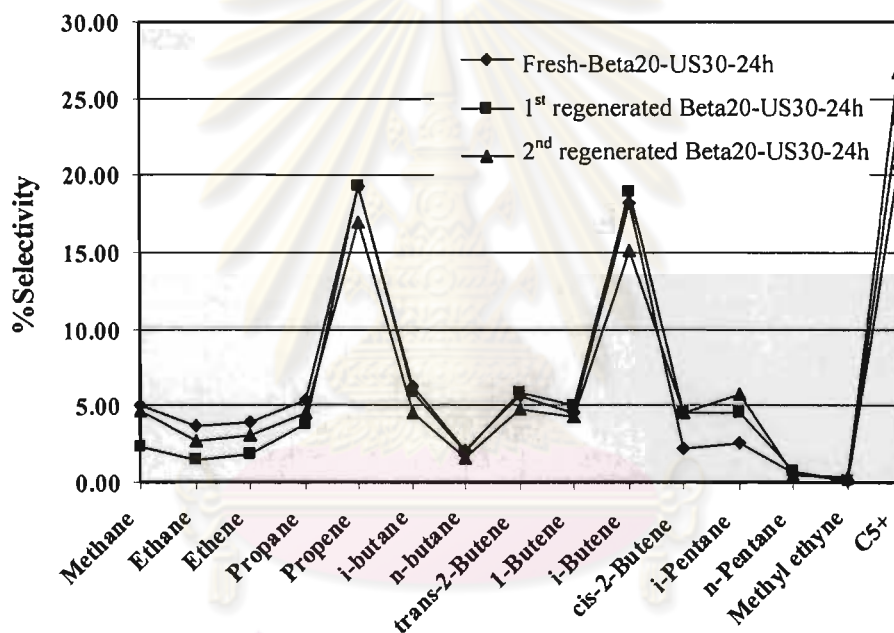


Figure 4.65 Distribution of gas fraction obtained by catalytic cracking of HDPE using the fresh and the regenerated Beta20-US30-24h catalyst (Condition: 10 wt% catalyst of plastic, N₂ flow of 20 cm³/min, 400°C, and reaction time of 40 min)

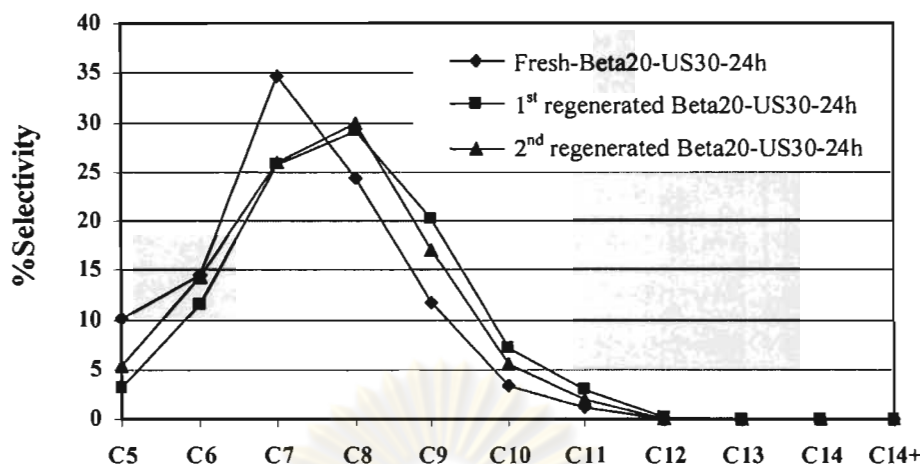


Figure 4.66 Carbon number distributions of liquid fraction obtained by catalytic cracking of HDPE using the fresh and the regenerated Beta20-US30-24h catalyst (Condition: 10 wt% catalyst of plastic, N₂ flow of 20 cm³/min, 400°C, and reaction time of 40 min)

4.6 Comparison of Activity of Zeolite beta, ZSM-5, and Fe-MFI Catalysts in HDPE Cracking

ZSM-5 with the Si/Al ratio of 60 was synthesized by ultrasound irradiation method and crystallized for 24 h. Tetrapropylammonium hydroxide (TPAOH) was used as structure-directing agent with the TPAOH/SiO₂ of 0.1. Fe-MFI with the Si/Fe of 60 was prepared by xerogel method and crystallized for 48 h. Textural properties of calcined zeolite beta, ZSM-5 and Fe-MFI catalysts are summarized in Table 4.19. Beta60-US30-24h shows the smallest particle size of 0.19 μm, resulting in the highest BET specific surface area and external surface area. Although the particle size of ZSM-5 catalyst are extremely larger than others, the BET specific surface area and external surface area of both ZSM-5 and Fe-MFI catalysts are not different. Considering the acidity of all three catalysts, ZSM-5 sample exhibits the highest total acidity, whereas the lowest total acidity is presented in Fe-MFI sample. It is known that the BET specific surface area and especially the external surface area play an important role on enhancing the activity of catalysts as well as acidity.

Table 4.19 Textural properties of calcined zeolite beta, ZSM-5 and Fe-MFI catalysts

Catalyst	Particle size ^a (μm)	S _{BET} ^b (m ² /g)	S _{ext} ^c (m ² /g)	Acidity ^d (mmol/g)		
				Weaker acid site ^e	Stronger acid site ^f	Total ^g
Beta60-US30-24h	0.19	784	62	0.66	0.59	1.25
ZSM-5	2.7	440	49	2.30	0.06	2.36
Fe-MFI	0.32	440	50	0.40	-	0.40

^a particle size estimated by SEM images.

^b Specific surface area determined by application of the BET-plot method.

^c external surface area determined by application of the t-plot method.

^d Obtained by NH₃ temperature programmed desorption.

^e Obtained at temperature around 170°C.

^f Obtained at temperature around 430°C.

^g Summation of number of weaker acid site and stronger acid site.

The catalytic activity of Beta60-US30-24h was compared with ZSM-5 and Fe-MFI catalysts which were synthesized in our laboratory in degradation of HDPE at 400°C. Table 4.19 shows the values of %conversion and product yield obtained by the HDPE cracking over Beta60-US30-24h, ZSM-5 and Fe-MFI catalysts. The values of %conversion obtained in the HDPE cracking over the three catalysts are not different. All three catalysts exhibit a high performance with the conversion over 95% in HDPE wastes cracking with small amount of residue. The significant differences are shown in the %product yield and the ratio of distillate oil and heavy oil. ZSM-5 catalyst presents the highest %gas fraction yield (66.60%) and large amount of distillate oil (71.86%). It can be explained that the highest acidity of ZSM-5 enhances the cracking of smaller fragments (from primary step) on their acid sites located on micropore surface, resulting in the formation of gas fraction and lighter liquid products. It is in agreement with the normal rule for micro-sized zeolites that gas fractions are major product due to their high acidity.

On the other hand, nano-sized Beta60-US30-24h and Fe-MFI catalysts produce higher yields of liquid fraction than gas fraction due to the lower acidity of the two zeolites. It is remarkable that liquid product yield obtained in the catalytic cracking over Beta60-US30-24h is significant higher than that over Fe-MFI, moreover, Beta60-US30-24h shows a high selectivity to distillate oil compared to Fe-MFI. The yield of distillate oil of Beta60-US30-24h is 71.86% while that of Fe-MFI is 57.87%. This result suggests that the higher specific surface area and higher activity of Beta60-US30-24h provide better cracking of HDPE resulting in larger light hydrocarbon liquid.

Table 4.20 Values of %conversion and yield obtained by catalytic cracking of HDPE over zeolite beta, ZSM-5 and Fe-MFI catalysts (Condition: 10wt% catalyst of plastic, N₂ flow of 20 cm³/min, 400°C, and reaction time of 40 min)

	Beta60-US30-24h	ZSM-5	Fe-MFI
%Conversion*	96.20	96.47	95.20
%Yield*			
1. gas fraction	37.63	66.60	40.60
2. liquid fraction	58.57	29.87	54.60
- % distillate oil	72.37	71.86	57.87
- % heavy oil	27.63	28.14	42.13
3. residue	3.80	3.53	4.80
- wax	2.83	2.84	4.23
- solid coke	0.97	0.69	0.57
Total volume of liquid fraction (cm ³)	4.17	1.97	3.85

* Deviation within 0.5% for conversion, 0.6% for yield of gas fraction, 0.4% for yield of liquid fraction, and 0.5% for yield of residue

Figure 4.67 shows distribution of gas fraction obtained by catalytic cracking of HDPE over Beta60-US30-24h, ZSM-5 and Fe-MFI catalysts at 400°C. The major components for catalytic cracking over ZSM-5 are mainly C₄ (n-butane) while that over Fe-MFI is C₃ (propene), and that over Beta60-US30-24h are mainly C₃ (propene), C₄ (i-butene). However, the vapor of C₅⁺ which has higher boiling point

than that of C₅ (n-pentane) is obviously detected in high amount for all catalysts. The gas fraction distributions of all three catalysts are different because shape and size selectivity of products depend on pore size of catalysts. Both ZSM-5 and Fe-MFI are medium pore, while zeolite beta is large pore zeolite. Therefore, zeolite beta provides selectivity to larger gas molecules (i-butene) than the two catalysts.

Figure 4.68 show carbon number distribution of distillate oil obtained by catalytic cracking of HDPE over Beta60-US30-24h, ZSM-5 and Fe-MFI catalysts at 400°C. The major liquid products of both Beta60-US30-24h and ZSM-5 are distributed in the range of C₇ and C₈. That is comparable to the distribution of distillate oil of SUPELCO standard gasoline fraction based on the boiling point range using n-paraffins as reference. In case of catalytic cracking of Fe-MFI, the lighter hydrocarbons in the range of C₆ and C₇ are major liquid products.

According to the results mentioned above, Beta60-US30-24h shows considerably largest amount of liquid fraction and distillate oil, Moreover, it provides highest selectivity to the liquid products in the range of C₇ and C₈ which are in the boiling point range of gasoline production. Therefore, Beta60-US30-24h is a best powerful catalyst for the HDPE degradation

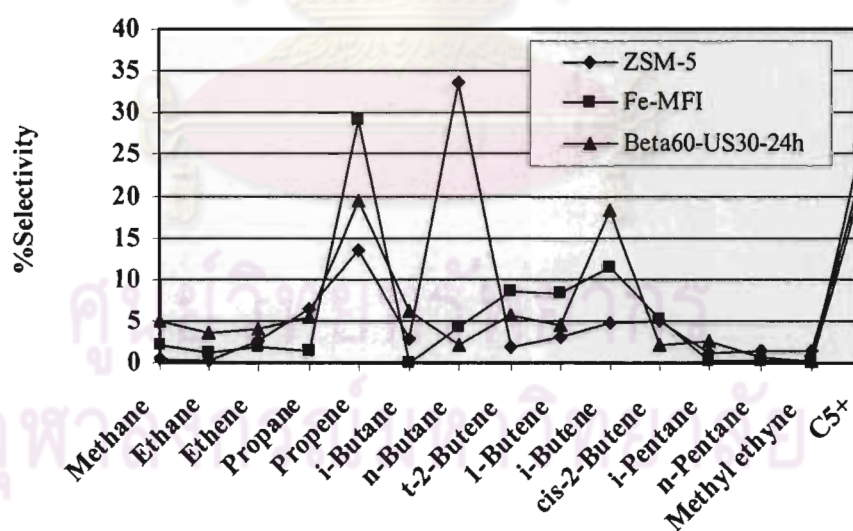


Figure 4.67 Distribution of gas fraction obtained by catalytic cracking of HDPE over zeolite beta, ZSM-5 and Fe-MFI catalysts (Condition: 10 wt% catalyst of plastic, N₂ flow of 20 cm³/min, 400°C, and reaction time of 40 min)

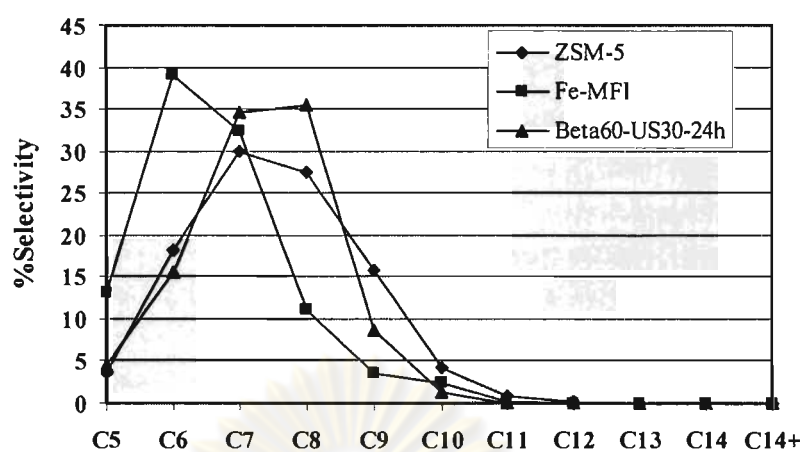


Figure 4.68 Carbon number distributions of liquid fraction obtained by catalytic cracking of HDPE over zeolite beta, ZSM-5 and Fe-MFI catalysts (Condition: 10 wt% catalyst of plastic, N₂ flow of 20 cm³/min, 400°C, and reaction time of 40 min)

ศูนย์วิทยทรัพยากร
จุฬาลงกรณ์มหาวิทยาลัย

CHAPTER V

CONCLUSION

Zeolite beta nanoparticles were synthesized from a freshly prepared silica xerogel mixed with aluminium isopropoxide and a solution of tetraethylammonium hydroxide, followed by hydrothermal crystallization at 135°C for various periods. Application of ultrasound irradiation during the gel formation step did not affect the structure and crystallinity but had significant effect the particle size of zeolite beta. Prolongation of irradiation period from 30 to 120 min does not significant affect the structure, the particle size and specific surface area of zeolite beta. XRD patterns show that formation of zeolite beta can be achieved after 16 h and pure fully crystalline zeolite beta is obtained at 20 h for both synthesis methods, with and without ultrasound irradiation. All samples exhibit a type I isotherm which is typical for microporous materials. The specific surface area in the micropores decreases with the increasing of aluminum content. Beta20-US30-24h shows the lowest relative intensities of octahedral Al to tetrahedral Al indicating that almost all aluminum atoms incorporated into the tetrahedral framework position. For the Si/Al ratios in a range from 40 to 80, the total acidity is not much different for both synthesis methods. For the low Si/Al ratio of 20, the total acidity of Beta20-US30-24h is higher than the total acidity of Beta20-24h. Ultrasound irradiation caused not only yield of zeolite beta increased but also more aluminum incorporated into the tetrahedral framework position resulting in higher acidity.

The catalytic property of synthesized zeolite beta was investigated in polypropylene and high density polyethylene catalytic cracking under different conditions. Crystallization time of 24 h is an optimum condition for zeolite beta synthesis due to a high selectivity to distillate oil and less amounts of coke deposited on its surface. The cracking of high density polyethylene is more difficult than that of polypropylene. When zeolite beta was used as catalyst, the conversions of both plastics are greatly more than that in the absence of catalyst. The Si/Al ratios in

catalyst in the range from 40 to 80 do not affect plastic conversions and product yields. Application of ultrasound radiation to the sample with the low Si/Al ratio of 20 provides the highest conversion as well as liquid product yield due to the highest acidity of the catalyst. The plastic conversions and yields of liquid products depend on the cracking temperature and the plastic to catalyst ratio. The value of % conversion increases when reaction temperature and plastic to catalyst ratio increase. The higher acidity causes higher efficiency in cracking PP and HDPE to products and fewer residues was left in the catalytic reactor. The product selectivity is affected slightly. The gas products obtained by polypropylene and high density polyethylene cracking are mainly propene, i-butene and C_5^+ . The liquid products obtained by cracking of both types of plastic are mainly in the boiling point range from C_6 to C_9 which is similar to that for commercial gasoline fraction hydrocarbon based on the boiling point range using n-paraffins as reference. The used zeolite beta catalyst can be regenerated easily in a furnace and its cracking activity still does not change significantly.

The suggestions for future work

1. To investigate the type of hydrocarbon components in liquid fraction product.
2. To compare zeolite beta with other zeolite and mesoporous materials for catalytic cracking of HDPE and PP under the same condition.
3. To investigate the efficiency of zeolite beta for catalytic cracking of mixed plastic containing HDPE, LDPE, PP, PS.

ศูนย์วิทยทรัพยากร
จุฬาลงกรณ์มหาวิทยาลัย

REFERENCES

- [1] Plastic recycling information sheet [Online]. 2004. Available from: <http://www.wasteonline.org.uk/resources/InformationSheets/Plastics.htm> [2008, February 29]
- [2] Michaeli, W. *Plastic Processing: An Introduction*, pp. 1-2, 13. New York: Hanser Publishers, 1995.
- [3] Recycling Plastics [Online]. Available from: <http://www.polymer.com/dotcom/home.html> [2006, August 5]
- [4] Plastics: Future Contract [Online]. Available from: <http://www.ncdex.com> [2007, December 2]
- [5] Lotfi, A. Plastic Recycling [Online]. 2007. Available from: <http://www.lotfi.net/recycle/plastic.html#intro> [2008, February 11]
- [6] Yuva, J. Plastics Are on the Move [Online]. ISM Chemical Group. 2006. Available from: <http://www.ism.ws/pubs/EmailNewsletters/ChemicalsNewsletter/eDigestChemicalDetail.cfm?ItemNumber=15575> [2007, July 20]
- [7] Marcilla, A.; Ruiz-Femenia, R.; and Hernandez, J. Thermal and catalytic pyrolysis of crosslinked polyethylene. *J. Anal. Appl. Pyrol.* 76(2006): 254.
- [8] Marcilla, A.; Gómez, A.; Menargues, S.; García-Martinez, J.; and Cazorla-Amorós, MD. Catalytic cracking of ethyl-vinyl acetate copolymers: comparison of different zeolite. *J. Anal. Appl. Pyrol.* 68-69(2003): 495-506.
- [9] Ali, S.; Garforth, A. A.; Harris, D. H.; Rawlence, D. J.; and Uemichi, Y. Polymer waste recycling over used catalyst. *Catal. Today* 75(2002): 247.
- [10] Serrano, D. P.; Aguado, J.; Escola, J. M.; Rodriguez, J. M.; and Miguel, G. S. An investigation into the catalytic cracking of LDPE using Py-GC/MS. *J. Anal. Appl. Pyrol.* 74(2005): 370.
- [11] Aguado, J.; and Serrano, D. P. *Feedstock Recycling of plastic wastes*. pp. 154. The royal Society of Chemistry, Cambridge, 1999.
- [12] Kim, J. R.; Yoon, J. H.; and Park, D. W. Catalytic recycling of the mixture of polypropylene and polystyrene. *Polym. Degrad. Stab.* 76(2002): 61.

- [13] Kaminsky, W.; Schlesselmann, B.; and Simon, C. Olefins from polyolefins and mixed plastic by pyrolysis. *J. Anal. Appl. Pyrol.* 32(1995): 19.
- [14] Conesa, J. A.; Fant, R.; Marcilla, A.; and Garcia, A. N. Pyrolysis of polyethylene in a fluidized bed reactor. *Energy Fuels* 8(1994): 1238.
- [15] Wanpler, T. P. Thermometric behavior of polyolefins. *J. Anal. Appl. Pyrol.* 15(1989): 187.
- [16] Adams, C. J.; Earle, M. J.; and Seddon, K. R. Catalytic cracking reactions of polyethylene to light alkanes in ionic liquid. *Green Chem.* (2000): 21-23.
- [17] Lin, Y.-H.; and Yang, M.-H. Catalytic pyrolysis of polyolefin waste into valuable hydrocarbons over reused catalyst from refinery FCC units. *Appl. Catal., A: General* 328(2007): 132-139.
- [18] Garcia, R. A.; Serrano, D. P.; and Otero, D. Catalytic cracking of HDPE over hybrid zeolitic-mesoporous materials. *J. Anal. Appl. Pyrol.* 74(2005): 379.
- [19] Manos, G.; Yusof, I. Y.; Papayannakos, N.; and Gangas, N. H. Catalytic cracking of polyethylene over clay catalysts: Comparison with an ultrastable Y zeolite. *Ind. Eng. Chem. Res.* 40(2001): 2220.
- [20] Serrano, D. P.; Aguado, J.; and Escola, J. M. Catalytic conversion of polystyrene over HMCM-41, HZSM-5 and amorphous SiO₂-Al₂O₃: comparison with thermal cracking. *Appl. Catal., B: Environmental* 25(2000): 181.
- [21] Ooi, Y. S.; Zakaria, R.; Mohamed, R. A.; and Bhatia, S. Synthesis of composite material MCM-41/Beta and its catalytic performance in waste used palm oil cracking. *Appl. Catal., A: General* 274(2004): 15-23.
- [22] Altwasser, S.; Welker, C.; Traa, Y.; and Weitkamp, J. Catalytic cracking of n-octane on small-pore zeolites. *Micropor. Mesopor Mater.* 83(2005): 345.
- [23] Nakao, R.; Kubota, Y.; Katada, N.; Nishiyama, N.; Kunimori, K.; and Tomishig, K. Performance and characterization of BEA catalysts for catalytic cracking. *Appl. Catal., A: General* 273(2004): 63-73.
- [24] Bonetto, L.; Cambor, M. A.; and Corma, A. Optimization of zeolite beta in cracking catalysts: Influence of crystallite size. *Appl. Catal., A: General* 82 (1992): 37-50.

- [25] Manos, G.; Gaeforth, A.; and Dwyer, J. Catalytic degradation of HDPE over different zeolitic structures. *Ind. Eng. Chem. Res.* 39(2000): 1198.
- [26] Serrano, D. P.; Aguado, J.; and Escola, J. M. Catalytic cracking of a polyolefin mixture over different acid solid catalysts. *Ind. Eng. Chem. Res.* 39(2000): 1177.
- [27] Marcilla, A.; Gómez-Siurana, A.; and Valdés, F. Catalytic pyrolysis of LDPE over H-beta and HZSM-5 zeolites in dynamic conditions: Study of the evolution of the process. *J. Anal. Appl. Pyrol.* 79(2007): 433-442.
- [28] Marcilla, A.; Gómez-Siurana, A.; and Valdés, F. Catalytic cracking of low-density polyethylene over H- Beta and HZSM-5 zeolites: Influence of the external surface. Kinetic model. *Polym. Degrad. Stab.* 92(2007): 197-204.
- [29] Aguado, J.; Serrano, D. P.; Escola, J. M.; Garagorri, E.; and Fernández, J. A. Catalytic conversion of polyolefins into fuels over zeolite beta. *Polym. Degrad. Stab.* 69(2000): 11-16.
- [30] Lee, Y. J.; Kim, J. H.; Kim, S. H.; Hong, S. B.; and Seo, G. Nanocrystalline Beta zeolite: An efficient solid acid catalyst for the liquid-phase degradation of high-density polyethylene. *Appl. Catal., B: Environmental* [online]. 2008. Available from: <http://www.sciencedirect.com> [2008, March 17]
- [31] Breck, D.W. *Zeolite Molecular Sieves: Structure, Chemistry, and use*. pp. 3-20. New York: John Wiley & Sons, 1997.
- [32] Secondary Building Units (SBU's) in zeolites [Online]. Available from: <http://www.ch.ic.ac.uk/vchemlib/course/zeolite/structure.html> [2007, November 12]
- [33] Szostak, R. *Zeolite Molecular Sieves. Principles of Synthesis and Identification*. pp. 3-42. New York Van: Nostrand Reinhold, 1989.
- [34] Lin, Y. H.; Yang, M. H.; Yeh, T. F.; and Ger, M. D. Catalytic degradation of HDPE over mesoporous and microporous catalytic in a fluidized-bed reactor. *Polym. Degrad. Stab.* 86(2004): 121.
- [35] Garforth, A.; Fiddy, S.; Lin, Y. H.; and Sharratt, P. N. Catalytic degradation of HDPE: An evaluation of mesoporous and microporous catalysts using thermal analysis. *Thermochim. Acta* 294(1997): 65.

- [36] Aguado, J.; Sotelo, J. L.; Serrano, D. P.; Callers, J. A.; and Escola, J. M. Catalytic conversion of polyolefins into liquid fuels over MCM-41: Comparison with ZSM-5 and amorphous $\text{SiO}_2\text{-Al}_2\text{O}_3$. *Energy Fuels* 11(1997): 1225.
- [37] Derouane, E. G. New aspects of molecular shape-selectivity: Catalytic by zeolite ZSM-5. *Stud. Surf. Sci. Catal.* 5(1980): 5.
- [38] Wadlinger, R. L.; Kerr, G. T.; and Rosinski, E. J. *US Patent 3 308 068* (1967).
- [39] Keading, W. W.; Chu, C.; Young, L. B.; Weinstein, B.; and Butter, S. A. Selective alkylation of toluene with methanol to produce para-xylene. *J. Catal.* 67(1981): 159.
- [40] Prasetyoko, D.; Ramli, Z.; Endud, S.; Hamdan, H.; and Sulikowski, B. Conversion of rice husk ash to zeolite beta. *Waste Manage.* 20(2006): 1173-1179.
- [41] Jensen, J. C.; Creighton, E. J.; Njo, S. L.; Koningsveld, H.; and Bekkum, H. On the remarkable behavior of zeolite beta in acid catalysis. *Catal. Today* 38(1997): 205-206.
- [42] Barthoment, D. Acidic catalysts with zeolites. *Zeolite Science and Technology*, Martinus Nijhoff Publishers, 1984.
- [43] Sun, J.; Zhu, G.; Chen, Y.; Li, J.; Wang, L.; Peng, Y.; Li, H.; and Qiu, S. Synthesis, surface and crystal structure investigation of the large zeolite beta crystal. *Micropor. Mesopor Mater.* 102(2007): 242-248.
- [44] Newsam, J. M.; Treacy, M. J.; Koetsier, W.; and deGruyter, C. B. Structural Characterization of zeolite beta. *Proc. R. Soc. Lond.* A420(1988): 375.
- [45] Treacy, M. J.; and Newsam, J. M. Two new three-dimensional twelve-ring zeolite frameworks of which zeolite beta is a disordered intergrowth. *Nature* 332(1988): 249.
- [46] Corma, A.; Navarro, M. T.; Rey, F.; Rius, J.; and Valencia, S. Pure polymorph C of zeolite beta synthesized by using framework isomorphous substitution as a structure-directing mechanism. *Angew. Chem. Int. Ed.* 40(2001): 2277.
- [47] Corma, A.; Navarro, M. T.; Rey, F.; and Valencia, S. Synthesis of pure polymorph C of Beta zeolite in a fluoride-free system. *Chem. Commun.* 16(2001): 1486.
- [48] Leonid, V. A. *Elements of X-ray crystallography*. pp. 4-25. New York: Mcgraw-hill, 1997.

- [49] Skoog, D. A. *Principles of Instrumental Analysis*. 4th ed. pp. 363-364. New York: Harcourt Brace College Publishers, 1997.
- [50] Myers, D. *Surface, Interfaces and Colloids: Principles and Applications*. 2nd ed. pp. 550-556. USA: John Wiley & Sons, 1999.
- [51] Ding, L.; Zheng, Y.; Hong, Y.; and Ring, Z. Effect of particle size on the hydrothermal stability of zeolite beta. *Micropor. Mesopor Mater.* 101(2007): 432-439.
- [52] Basic operating principles of the sorptomatic [Online]. 1990. Available from: <http://saf.chem.ox.ac.uk./Instruments/BET/sorptprin> [2005, November]
- [53] Analysis software user's manual, BELSORP, BEL JAPAN, INC. 57.
- [54] Elliott, P. B.; Leslie, G. J.; and Paul, P. H. The determination of pore volume and area distributions in porous substances. I Computations from nitrogen isotherms. *Contribution from the multiple fellowships of Baugh and Sons Company, Mellon Institute* 73(1995): 373.
- [55] Brunauer, S.; Emmett, P. M.; and Teller, E. Adsorption of gases in multimolecular layers. *The Bureau of chemistry and solids and George Washington University* 60(1938): 309.
- [56] Temperature-programmed desorption (TPD) for characterizing the acid sites on oxide surfaces-supplier data by micromeritics [Online]. 2006. Available from: <http://www.azonano.com/details.asp?ArticleID=1475> [2007, October 10]
- [57] Hunger, M.; Schenk, U.; Breuninger, R.; Glaser, R.; and Weikamp, J. Characterization of the acid sites in MCM-41 type materials by spectroscopic and catalytic technique. *Micropor. Mesopor Mater.* 27(1999): 261.
- [58] Simon-Masseron, A.; Marques, J. P.; Lopes, J. M.; Ribeiro, F. R.; Gener, I.; and Guisnet, M. Influence of the Si/Al ratio and crystal size on the acidity and activity of HBEA zeolites. *Appl. Catal., A: General* 316(2007): 75-82.
- [59] Zheng, Y.; and Ding, L. Nanocrystalline zeolite beta: The effect of template agent on crystal size. *Mater. Res. Bull.* 42(2007): 584-590.
- [60] Andaç, Ö.; Tatlıer, M.; Sirkecioğlu, A.; Ece, I.; and Erdem-Şenatalar, A. Effects of ultrasound on zeolite A synthesis. *J. Micropor. Mesopor. Mater.* 79(2005): 225-233.

- [61] Suslick, K. S. The Chemistry of Ultrasound [online]. Available from: <http://www.scs.uiuc.edu/suslick/britannica.html> [2007, July 14]
- [62] Mason, T. J. *Practical Sonochemistry: user's guide to applications in chemistry and chemical engineering*. pp. 20-30. London: Ellis Horwood, 1991.
- [63] Suslick, K. S. Executive Summary: The chemical and physical effect of ultrasound [online]. Available from: <http://www.scs.uiuc.edu/suslick/execsummsono.html> [2007, October 8]
- [64] He, J.; Yang, X.; Evans, D. G.; and Duan, X. New methods to remove organic templates from porous materials. *Mater. Chem. Phys.* 77(2002): 270-276.
- [65] Nelson, W. L. *Petroleum Refinery Engineering*. 4th ed. pp. 759-818. Singapore: Mcgraw-hill, 1987.
- [66] Serge, R. *Thermal and Catalytic Process in Petroleum Refining*. pp. 293-403. New York: Maecel Dekker, 2003.
- [67] Oil refinery: Cracking [Online]. 2006. Available from: <http://www.schoolscience.co.uk/content/4/chemistry/petroleum/knowl/4/cracking.html> [2007, December 24]
- [68] Odian, G. *Principle of Polymerization*. 4th ed. pp. 209-235. Canada: Wiley & Sons, 2004.
- [69] Yury, V. K. Chemical mechanisms of catalytic cracking over solid acidic catalyst: alkanes and alkenes. *Taylor & Francis* 48(2001): 85.
- [70] Scherzer, J. Octane-enhancing, zeolitic FCC catalyst: scientific and technical aspect. *Catal. Rev.-Sci. Eng.* 31(1989): 83.
- [71] Greensfflder, B. S.; and Voge, H. H.; Good, G. M. Catalytic and thermal cracking of pure hydrocarbons. *Ind. Eng. Chem.* 41(1949): 2573.
- [72] Thomas, C. L. Chemistry of cracking catalysts. *Ind. Eng. Chem.* 41(1949): 2564.
- [73] Sie, S. T. Acid-catalyzed cracking of paraffinics Part2. Evidence for the protonnated cyclopropane mechanism from catalytic cracking experiments. *Indian Eng. Chem.* 32(1993): 397.
- [74] Williams, B. A.; Babitz, S. M.; Miller, J. T.; Snurr, R. Q.; and Kung, H. H. The role of acid strength and pore diffusion in the enhanced cracking activity of steamed zeolites Y. *Appl. Catal., A.* 32(1999): 161.

- [75] Cumming, K. A.; and Wojciechowski, B. W. Hydrogen transfer, coke formation and catalyst decay and their role in the chain mechanism of catalytic cracking. *Catal. Rev. Sci. Eng.* 38(1996): 101.
- [76] Wojciechowski, B. W.; and Abbot, J. The mechanism of catalytic cracking of n-alkanes on ZSM-5 zeolite. *J. Chem. Eng.* 63(1985): 462.
- [77] Makkee, M.; Wissink, M.; and Moulijn, J. A. Gasoline conversion: reactivity towards cracking with equilibrated FCC and ZSM-5 catalysts. *Appl. Catal., A: General* 223(2002): 85.
- [78] Serrano, D. P.; Aguado, J.; Escola, J. M.; and Rodriguez, J. M. Influence of nanocrystalline HZSM-5 external surface on the catalytic cracking of polyolefins. *J. Anal. Appl. Pyrol.* 74(2005): 353-360.





APPENDICES

ศูนย์วิทยทรัพยากร
จุฬาลงกรณ์มหาวิทยาลัย

Appendix

A-1 Calculation of Selectivity to Other Hydrocarbons

% Selectivity of gas fraction and liquid fraction

$$\% \text{ Selectivity of X} = \frac{\text{concentration of X} \times 100}{\text{total concentration of fractions}}$$

$$\text{Concentration of X} = \frac{b \times c}{a}$$

a = Peak area of X in standard gas or liquid fraction

b = % molar of X in standard gas or liquid fraction

c = Peak area of X in sample products



ศูนย์วิทยทรัพยากร
จุฬาลงกรณ์มหาวิทยาลัย

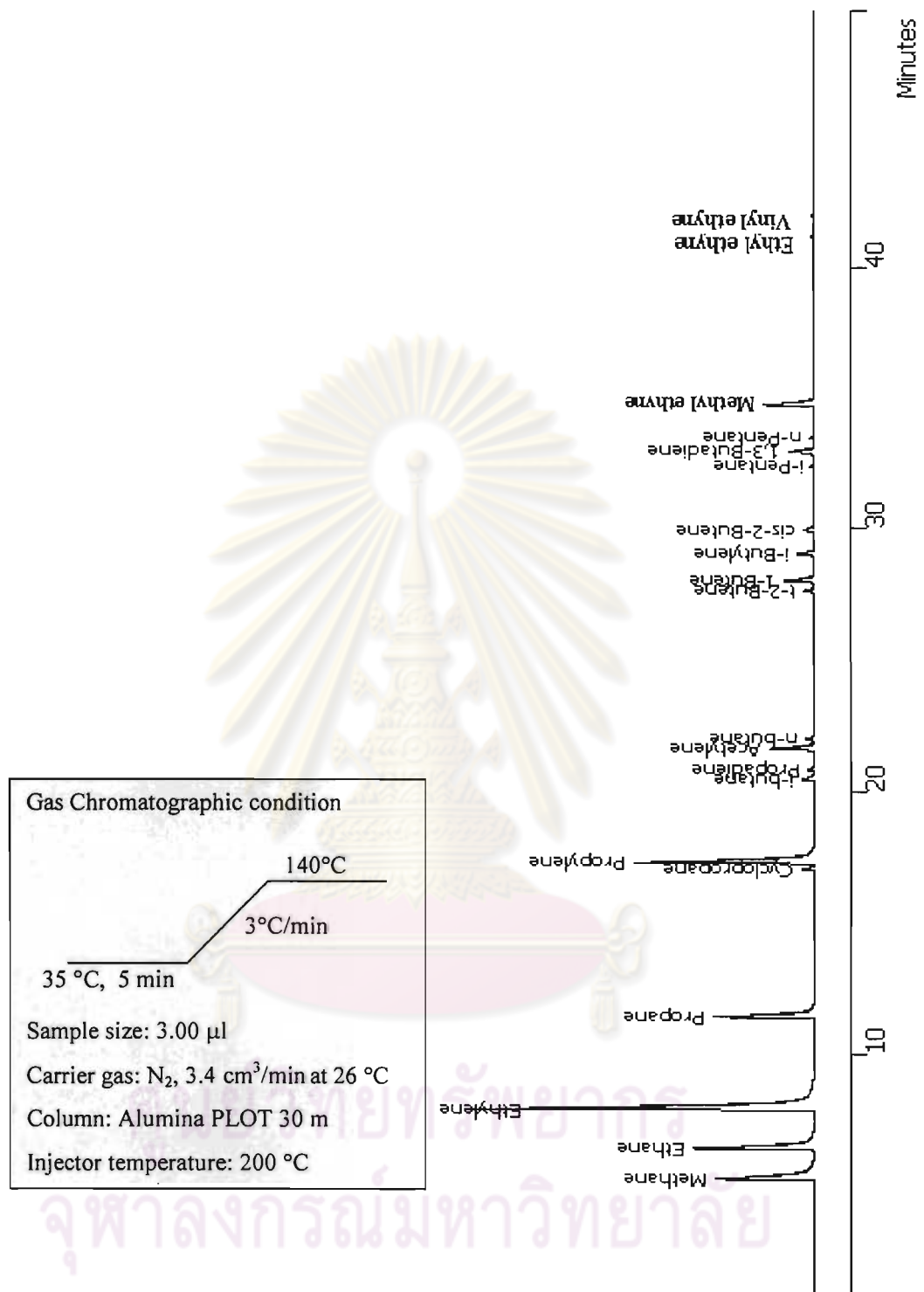


Figure A-1 Gas chromatogram of standard mixture gas.

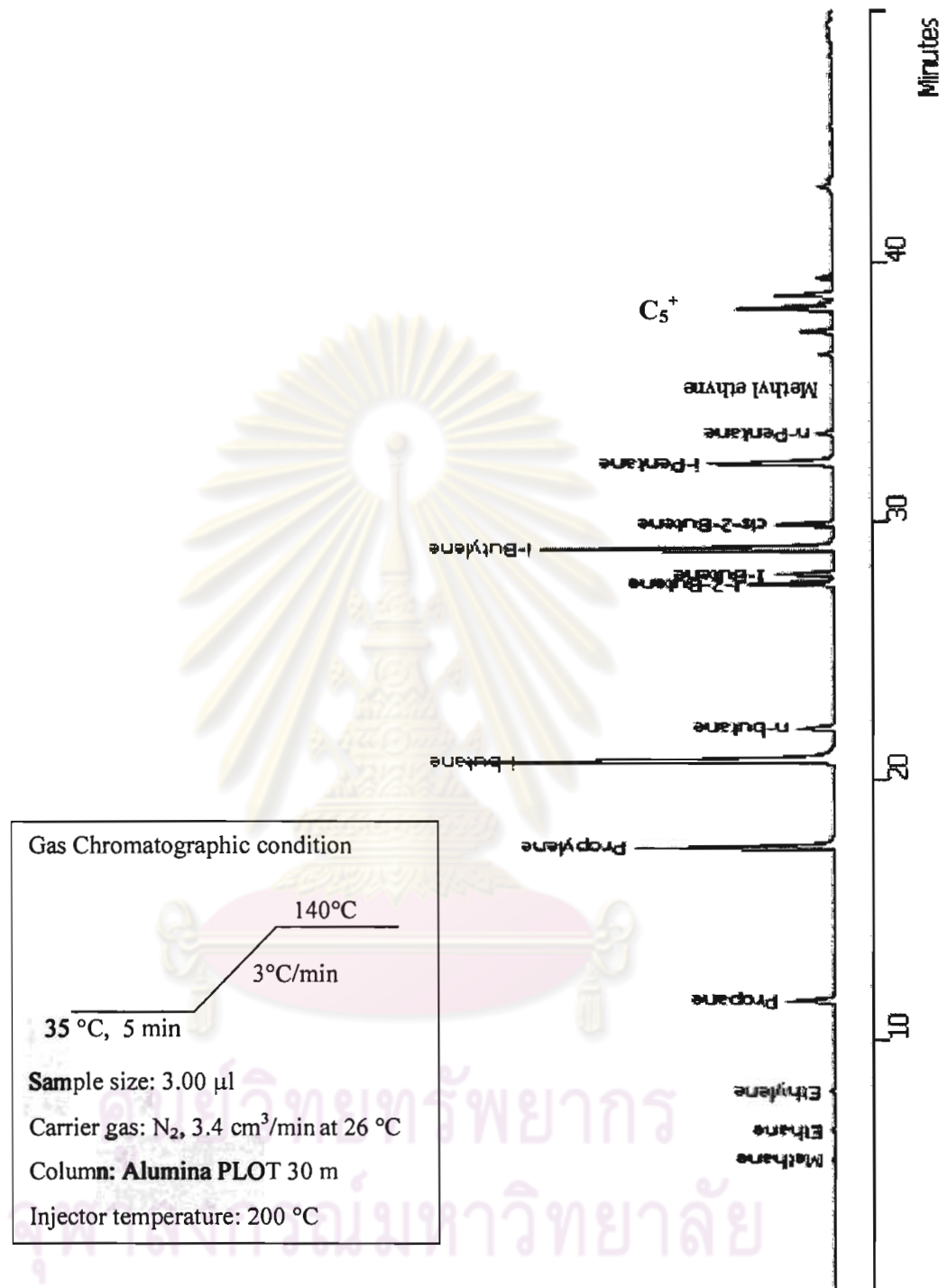


Figure A-2 Gas chromatogram of gas product obtained from catalytic cracking of PP waste over Beta20-US30-24h at 400°C

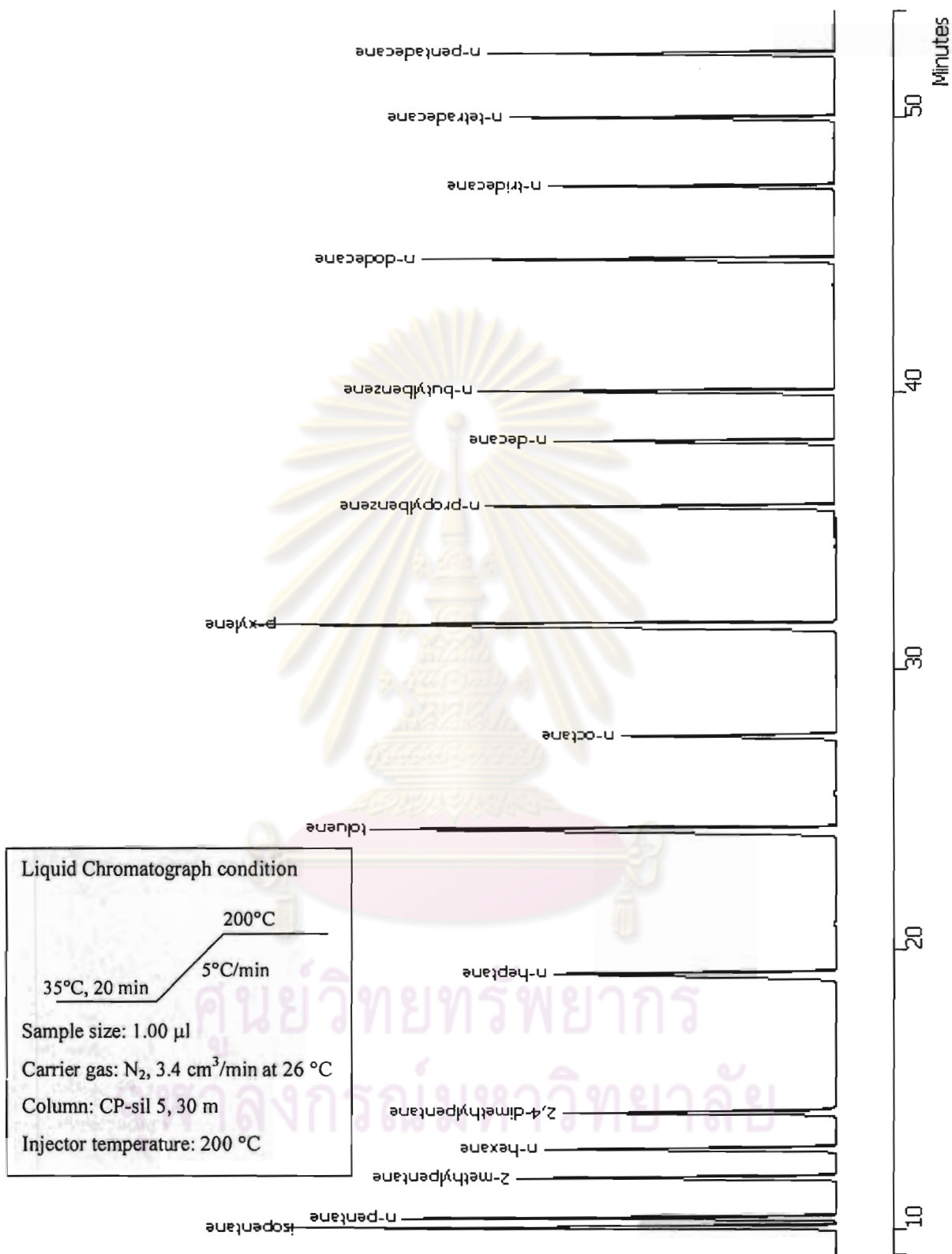


Figure A-3 Liquid chromatogram of standard gasoline (SUPELCO).

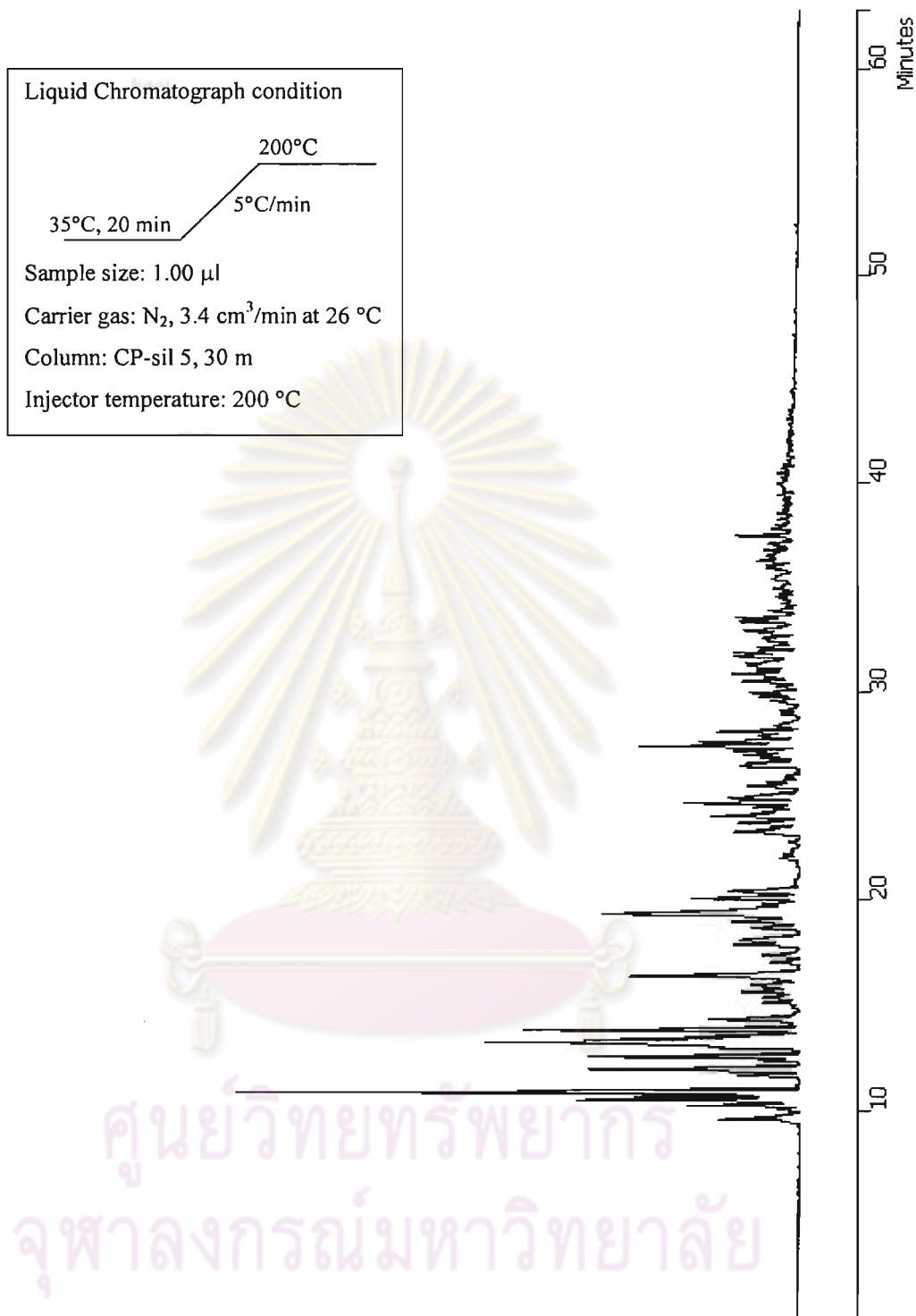


Figure A-4 Liquid chromatogram of liquid product obtained from catalytic cracking of PP waste over Beta20-US30-24h at 400°C

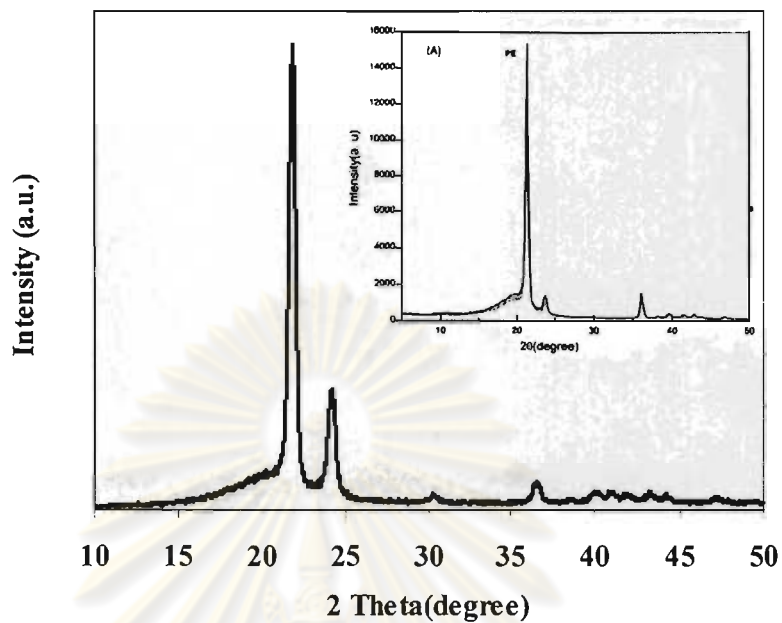


Figure A-5 XRD pattern of plastic waste. Insert shows the XRD patterns for HDPE.

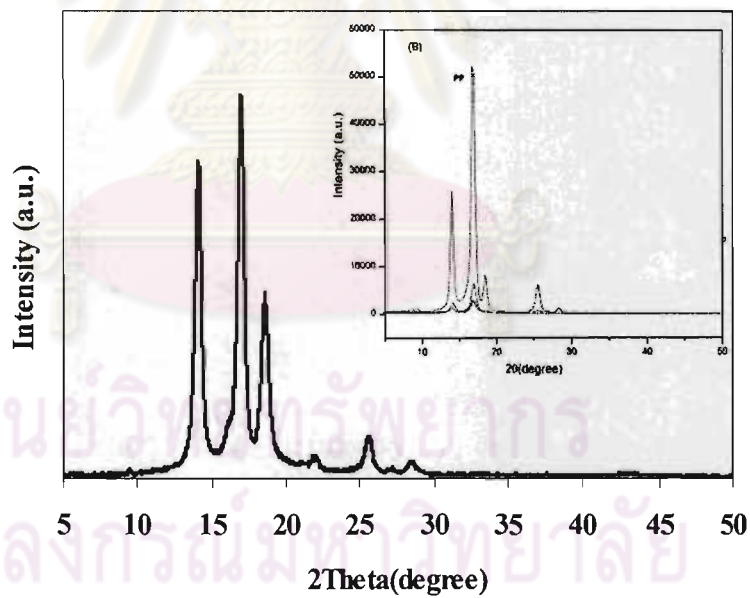


Figure A-6 XRD pattern of plastic waste. Insert shows the XRD patterns for PP.

VITAE

Miss Thidarat Kunawong was born on August 2, 1982 in Loei, Thailand. She graduated with Bachelor's Degree in Chemistry from Faculty of Science, Khonkaen University in 2005. She continued her study in Chemistry, Faculty of Science, Chulalongkorn University in 2005 and completed in 2008.



ศูนย์วิทยทรัพยากร
จุฬาลงกรณ์มหาวิทยาลัย